Tracing alteration of ultramafic rocks in the Samail ophiolite

Juan Carlos de Obeso

Submitted in partial fulfillment of the
requirements for the degree of
Doctor of Philosophy
in the Graduate School of Arts and Sciences

COLUMBIA UNIVERSITY

2019

ABSTRACT

Tracing alteration of ultramafic rocks in the Samail ophiolite

Juan Carlos de Obeso

Alteration of ultramafic rocks is ubiquitous to their occurrence near the surface. Primary mantle minerals like olivine and pyroxenes are unstable at low pressure and temperatures and undergo hydration (serpentinization), carbonation and weathering reactions forming hydrated and carbonated minerals. Employing a variety of analytical techniques including: electron microprobe, X-Ray diffraction, major and trace element geochemistry, Mg isotopes geochemistry and geochemical modelling this work seeks to contrain conditions of alteration and trace changes in composition of peridotite during alteration.

In Wadi Fins in the southeast of Oman peridotites outcrop at the bottom of a canyon overlaid by a thick sequence $\sim$ 1.5 km of Cretaceous to Eocene shallow oceanic limestones and dolostones. The peridotites exhibit different types of alteration. While the common view is that serpentinization and carbonation of peridotites is isochemical this is not the case for alteration in Wadi Fins. Peridotites tens of meters below the unconformity are characterized by a striking grid of carbonate and serpentine veins. The calcite veins and relatively low MgO/SiO_2 suggest that the peridotites reacted with a hydrous fluid derived from interaction of seawater with the overlying sediments composed of limestones with minor amounts of chert. This is further affirmed by average $\delta^{13}C$, $\delta^{18}O$ and $^{87}Sr/^{86}Sr$ from carbonate veins in the peridotites that are similar to values of the sediments. Clumped isotope thermometry on calcite veins in peridotite establish that they formed at 25–60 ℃. Reaction path modeling of carbonate- quartz derived fluids with peridotite reproduces the

observed mineral assemblage composed of carbonate and serpentine with similar Mg and MgO/SiO_2 at high water to rock ratios, with carbon, H_2O and silica added to the rock by the reacting fluid.

Close to the unconformity the altered peridotites are characterized by concentric alteration halos recording variable fO_2 and fS_2. The partially serpentinized cores preserved primary minerals and record extremely low oxygen fugacities ($fO_2 \sim 10^{-75}$ bars). Two alteration zones are present evident from the alteration color. These zones exhibit non-isochemical alteration characterized by intergrowths of stevensite/lizardite. The alteration zones record progressively higher (fO_2) recorded by Ni-rich sulfides and iron oxides/hydroxides. The alteration zones lost 20-30% of their initial magnesium content, together with mobilization of iron over short distances from inner green zones into outer red zones, where iron was reprecipitated in goethite intermixed with silicates due to higher fO_2.

The loss of magnesium in this peridotites motivated the final section of work. Mg isotopic compositions of partially serpentinized harzburgites and dunites in Oman are identical to average mantle and bulk silicate Earth (δ^{26}Mg=-0.25‰) while altered peridotites from Wadi Fins get heavier with increasing alteration. Analyses of peridotite alteration products including samples from Wadi Fins and carbonates from Wadi Tayin were used to show that isochemical serpentinization at low W/R does not fractionate Mg isotopes. I propose a mechanism that with increasing W/R and co-precipitation of Mg-carbonates and serpentine leads to carbonates with light isotopic compositions (Magnesite δ^{26}Mg =-3.3 and dolomite δ^{26}Mg=-1.91) and serpentine with heavy compositions (up to δ^{26}Mg =-0.96 in serpentine veins). This complementary enrichment-depletion and

the finite ^{14}C ages of the carbonates suggest that serpentinization is ongoing along carbonation in Oman at ambient temperatures. Rates of calcite precipitation in travertines inferred from $\Delta^{26}Mg_{cal-fl}$ suggest that travertine formation in Oman sequesters a total of 10^6-10^7 kg CO_2/yr.

Contents

List of Figures

List of Tables

Acknowledgements

The completion of this thesis would not be possible without the guidance and support of many people. First and foremost, I would like to thank Peter Kelemen. He took a chance with me 6 years ago. An unconventional Mexican graduate student candidate with a chemical engineering degree and little geology background. Peter enthusiasm for science is contagious, his commitment to ask and answer important scientific questions is unmatched. He always pushed for a bit more of me and that helped shaped this dissertation and ongoing research projects. From Peter I have learned to explore the Earth as a geologist. During these years Peter gave me several "once-in-a-lifetime" opportunities to see parts of the world I never would have dreamed of reaching and the opportunity of participating in projects reaching far beyond what I have ever expected to do as a scientist. Apart from being such a capable and patient mentor he has become a good friend and colleague.

I like to thank Steve L. Goldstein and Marc Spiegelman for being part of my advisory committee. They provided critical input and support for the work presented in this dissertation.

A lot of the laboratory work done for this dissertation is possible as a result of mentoring and teaching from multiple people at Lamont that sacrifice some of there time to help me. Jean Hanley and Karen Benedetto helped with in the rock prep lab and made themselves always available for technical and non-technical questions. Gary Mezko and Cathleen Doherty teached me the flux fusion protocol used for ICP-OES and how to reduce the data. I learned the basics of rock digestions for trace elements and isotopes

from Conny Class. A lot of the clean lab work would not been possible without the help of Louise Bolge, she provided technical guidance, support and encouragement for eternal rounds of perchloric acid fuming, HF:HNO_3 digestions and standard preparations for complex samples. This dissertation benefits from work performed at the American Museum of Natural History. Adrian Fiege, Julianne Gross and Beth Goldoff are gratefully acknowledged for microprobe training and assistance. I would also like to thank George Harlow and Karin Block for allowing me to use their XRD instruments. Reaction path modeling benefited from training with Amelia Paukert and a customized database built by Frieder Klein. Both are acknowledged for their help. Lisa and Tony Falk received me in their home at Woods Hole. Lisa helped me with clumped isotope measurements. Their hospitality during a harsh Cape Cod winter week is appreciated. Friends in Lamont are thanked for long conversations and allowing me to learn of other fields: Laura Haynes, Frankie Pavia, Genevieve Coffey, James Gibson, Lucy Tweed, Laura Gruenberg, Hannah Rabinowitz, Natalie Accardo, Mike Sandstrom, Sean Kinney, Steven Boswell and many more.

I need to thank John Higgins at Princeton University for hosting me in his lab for the magnesium isotope work. Everyone in his laboratory provided friendly assistance and guidance during my visits. Above all I thank Danielle Santiago Ramos, she was instrumental to get the measurements done, providing assistance and time for sample purification and measurement. D. Nothaft is thanked for help powdering and cutting samples and for hosting me in Boulder for a quick exploratory Raman session.

I owe a great debt of gratitude to other mentors and collaborators, at Lamont and beyond: Dave Walker, Margot Godard, Juerg Matter, Jude Coogon, Craig Manning, Emily

Cooperdock, Michelle Harris, Alexis Templeton and Eric Ellison. A multitude of collaborators from the Oman Drilling Project Science are gratefully acknowledged.

I thank everyone at the Sultanate of Oman Public Authority for Mining, especially Dr. Ali Al Rajhi for facilitating our fieldwork in Oman.

I would like to give special thanks to my friends and family. My parents and siblings provided constant and unconditional support through the years. My brother Alvaro provided invaluable hours of talks about navigating academia in a foreign country. My parents Pilar and Juan Carlos always encouraged me to follow my dreams, if I am here it is because of them. Jorge and Pilar LdL are thanked for their help during my early years in NYC. Thanks to los chilenos who became our family in NYC. My mexican friends in NY that were always available to have some tacos and take my mind away from research for a few hours among the many of them I want to acknowledge Diego Villarreal, Andres Lajous and Sara Hidalgo.

Above all, I would like to thank my wife Susana. Susana took a leap of faith 8 year sacrificing some of her personal projects. This work belongs to her as much as anyone else, and its completion would've been impossible without her support. Gracias totales.

Financial support from the National Science Foundation, Sloan Foundation and from Consejo Nacional de Ciencia y Tecnologıa (CONACYT) is gratefully acknowledged.

”Y si el ideal no ha de cumplirse jamás mejor es padecer la perpetua tentación de lo imposible”

Pez

1 Introduction

This thesis addresses alteration processes of ultramafic rocks in the Samail ophiolite in eastern Oman. Ultramafic rocks or peridotites are far from equilibrium with hydrous fluid in near surface conditions and undergo hydration (serpentinization) and carbonation reaction dramatically changing mineralogy and physical characteristics of the rocks. Most of these reactions are usually thought to proceed under isochemical conditions, this means only incorporating water and CO_2 without changing the major element composition of the rocks (e.g., Coleman and Keith 1971; Kelemen et al. 2011; Komor, Elthon, and Casey 1985; O'Hanley 1996). This thesis focuses on conditions in which this is not the case. In some circumstances, serpentinization, carbonation and weathering produce drastic changes in major element ratios, which are important for many reasons, including their effect on volume changes and permeability during alteration, design of engineered systems that emulate natural carbon mineralization, and sustaining the conditions for abiotic hydrocarbon synthesis, chemosynthetic subsurface ecosystems and the origin of life on this and other planets.

1.1 Processes of alteration of ultramafic rocks

Shallow mantle peridotite is mainly composed of olivine, orthopyroxene, clinopyroxene and Cr-spinel. These minerals are unstable in the presence of water at low temperatures and pressures, and undergo hydration, carbonation and oxidation reactions. The importance of these reactions has been made clear over the past 40 years (e.g Evans 2010; Moody 1976; Neal and Stanger 1985; O'Hanley 1996; Ulmer and Trommsdorff 1995). Hydration of peridotites, commonly known as serpentinization involves drastic changes in

the rheology of the rocks; density decreases and the rock becomes weaker (Escartín, Hirth, and Evans 1997). Serpentinization at relatively low time integrated water-rock ratios produces strongly reducing conditions as Fe^{2+} oxidizes to Fe^{3+} (Bach and Klein 2009; Frost 1985; Früh-Green et al. 2004; Schwarzenbach, Gazel, and Caddick 2014). The resulting fluids are among the most reduced on Earth, saturated in metal alloys such as awaruite (Ni_2Fe to Ni_3Fe), wairauite (CoFe) and native copper (Cu), and sulfides including heazlewoodite (Ni_3S_2) and polydymite (Ni_3S_4) (Abrajano et al. 1988; Chamberlain et al. 1965; Frost 1985; Klein and Bach 2009; Lorand 1988; Nickel 1959; Schwarzenbach, Gazel, and Caddick 2014). The fluids commonly have high concentration of molecular hydrogen (Abrajano et al. 1990; Kelley et al. 2005; Neal and Stanger 1985; Sleep et al. 2004; Thayer 1966) and methane (e.g. Etiope, Schoell, and Hosgörmez 2011; Hitch et al. 1980; Holm and Charlou 2001; Miller et al. 2016; Proskurowski et al. 2008; Rempfert et al. 2017; Russell 2007). These compounds may form the basis for abiotic synthesis of more complex hydrocarbons, and are a potential source of energy for chemosynthetic organisms. Locations where these processes operated have been proposed as a potential place for the emergence of life on Earth (Evans 2010; McCollom and Seewald 2013; Russell 2007; Sleep et al. 2004) and could provide a source of energy for hypothesized life in other planetary bodies (Russell et al. 2014; Vance et al. 2007).

Water in the serpentine mineral structure is carried down during subduction of altered ocean crust and released into the mantle during deserpentinization (Hacker 2003; Hattori and Guillot 2003; Ulmer and Trommsdorff 1995). This process also cycles several elements that incorporate into serpentinites like sulfur, boron and chlorine (Alt and Shanks 1998; Alt et al. 2013; Barnes and Sharp 2006; Bonatti, Lawrence, and Morandi 1984; Boschi

et al. 2013; Thompson and Melson 1970). On land, low temperature serpentinization is ubiquitous to peridotite massifs (Barnes, O'Neil, and Trescases 1978; Clark and Fontes 1990; Kelemen and Matter 2008; Kelemen et al. 2011; Neal and Stanger 1985; Paukert et al. 2012; Sánchez-Murillo et al. 2014). Carbonation of peridotites has been linked to past climate change (Jagoutz, Macdonald, and Royden 2016; Reusch 2011) and represents a significant carbon sink in the seafloor (Alt et al. 2012). Carbonation of seafloor peridotites forms spectacular carbonate chimneys at the Lost City hydrothermal field (Kelley et al. 2005; Rouméjon et al. 2014) and the Baie de Prony in New Caledonia (Launay and Fontes 1985; Monnin et al. 2014). On land carbonation reactions present as magnesium carbonate deposits and extensive travertine deposits (e.g. Falk et al. 2016; Kelemen and Matter 2008; Kelemen et al. 2011; Matter and Kelemen 2009; Mervine et al. 2014; Real et al. 2016). The carbonation reactions of mantle minerals have been proposed as potential sink of anthropogenic CO_2 emissions (Lackner et al. 1995; Seifritz 1990). Fluids with high pH, low fO_2 and low DIC are a direct result of serpentinization and carbonation reactions (Barnes and O'Neil 1969; Bruni et al. 2002; Paukert et al. 2012).

Reaction pathways for serpentinization and carbonation change depending on alteration conditions. Variation in temperature, pressure, fluid composition, fluid/rock (W/R) or mineralogy of the protolith can lead to diverse reaction pathways. During serpentinization at low temperatures (<200°C) lizardite and chrysotile ($Mg_2Si_2O_5(OH)_4$) are the main serpentine minerals (Evans 2004; Evans et al. 1976) while iron preferentially forms Fe-rich brucite ($(Mg,Fe)(OH)_2$) (Klein and Bach 2009; Klein, Bach, and McCollom 2013; Seyfried, Foustoukos, and Fu 2007). At higher temperatures antigorite ($(Mg,Fe)_{2.93}Si_{2.07}O_{5.18}(OH)_{3.78}$) is the main serpentine mineral (Evans 2004; Evans et al.

1976) and magnetite (Fe_3O_4) becomes the main sink for iron (Klein et al. 2014). Higher concentration of CO_2 in the fluids leads to the formation of carbonates instead of hydroxides while increased SiO_2 activity results in the formation of talc (Bach et al. 2004; Frost and Beard 2007; Hemley et al. 1977) and/or quartz (Streit, Kelemen, and Eiler 2012). As fluid-rock ratios increase, the alteration system becomes fluid-dominated, resulting in more oxidizing and alkaline conditions that produce opaque mineral assemblages recording variable oxygen fugacity (Alt and Shanks 1998; Eckstrand 1975; Frost 1985; Klein and Bach 2009; Schwarzenbach, Gazel, and Caddick 2014; Schwarzenbach et al. 2012).

Systematic changes in major element ratios, produced by peridotite alteration, have been observed, particularly for alteration at < 50℃. During seafloor weathering pervasive loss of magnesium has been documented in peridotites (Snow and Dick 1995). Systematically elevated Si/Mg compared to residues of mantle melt extraction – often attributed to Mg loss, but sometimes due to Si gain - is also observed in ophiolites, in which many partially serpentinized peridotites show Si/Mg higher than residual peridotites at the same Al/Si by 5 to 10% (e.g., Monnier et al. 2006, Figure 5, Obeso and Kelemen 2018, Figure 13). Much higher Si/Mg (molar ratio 1:1, weight ratio $SiO_2/MgO \sim 1.5$) is observed some localities rich in "deweylite" (Beinlich et al. 2010 and this work), composed of microcrystalline mixtures of serpentine and clay or talc (Bish and Brindley 1978; Faust and Fahey 1962).

1.2 Brief geological setting

All the work presented in this thesis involves samples collected in the mantle section of the Samail ophiolite in the Sultanate of Oman. The Samail ophiolite is a section of oceanic crust and underlying mantle that was thrust soon after formation into the Arabian

continental margin in the late Cretaceous (Boudier, Nicolas, and Ildefonse 1996; Hacker 1994; Hacker, Mosenfelder, and Gnos 1996; Nicolas et al. 2000; Rioux et al. 2012, 2013; Tilton, Hopson, and Wright 1981; Warren et al. 2005). It is the largest and best-preserved ophiolitic sequence in the planet and runs as a semi-continuous belt of ∼480 km and up to 80km wide striking NW to SE along the coast of the United Arab Emirates and the Sultanate of Oman (Coleman and Hopson 1981) (Figure 1).

The mantle section of the ophiolite is mainly composed of highly depleted, residual mantle peridotites (mostly harzburgites, e.g. Godard, Jousselin, and Bodinier 2000; Hanghøj et al. 2010; Monnier et al. 2006), together with 5 to 15% dunite (Boudier and Coleman 1981; Braun 2004; Braun and Kelemen 2002; Collier 2012; Kelemen, Braun, and Hirth 2000). The degree of alteration ranges from ∼ 20% serpentinization in "fresh" rock to nearly 100% replacement of the anhydrous silicates and oxides (olivine, pyroxenes, spinel) with hydrous minerals (mostly serpentine, but also brucite or talc), carbonates (magnesite, dolomite, calcite, hydrous Mg carbonates), and Fe-oxides and oxy-hydroxides (magnetite, hematite, goethite). Alteration likely occurred throughout the history of the ophiolite and continues to the present day (Chavagnac et al. 2013; Clark and Fontes 1990; Kelemen and Matter 2008; Kelemen et al. 2011; Mervine et al. 2014, 2015; Monnin et al. 2011; Neal and Stanger 1985; Streit, Kelemen, and Eiler 2012).

1.3 Outline of thesis

This thesis investigates alteration conditions of mantle peridotites in Oman that led to major element mobility. I focus on petrological, geochemical and modeling approaches to constrain chemical changes associated with serpentinization and carbonation reactions

primarily at low temperatures.

Chapter 2 presents results of analyses of a pervasively serpentinized and carbonated suite of peridotites from Wadi Fins, along the north facing coast of Oman near the town of Fins. Using bulk rock chemistry, clumped isotope thermometry and reaction path modeling, I show that these rocks were serpentinized at low temperatures and high water/rock ratio (W/R) during reaction with fluids derived from pore water in the overlying limestones. This alteration setting provides a window into the modification of peridotites by fluids similar to seawater at low temperatures, far from oceanic spreading ridges, and provides insights on the behavior of proposed engineered mineral carbonation using seawater as the carbon bearing fluid.

Chapter 3 investigates an outcrop in Wadi Fins upstream of that described in Chapter 2, closer to the Cretaceous unconformity where limestones overlie altered, weathered peridotites. The peridotites in the outcrop are heavily altered and exhibit concentric zoning, with variable composition and mineralogy. The cores are partially serpentinized harzburgites while the weathered/altered areas are depleted in magnesium and iron. Iron appears to be remobilized from a central, high Si zone, to a peripheral, iron-rich, oxidized zone. I use geochemical, petrological and mineralogical data complemented by reaction path modeling to show that changes in bulk chemistry are associated with changes in oxygen fugacity and variable W/R. The results show that iron is mobile at small scales during alteration, while up to 25% of the magnesium is leached out resulting in Si-rich rocks.

Chapter 4 builds on the idea of magnesium mobility during alteration. Mg-rich alteration minerals are common across the ophiolite. They occur as silicates (serpentine),

hydroxides (brucite) and carbonates (magnesite, dolomite, huntite). Each one of these minerals has a different magnesium isotope fractionation during hydrous alteration (Li et al. 2015; Pinilla et al. 2015; Ryu et al. 2016; Schott et al. 2016; Wang et al. 2019). I use this fractionation to show that magnesium is mobilized during alteration of peridotites in Oman, removed from peridotites and deposited in Mg-rich carbonate veins. I propose a mechanism in which Mg isotope ratios in silicates become heavier, and carbonates lighter, as alteration proceeds. These results allowed me to estimate the amount of carbonates and silicate reacting in the modern system. These results are consistent with previous estimates from reaction path modeling (Paukert et al. 2012) and estimates of carbon mineralization using different methods (Kelemen et al. 2011; Mervine et al. 2014).

References

Abrajano, T.A. et al. (1988). "Methane-hydrogen gas seeps, Zambales Ophiolite, Philippines: Deep or shallow origin?" In: *Chemical Geology* 71.1-3, pp. 211–222. ISSN: 00092541. DOI: 10.1016/0009-2541(88)90116-7.

Abrajano, T.A. et al. (1990). "Geochemistry of reduced gas related to serpentinization of the Zambales ophiolite, Philippines." In: *Applied Geochemistry* 5.5-6, pp. 625–630. ISSN: 0883-2927. DOI: 10.1016/0883-2927(90)90060-I.

Alt, Jeffrey C. and Wayne C. Shanks (1998). "Sulfur in serpentinized oceanic peridotites: Serpentinization processes and microbial sulfate reduction." In: *Journal of Geophysical Research* 103.November 2015, p. 9917. ISSN: 0148-0227. DOI: 10.1029/98JB00576.

Alt, Jeffrey C. et al. (2012). "Uptake of carbon and sulfur during seafloor serpentinization and the effects of subduction metamorphism in Ligurian peridotites." In: *Chemical Geology* 322-323, pp. 268–277. ISSN: 0009-2541. DOI: 10.1016/J.CHEMGEO.2012.07.009.

Alt, Jeffrey C. et al. (2013). "The role of serpentinites in cycling of carbon and sulfur: Seafloor serpentinization and subduction metamorphism." In: *Lithos* 178, pp. 40–54. ISSN: 00244937. DOI: 10.1016/j.lithos.2012.12.006.

Bach, Wolfgang and Frieder Klein (2009). "The petrology of seafloor rodingites: Insights from geochemical reaction path modeling." In: *Lithos* 112.1-2, pp. 103–117. ISSN: 00244937. DOI: 10.1016/j.lithos.2008.10.022.

Bach, Wolfgang et al. (2004). "Seawater-peridotite interactions: First insights from ODP Leg 209, MAR 15°N." In: *Geochemistry, Geophysics, Geosystems* 5.9, n/a–n/a. ISSN: 15252027. DOI: 10.1029/2004GC000744.

Barnes, Ivan and James R. O'Neil (1969). "The Relationship between Fluids in Some Fresh Alpine-Type Ultramafics and Possible Modern Serpentinization, Western United States." In: *Geological Society of America Bulletin* 80.10, p. 1947. ISSN: 0016-7606. DOI: 10.1130/0016-7606(1969)80[1947:TRBFIS]2.0.CO;2.

Barnes, Ivan, James R. O'Neil, and J.J Trescases (1978). "Present day serpentinization in New Caledonia, Oman and Yugoslavia." In: *Geochimica et Cosmochimica Acta* 42.1, pp. 144–145. ISSN: 00167037. DOI: 10.1016/0016-7037(78)90225-9.

Barnes, Jaime D. and Zachary D. Sharp (2006). "Achlorine isotope study of DSDP/ODP serpentinized ultramafic rocks: Insights into the serpentinization process." In: *Chemical Geology* 228.4, pp. 246–265. ISSN: 00092541. DOI: 10.1016/j.chemgeo.2005.10.011.

Beinlich, Andreas et al. (2010). "CO2 sequestration and extreme Mg depletion in serpentinized peridotite clasts from the Devonian Solund basin, SW-Norway." In: *Geochimica et Cosmochimica Acta* 74.24, pp. 6935–6964. ISSN: 00167037. DOI: 10.1016/j.gca.2010.07.027.

Bish, David L. and G.W. Brindley (1978). "Deweylites, mixtures of poorly crystalline hydrous serpentine and talc-like minerals." In: *Mineralogical Magazine* 42, pp. 75–79. ISSN: 0026-461X. DOI: 10.1180/minmag.1978.042.321.09.

Bonatti, Enrico, James R. Lawrence, and Noris Morandi (1984). "Serpentinization of oceanic peridotites: temperature dependence of mineralogy and boron content." In: *Earth and Planetary Science Letters* 70.1, pp. 88–94. ISSN: 0012821X. DOI: 10.1016/0012-821X(84)90211-5.

Boschi, Chiara et al. (2013). "Serpentinization of mantle peridotites along an uplifted lithospheric section, Mid Atlantic Ridge at 11° N." In: *Lithos* 178, pp. 3–23. ISSN: 00244937. DOI: 10.1016/j.lithos.2013.06.003.

Boudier, Françoise and Robert G. Coleman (1981). "Cross section through the peridotite in the Samail ophiolite, southeastern Oman Mountains." In: *Journal of Geophysical Research: ...* 86.B4, p. 2573. ISSN: 0148-0227. DOI: 10.1029/JB086iB04p02573.

Boudier, Françoise, Adolphe Nicolas, and Benoit Ildefonse (1996). "Magma chambers in the Oman ophiolite: fed from the top and the bottom." In: *Earth and Planetary Science Letters* 144.1-2, pp. 239–250. ISSN: 0012821X. DOI: 10.1016/0012-821X(96)00167-7.

Braun, Michael Geoffrey (2004). "Petrologic and Microstructural Constraints on Focused Melt Transport in Dunites and Rheology of the Shallow Mantle." PhD thesis. WHOI/MIT.

Braun, Michael Geoffrey and Peter B. Kelemen (2002). "Dunite distribution in the Oman Ophiolite: Implications for melt flux through porous dunite conduits." In: *Geochemistry, Geophysics, Geosystems* 3.11, pp. 1–21. ISSN: 15252027. DOI: 10.1029/2001GC000289.

Bruni, Jessica et al. (2002). "Irreversible water–rock mass transfer accompanying the generation of the neutral, Mg–HCO3 and high-pH, Ca–OH spring waters of the Genova province, Italy." In: *Applied Geochemistry* 17.4, pp. 455–474. ISSN: 08832927. DOI: 10.1016/S0883-2927(01)00113-5.

Chamberlain, J A et al. (1965). "NATIVE METALS IN THE MUSKOX INTRUSION." In: *Canadian Journal of Earth Sciences* 2.3, pp. 188–215. ISSN: 0008-4077. DOI: 10.1139/e65-017.

Chavagnac, Valerie et al. (2013). "Characterization of hyperalkaline fluids produced by low-temperature serpentinization of mantle peridotites in the Oman and Ligurian ophiolites." In: *Geochemistry, Geophysics, Geosystems* 14.7, pp. 2496–2522. ISSN: 15252027. DOI: 10.1002/ggge.20147.

Clark, Ian D. and Jean-Charles Fontes (1990). "Paleoclimatic reconstruction in northern Oman based on carbonates from hyperalkaline groundwaters." In: *Quaternary Research* 33.3, pp. 320–336. ISSN: 00335894. DOI: 10.1016/0033-5894(90)90059-T.

Coleman, Robert G. and Clifford A. Hopson (1981). "Introduction to the Oman Ophiolite Special Issue." In: *Journal of Geophysical Research: Solid Earth* 86.B4, pp. 2495–2496. ISSN: 01480227. DOI: 10.1029/JB086iB04p02495.

Coleman, Robert G. and T. E. Keith (1971). "A Chemical Study of Serpentinization — Burro Moutain, California." In: *Journal of Petrology* 12.2, pp. 311–328.

Collier, Martin Lee (2012). "Spatial-Statistical Properties of Geochemical Variability as Constraints on Magma Transport and Evolution Processes at Ocean Ridges." PhD thesis. Columbia University.

Eckstrand, O R (1975). "The Dumont serpentinite; a model for control of nickeliferous opaque mineral assemblages by alteration reactions in ultramafic rocks." In: *Economic Geology* 70.1, pp. 183–201. DOI: 10.2113/gsecongeo.70.1.183.

Escartín, J., G. Hirth, and B. Evans (1997). "Effects of serpentinization on the lithospheric strength and the style of normal faulting at slow-spreading ridges." In: *Earth and Planetary Science Letters* 151.3-4, pp. 181–189. ISSN: 0012-821X. DOI: 10.1016/S0012-821X(97)81847-X.

Etiope, Giuseppe, Martin Schoell, and Hakan Hosgörmez (2011). "Abiotic methane flux from the Chimaera seep and Tekirova ophiolites (Turkey): Understanding gas exhalation from low temperature serpentinization and implications for Mars." In: *Earth and Planetary Science Letters* 310.1-2, pp. 96–104. ISSN: 0012-821X. DOI: 10.1016/J.EPSL.2011.08.001.

Evans, Bernard W. (2004). "The Serpentinite Multisystem Revisited: Chrysotile Is Metastable." In: *International Geology Review* 46.6, pp. 479–506. ISSN: 0020-6814. DOI: 10.2747/0020-6814.46.6.479.

Evans, Bernard W. (2010). "Lizardite versus antigorite serpentinite: Magnetite, hydrogen, and life(?)" In: *Geology* 38.10, pp. 879–882. ISSN: 0091-7613. DOI: 10.1130/G31158.1.

Evans, Bernard W. et al. (1976). "Stability of chrysotile and antigorite in the serpentinite multisystem." In: *Schweizerische mineralogische und petrographische Mitteilungen* 56, pp. 79–93.

Falk, Elisabeth S. et al. (2016). "Controls on the stable isotope compositions of travertine from hyperalkaline springs in Oman: Insights from clumped isotope measurements." In: *Geochimica et Cosmochimica Acta* 192, pp. 1–28. ISSN: 00167037. DOI: 10.1016/j.gca.2016.06.026.

Faust, George and Joseph Fahey (1962). "The Serpentine-Group Minerals: Geological Survey Professional Paper 384-A." In: p. 99.

Frost, Ronald B. (1985). "On the stability of sulfides, oxides, and native metals in serpentinite." In: *Journal of Petrology* 26.June 1983, pp. 31–63. ISSN: 00223530. DOI: 10.1093/petrology/26.1.31.

Frost, Ronald B. and James S. Beard (2007). "On silica activity and serpentinization." In: *Journal of Petrology* 48.0, pp. 1351–1368. ISSN: 00223530. DOI: 10.1093/petrology/egm021.

Früh-Green, Gretchen L. et al. (2004). "Serpentinization of oceanic peridotites: Implications for geochemical cycles and biological activity." In: *AGU Monograph*. Vol. 144, pp. 119–136. DOI: 10.1029/144GM08.

Godard, Marguerite, David Jousselin, and Jean-Louis Bodinier (2000). "Relationships between geochemistry and structure beneath a palaeo-spreading centre: a study of the

mantle section in the Oman ophiolite." In: *Earth and Planetary Science Letters* 180.1-2, pp. 133–148. ISSN: 0012821X. DOI: 10.1016/S0012-821X(00)00149-7.

Hacker, Bradley R. (1994). "Rapid Emplacement of Young Oceanic Lithosphere: Argon Geochronology of the Oman Ophiolite." In: *Science* 265.5178, pp. 1563–1565. ISSN: 0036-8075. DOI: 10.1126/science.265.5178.1563.

Hacker, Bradley R. (2003). "Subduction factory 2. Are intermediate-depth earthquakes in subducting slabs linked to metamorphic dehydration reactions?" In: *Journal of Geophysical Research* 108.B1, p. 2030. ISSN: 0148-0227. DOI: 10.1029/2001JB001129.

Hacker, Bradley R., Jed L. Mosenfelder, and E Gnos (1996). "Rapid emplacement of the Oman ophiolite: Thermal and geochronologic constraints." In: *Tectonics* 15.6, pp. 1230–1247. ISSN: 02787407. DOI: 10.1029/96TC01973.

Hanghøj, Karen et al. (2010). "Composition and Genesis of Depleted Mantle Peridotites from the Wadi Tayin Massif, Oman Ophiolite; Major and Trace Element Geochemistry, and Os Isotope and PGE Systematics." In: *Journal of Petrology* 51.1-2, pp. 201–227. ISSN: 0022-3530. DOI: 10.1093/petrology/egp077.

Hattori, Kéiko H. and Stéphane Guillot (2003). "Volcanic fronts form as a consequence of serpentinite dehydration in the forearc mantle wedge." In: *Geology* 31.6, pp. 525–528. DOI: 10.1130/0091-7613(2003)031<0525:VFFAAC>2.0.CO;2.

Hemley, J J et al. (1977). "Mineral equilibria in the MgO-SiO 2 -H 2 O system; II, Talc-antigorite-forsterite-anthophyllite-enstatite stability relations and some geologic implications in the system." In: *American Journal of Science* 277.4, pp. 353–383. ISSN: 0002-9599. DOI: 10.2475/ajs.277.4.353.

Hitch, B. F. et al. (1980). *The solubility of (α-Al(OH)3) in 1 molal NaCl as a function of pH and temperature*. Tech. rep. Oak Ridge National Laboratory Report ORNL-5623.

Holm, Nils G. and Jean Luc Charlou (2001). "Initial indications of abiotic formation of hydrocarbons in the Rainbow ultramafic hydrothermal system, Mid-Atlantic Ridge." In: *Earth and Planetary Science Letters* 191.1-2, pp. 1–8. ISSN: 0012-821X. DOI: 10.1016/S0012-821X(01)00397-1.

Jagoutz, Oliver, Francis A Macdonald, and Leigh Royden (2016). "Low-latitude arc–continent collision as a driver for global cooling." In: *Proceedings of the National Academy of Sciences* 113.18, pp. 4935–4940. ISSN: 0027-8424. DOI: 10.1073/pnas.1523667113.

Kelemen, Peter B., Michael Geoffrey Braun, and Greg Hirth (2000). "Spatial distribution of melt conduits in the mantle beneath oceanic spreading ridges: Observations from the

Ingalls and Oman ophiolites." In: *Geochemistry, Geophysics, Geosystems* 1.7, n/a–n/a. ISSN: 15252027. DOI: 10.1029/1999GC000012.

Kelemen, Peter B. and Jürg M. Matter (2008). "In situ carbonation of peridotite for CO2 storage." In: *Proceedings of the National Academy of Sciences* 105.45, pp. 17295–17300. ISSN: 0027-8424. DOI: 10.1073/pnas.0805794105.

Kelemen, Peter B. et al. (2011). "Rates and Mechanisms of Mineral Carbonation in Peridotite: Natural Processes and Recipes for Enhanced, in situ CO 2 Capture and Storage." In: *Annual Review of Earth and Planetary Sciences* 39.1, pp. 545–576. ISSN: 0084-6597. DOI: 10.1146/annurev-earth-092010-152509.

Kelley, Deborah S. et al. (2005). "A Serpentinite-Hosted Ecosystem: The Lost City Hydrothermal Field." In: *Science* 307.5714, pp. 1428–1434. DOI: 10.1126/science.1102556.

Klein, Frieder and Wolfgang Bach (2009). "Fe-Ni-Co-O-S phase relations in peridotite-seawater interactions." In: *Journal of Petrology* 50.1, pp. 37–59. ISSN: 00223530. DOI: 10.1093/petrology/egn071.

Klein, Frieder, Wolfgang Bach, and Thomas M. McCollom (2013). "Compositional controls on hydrogen generation during serpentinization of ultramafic rocks." In: *Lithos* 178, pp. 55–69. ISSN: 00244937. DOI: 10.1016/j.lithos.2013.03.008.

Klein, Frieder et al. (2014). "Magnetite in seafloor serpentinite—Some like it hot." In: *Geology* 42, pp. 135–138. ISSN: 0091-7613. DOI: 10.1130/g35068.1.

Komor, Stephen C., Don Elthon, and John F. Casey (1985). "Serpentinization of cumulate ultramafic rocks from the North Arm Mountain massif of the Bay of Islands ophiolite." In: *Geochimica et Cosmochimica Acta* 49.11, pp. 2331–2338. ISSN: 00167037. DOI: 10.1016/0016-7037(85)90233-9.

Lackner, Klaus S. et al. (1995). "Carbon dioxide disposal in carbonate minerals." In: *Energy* 20.11, pp. 1153–1170. ISSN: 03605442. DOI: 10.1016/0360-5442(95)00071-N.

Launay, J and J C Fontes (1985). "Les sources thermales de Prony (Nouvelle-Caledonie) et leurs precipites chimiques; exemple de formation de brucite primaire." In: *Geologie de la France* 1985.1, pp. 83–100. ISSN: 0246-0874, 0246-0874.

Li, Weiqiang et al. (2015). "Experimental calibration of Mg isotope fractionation between dolomite and aqueous solution and its geological implications." In: *Geochimica et Cosmochimica Acta* 157, pp. 164–181. ISSN: 00167037. DOI: 10.1016/j.gca.2015.02.024.

Lorand, J.P. (1988). "Fe⊠Ni⊠Cu sulfides in tectonite peridotites from the Maqsad district, Sumail ophiolite, southern Oman: Implications for the origin of the sulfide component in the oceanic upper mantle." In: *Tectonophysics* 151.1-4, pp. 57–73. ISSN: 00401951. DOI: 10.1016/0040-1951(88)90240-5.

Matter, Jürg M. and Peter B. Kelemen (2009). "Permanent storage of carbon dioxide in geological reservoirs by mineral carbonation." In: *Nature Geosci* 2.12, pp. 837–841. ISSN: 1752-0894.

McCollom, Thomas M. and Jeffrey S Seewald (2013). "Serpentinites, hydrogen, and life." In: *Elements* 9.2, pp. 129–134. ISSN: 18115209. DOI: 10.2113/gselements.9.2.129.

Mervine, Evelyn M. et al. (2014). "Carbonation rates of peridotite in the Samail Ophiolite, Sultanate of Oman, constrained through 14C dating and stable isotopes." In: *Geochimica et Cosmochimica Acta* 126, pp. 371–397. ISSN: 00167037. DOI: 10.1016/j.gca.2013.11.007.

Mervine, Evelyn M. et al. (2015). "Applications and limitations of U-Th disequilibria systematics for determining ages of carbonate alteration minerals in peridotite." In: *Chemical Geology* 412, pp. 151–166. ISSN: 00092541. DOI: 10.1016/j.chemgeo.2015.07.023.

Miller, Hannah M. et al. (2016). "Modern water/rock reactions in Oman hyperalkaline peridotite aquifers and implications for microbial habitability." In: *Geochimica et Cosmochimica Acta* 179, pp. 217–241. ISSN: 00167037. DOI: 10.1016/j.gca.2016.01.033.

Monnier, Christophe et al. (2006). "Along-ridge petrological segmentation of the mantle in the Oman ophiolite." In: *Geochemistry, Geophysics, Geosystems* 7.11, n/a–n/a. ISSN: 15252027. DOI: 10.1029/2006GC001320.

Monnin, C et al. (2014). "Fluid chemistry of the low temperature hyperalkaline hydrothermal system of Prony bay (New Caledonia)." In: *Biogeosciences* 11.20, pp. 5687–5706. ISSN: 17264189. DOI: 10.5194/bg-11-5687-2014.

Monnin, Christophe et al. (2011). "Characterization of hyperalkaline fluids produced by serpentinization of mantle peridotites in Oman and in Liguria (Northern Italy)." In: *Mineralog. Mag* 75, p. 1490.

Moody, Judith B. (1976). "Serpentinization: a review." In: *Lithos* 9.2, pp. 125–138. ISSN: 00244937. DOI: 10.1016/0024-4937(76)90030-X.

Neal, C. and G. Stanger (1985). "Past and present serpentinization of ultramafic rocks: An example from the Semail ophiolite nappe of northern Oman." In: *The Chemistry*

of Weathering. Ed. by JI Drewer. Dordrecht, Holland: D. Reidel Publishing Company, 249–275.

Nickel, Ernest Henry (1959). "The occurrence of native nickel-iron in the serpentine rock of the Eastern Townships of Quebec Province." In: *The Canadian Mineralogist* 6.3, pp. 307–319.

Nicolas, Adolphe et al. (2000). "Accretion of Oman and United Arab Emirates ophiolite–Discussion of a new structural map." In: *Marine Geophysical Researches*, pp. 147–179. DOI: 10.1023/A:1026769727917.

O'Hanley, David S. (1996). *Serpentinites: Records of Tectonic and Petrological History*. New York and Oxford: Oxford University Press, p. 227. ISBN: 0-19-508254-0.

Obeso, Juan Carlos de and Peter B. Kelemen (2018). "Fluid rock interactions on residual mantle peridotites overlain by shallow oceanic limestones: Insights from Wadi Fins, Sultanate of Oman." In: *Chemical Geology*. ISSN: 0009-2541. DOI: 10.1016/J.CHEMGEO.2018.09.022.

Paukert, Amelia N. et al. (2012). "Reaction path modeling of enhanced in situ CO2 mineralization for carbon sequestration in the peridotite of the Samail Ophiolite, Sultanate of Oman." In: *Chemical Geology* 330-331, pp. 86–100. ISSN: 00092541. DOI: 10.1016/j.chemgeo.2012.08.013.

Pinilla, Carlos et al. (2015). "Equilibrium magnesium isotope fractionation between aqueous Mg2+ and carbonate minerals: Insights from path integral molecular dynamics." In: *Geochimica et Cosmochimica Acta* 163, pp. 126–139. ISSN: 00167037. DOI: 10.1016/j.gca.2015.04.008.

Proskurowski, G. et al. (2008). "Abiogenic Hydrocarbon Production at Lost City Hydrothermal Field." In: *Science* 319.5863, pp. 604–607. ISSN: 0036-8075. DOI: 10.1126/science.1151194.

Real, Pablo Garcia del et al. (2016). "Clumped-isotope thermometry of magnesium carbonates in ultramafic rocks." In: *Geochimica et Cosmochimica Acta* 193, pp. 222–250. ISSN: 00167037. DOI: 10.1016/j.gca.2016.08.003.

Rempfert, Kaitlin R et al. (2017). "Geological and Geochemical Controls on Subsurface Microbial Life in the Samail Ophiolite , Oman." In: 8.February. DOI: 10.3389/fmicb.2017.00056.

Reusch, D. N. (2011). "New Caledonian carbon sinks at the onset of Antarctic glaciation." In: *Geology* 39.9, pp. 807–810. ISSN: 0091-7613. DOI: 10.1130/G31981.1.

Rioux, Matthew et al. (2012). "Rapid crustal accretion and magma assimilation in the Oman-U.A.E. ophiolite: High precision U-Pb zircon geochronology of the gabbroic crust." In: *Journal of Geophysical Research* 117.B7, B07201. ISSN: 0148-0227. DOI: 10.1029/2012JB009273.

Rioux, Matthew et al. (2013). "Tectonic development of the Samail ophiolite: High-precision U-Pb zircon geochronology and Sm-Nd isotopic constraints on crustal growth and emplacement." In: *Journal of Geophysical Research: Solid Earth* 118.5, pp. 2085–2101. ISSN: 21699313. DOI: 10.1002/jgrb.50139.

Rouméjon, Stéphane et al. (2014). "Serpentinization and fluid pathways in tectonically exhumed peridotites from the southwest Indian ridge (62-65°E)." In: *Journal of Petrology* 56.4. ISSN: 14602415. DOI: 10.1093/petrology/egv014.

Russell, Michael J. (2007). "The alkaline solution to the emergence of life: Energy, entropy and early evolution." In: *Acta Biotheoretica* 55.2, pp. 133–179. ISSN: 00015342. DOI: 10.1007/s10441-007-9018-5.

Russell, Michael J. et al. (2014). "The Drive to Life on Wet and Icy Worlds." In: *Astrobiology* 14.4, pp. 308–343. ISSN: 1531-1074. DOI: 10.1089/ast.2013.1110.

Ryu, Jong-Sik et al. (2016). "Experimental investigation of Mg isotope fractionation during mineral dissolution and clay formation." In: *Chemical Geology* 445, pp. 135–145. ISSN: 00092541. DOI: 10.1016/j.chemgeo.2016.02.006.

Sánchez-Murillo, Ricardo et al. (2014). "Geochemical evidence for active tropical serpentinization in the Santa Elena Ophiolite, Costa Rica: An analog of a humid early Earth?" In: *Geochemistry, Geophysics, Geosystems* 15, pp. 1783–1800. ISSN: 15252027. DOI: 10.1002/2013GC005213.

Schott, Jacques et al. (2016). "The control of carbonate mineral Mg isotope composition by aqueous speciation: Theoretical and experimental modeling." In: *Chemical Geology* 445, pp. 120–134. ISSN: 00092541. DOI: 10.1016/j.chemgeo.2016.03.011.

Schwarzenbach, Esther M., Esteban Gazel, and Mark J. Caddick (2014). "Hydrothermal processes in partially serpentinized peridotites from Costa Rica: evidence from native copper and complex sulfide assemblages." In: *Contributions to Mineralogy and Petrology* 168. ISSN: 0010-7999. DOI: 10.1007/s00410-014-1079-2.

Schwarzenbach, Esther M. et al. (2012). "Sulfur geochemistry of peridotite-hosted hydrothermal systems: Comparing the Ligurian ophiolites with oceanic serpentinites." In: *Geochimica et Cosmochimica Acta* 91, pp. 283–305. ISSN: 00167037. DOI: 10.1016/j.gca.2012.05.021.

Seifritz, W (1990). "CO2 disposal by means of silicates." In: *Nature* 345, p. 486.

Seyfried, William E., D.I. Foustoukos, and Qi Fu (2007). "Redox evolution and mass transfer during serpentinization: An experimental and theoretical study at 200°C, 500bar with implications for ultramafic-hosted hydrothermal systems at Mid-Ocean Ridges." In: *Geochimica et Cosmochimica Acta* 71.15, pp. 3872–3886. ISSN: 00167037. DOI: 10.1016/j.gca.2007.05.015.

Sleep, Norman H. et al. (2004). "H2-rich fluids from serpentinization: geochemical and biotic implications." In: *Proceedings of the National Academy of Sciences of the United States of America* 101, pp. 12818–12823. ISSN: 0027-8424. DOI: 10.1073/pnas.0405289101.

Snow, Jonathan E. and Henry J.B. Dick (1995). "Pervasive magnesium loss by marine weathering of peridotite." In: *Geochimica et Cosmochimica Acta* 59.20, pp. 4219–4235. ISSN: 00167037. DOI: 10.1016/0016-7037(95)00239-V.

Streit, Elisabeth, Peter B. Kelemen, and John Eiler (2012). "Coexisting serpentine and quartz from carbonate-bearing serpentinized peridotite in the Samail Ophiolite, Oman." In: *Contributions to Mineralogy and Petrology* 164.5, pp. 821–837. ISSN: 00107999. DOI: 10.1007/s00410-012-0775-z.

Thayer, T P (1966). "Serpentinization considered as a constant-volume metasomatic process." In: *American Mineralogist* 51.5-6, p. 685. ISSN: 0003-004X.

Thompson, Geoffrey and William G. Melson (1970). "Boron contents of serpentinites and metabasalts in the oceanic crust: Implications for the boron cycle in the oceans." In: *Earth and Planetary Science Letters* 8.1, pp. 61–65. ISSN: 0012821X. DOI: 10.1016/0012-821X(70)90100-7.

Tilton, G. R., C. a. Hopson, and J. E. Wright (1981). "Uranium-lead isotopic ages of the Samail Ophiolite, Oman, with applications to Tethyan ocean ridge tectonics." In: *Journal of Geophysical Research* 86.B4, p. 2763. ISSN: 0148-0227. DOI: 10.1029/JB086iB04p02763.

Ulmer, Peter and Volkmar Trommsdorff (1995). "Serpentine Stability to Mantle Depths and Subduction-Related Magmatism." In: *Science* 268.5212, pp. 858–861. DOI: 10.1126/science.268.5212.858.

Vance, Steve et al. (2007). "Hydrothermal Systems in Small Ocean Planets." In: *Astrobiology* 7.6, pp. 987–1005. ISSN: 1531-1074. DOI: 10.1089/ast.2007.0075.

Wang, Wenzhong et al. (2019). "Equilibrium Mg isotope fractionation among aqueous Mg2+, carbonates, brucite and lizardite: Insights from first-principles molecular dynamics simulations." In: *Geochimica et Cosmochimica Acta* 250, pp. 117–129. ISSN: 0016-7037. DOI: 10.1016/J.GCA.2019.01.042.

Warren, Clare J et al. (2005). "Dating the geologic history of Oman's Semail ophiolite: insights from U-Pb geochronology." In: *Contributions to Mineralogy and Petrology* 150.4, pp. 403–422. ISSN: 1432-0967. DOI: 10.1007/s00410-005-0028-5.

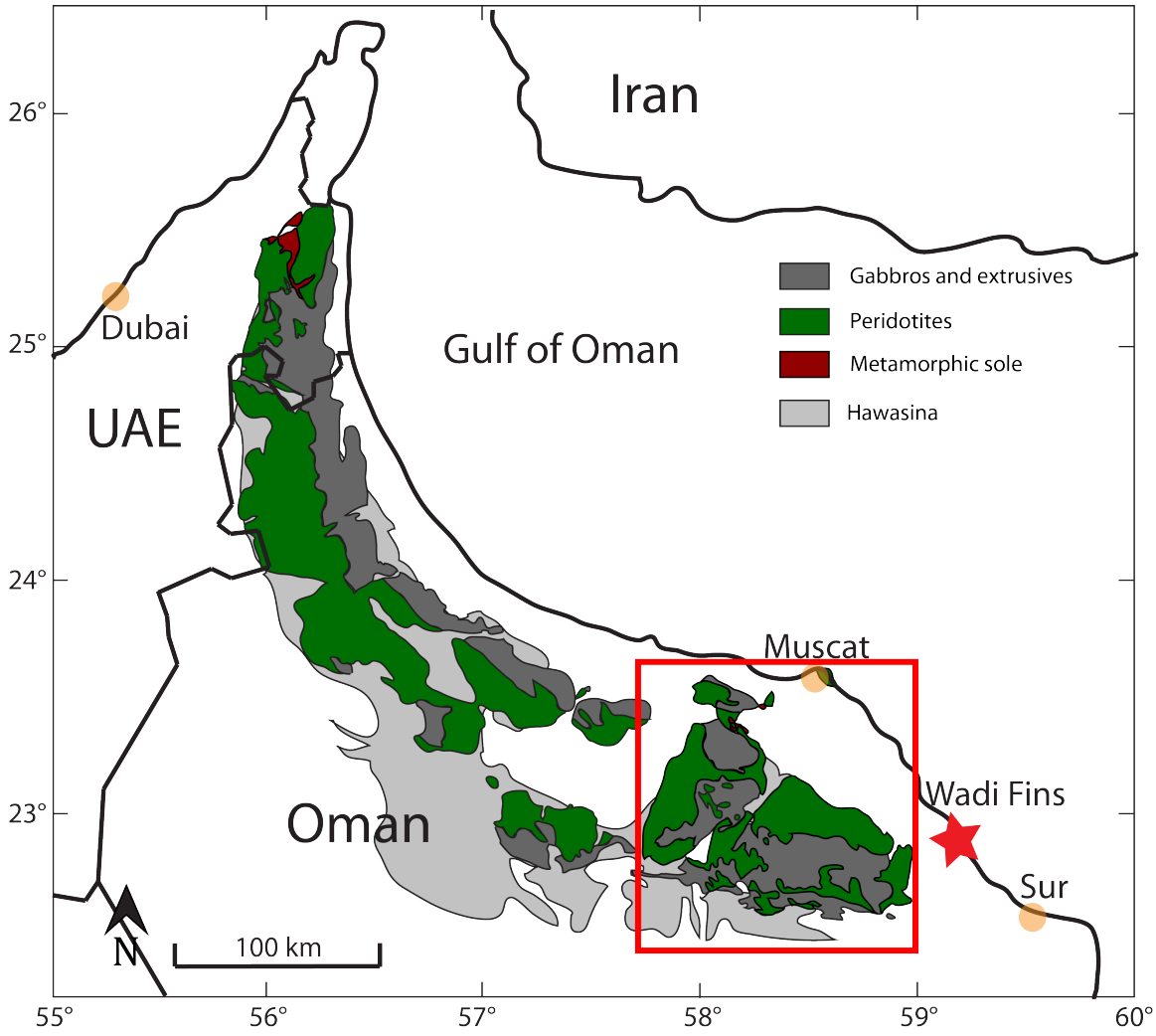

Figure 1.1: Simplified geologic map of the Samail ophiolite after Nicolas, Boudier, and France 2009. All samples used in this work come from the southern massifs (red square and Wadi Fins (red star).

2 Fluid rock interactions on residual mantle peridotites overlain by shallow oceanic limestones: Insights from Wadi Fins, Sultanate of Oman

This chapter has been published in Chemical Geology. The final publication is available at: https://www.sciencedirect.com/science/article/pii/S0009254118304625

Abstract

In the southeastern Oman Mountains the mantle section of the Samail ophiolite is unconformably capped by large units of Maastrichtian to Eocene limestones deposited in a shallow marine environment after ophiolite emplacement. In the vicinity of the town of Fins, a deep canyon carved by a stream has exposed mantle sections of the ophiolite. This section is composed of altered peridotites with high concentrations of calcium and small enrichments of silica compared to the Samail mantle protolith suggesting that the peridotites reacted with a hydrous fluid derived from interaction of seawater with the overlying sediments composed of limestones with minor amounts of chert. This is further affirmed by average δ^{13}C (-0.25 ‰VPDB), δ^{18}O (-5.53 ‰VPDB) and ^{87}Sr/^{86}Sr (0.70788) in the carbonate veins, consistent with values in the sediments. Clumped isotope thermometry on calcite veins in peridotite establish that they formed at 25-60 ℃. Reaction path modeling of carbonate-quartz derived fluids with peridotite reproduces the observed mineral assemblage composed of carbonate and serpentine with similar Mg# and MgO/SiO_2 at high water to rock ratios, with carbon, H_2O and silica added to the rock by the reacting fluid.

2.1 Introduction

Mantle peridotite, composed mainly of olivine ($(Mg,Fe)_2SiO_4$) and pyroxenes ($(Ca,Mg,Fe)_2Si_2O_6$), is unstable at Earth's surface conditions and reacts with hydrous fluids to form hydrated silicates (serpentinization), carbonates (carbonation) and oxides. These processes have significant geophysical and geochemical implications. The alteration of peridotite to serpentinite results in drastic changes in the rheology of the rocks (e.g. Escartín, Hirth, and Evans 1997; Guillot et al. 2015). Serpentinization of seafloor peridotites is a significant sink for several elements including sulfur, carbon, boron and chlorine (Alt and Shanks 1998; Alt et al. 2013; Barnes and Sharp 2006; Bonatti, Lawrence, and Morandi 1984; Boschi et al. 2013; Thompson and Melson 1970). On land, low temperature serpentinization and carbonation are ubiquitous in peridotite massifs (Barnes, O'Neil, and Trescases 1978; Clark and Fontes 1990; Kelemen and Matter 2008; Kelemen et al. 2011; Neal and Stanger 1985; Paukert et al. 2012; Sánchez-Murillo et al. 2014).

Reaction pathways for serpentinization change depending on temperature, pressure, fluid composition, fluid/rock (W/R) ratios, and primary mineralogy of the protolith. Secondary mineralogy for serpentinization reactions at low temperatures (<200℃) is characterized by the presence of lizardite and chrysotile ($Mg_3Si_2O_5(OH)_4$) as the main serpentine minerals (Evans 2004; Evans et al. 1976) while iron preferentially forms Fe-rich brucite ($(Mg,Fe)(OH)_2$) (Klein, Bach, and McCollom 2013; Klein et al. 2009; Seyfried, Foustoukos, and Fu 2007). At higher temperatures antigorite ($(Mg,Fe)_{2.93}Si_{2.07}O_{5.18}(OH)_{3.78}$) is the main serpentine mineral (Evans 2004; Evans et al. 1976) and magnetite ($Fe_3\ O_4$) becomes the main sink for iron (Klein et al. 2014). Early stages of serpentinization are

characterized by low water fluxes and strongly reducing conditions (e.g. Bach and Klein 2009; Frost 1985; Früh-Green et al. 2004; Schwarzenbach, Gazel, and Caddick 2014). As serpentinization advances, fluid fluxes increase, resulting in more oxidizing conditions. This leads to sharp changes in oxygen fugacity and secondary mineralogy (Schwarzenbach et al. 2012).

The objective of this paper is to provide constraints on the temperature, fluid composition and fluid source during alteration of mantle peridotite in Wadi Fins, Oman. The results have relevance for understanding carbonation and serpentinization of near-surface mantle peridotite during reaction with sediment-derived fluids.

2.2 Geologic setting

The Samail ophiolite along the northeast coast of Oman is among the largest and best sub-aerially exposed sections of oceanic crust and its underlying mantle in the world (Coleman 1977; Coleman and Hopson 1981; Lippard, Shelton, and Gass 1986; Pallister and Knight 1981). It was thrust over adjacent oceanic lithosphere soon after magmatic formation of oceanic crust at a submarine spreading ridge and then onto the margin of the Arabian subcontinent in the late Cretaceous (Boudier, Nicolas, and Ildefonse 1996; Hacker 1994; Hacker, Mosenfelder, and Gnos 1996; Nicolas et al. 2000; Rioux et al. 2012, 2013; Tilton, Hopson, and Wright 1981; Warren et al. 2005).

The mantle section of the ophiolite is mainly composed of highly depleted, residual mantle peridotites (mostly harzburgites, e.g. Godard, Jousselin, and Bodinier 2000; Hanghøj et al. 2010; Monnier et al. 2006), together with 5 to 15% dunite (Boudier and Coleman 1981; Braun and Kelemen 2002; Coleman 1981; Collier 2012; Kelemen, Braun,

and Hirth 2000). These peridotites, thrust toward the surface and then exposed by faulting and erosion, are far from equilibrium with water and carbon dioxide. This disequilibrium causes ubiquitous alteration. The alteration ranges from $\sim$ 20% serpentinization in "fresh" rock to nearly 100% replacement of the anhydrous silicates and oxides (olivine, pyroxenes, spinel) with hydrous minerals (mostly serpentine, but also brucite or talc), carbonates (magnesite, dolomite, calcite, hydrous Mg carbonates), and Fe-oxides and oxyhydroxides (magnetite, hematite, goethite). Alteration probably occurred throughout the history of the ophiolite, beginning near the axis of the oceanic spreading ridges where the Samail ophiolite crust formed (e.g., Gregory and Taylor 1981), followed by "high temperature" alteration in the late Cretaceous near the basal thrust where metasediments were subducted beneath peridotite $\sim$ 100℃, (Falk and Kelemen 2015; Nasir et al. 2007; Stanger 1985), and continuing to the present day (Chavagnac et al. 2013; Clark and Fontes 1990; Kelemen and Matter 2008; Kelemen et al. 2011; Mervine et al. 2014, 2015; Monnin et al. 2011; Neal and Stanger 1985; Streit, Kelemen, and Eiler 2012). Mantle peridotites of the Samail ophiolite in Oman were exposed by sub-aerial erosion in the late Cretaceous. They are locally capped by Late Cretaceous (Maastrichtian) laterites (Al-Khirbash 2015; Nolan et al. 1990), and elsewhere by fluvial conglomerates rich in peridotite cobbles. This was followed by a marine transgression, which deposited shallow marine carbonates over a broad region, including the Qahlah, Simsina and Jafnayn formations (Nolan et al. 1990; Wyns et al. 1992).

Outcrops of altered peridotite occur in Wadi Fins at the bottom of the water-carved canyon (Figure 1). These peridotites are unconformably overlain by up to 1-1.5 km. of sediment, mostly shallow water limestones, deposited from the Late Cretaceous (Maas-

trichtian) to the Eocene (e.g. Mann, Hanna, and Nolan 1990; Racey 1995; Searle and Graham 1982; Wyns et al. 1992). Regionally, the peridotite in Wadi Fins is pervasively serpentinized and crosscut by an extensive network of carbonate and serpentine-carbonate veins.

Clastic dikes (or "Neptunian veins") of fine-grained grey limestone intrude the peridotite, tapering downward and extending ∼10 m down from the unconformity (Figure 2). The clastic dikes are best exposed on the south wall of the Wadi where they are spaced roughly 2 to 4 meters apart. They contain angular clasts of altered peridotite, especially near their tips. Although these dikes are almost certainly coeval with formation of the carbonate veins in the underlying peridotite, they are cut by a network of somewhat younger carbonate veins.

2.3 Sample processing and analytical methods

Analyzed samples were collected during the 2013 and 2016 field seasons in Wadi Fins, Oman (Figure 1). Twenty-three peridotite and six limestone sub-samples were chipped using a jaw crusher and powdered using an alumina puck mill. These were used for elemental and mineralogical analysis. Billets of 16 peridotite samples were sent to Spectrum Petrographics (http://www.petrography.com/) for preparation of polished thin sections.

Powdered samples were analyzed by X-Ray diffraction (XRD), X-Ray fluorescence (XRF) and Inductively Coupled Plasma Optical Emission spectroscopy (ICP-OES) to obtain whole rock and mineralogical compositions. XRD analysis were performed using a Rigaku DMAX-Rapid Microdiffraction system at the American Museum of Natural History (AMNH), difractograms were analyzed using JADE software to identify main min-

erals. Major element X-Ray Flourescence and loss on ignition (LOI) analyses of the bulk rocks for 16 peridotite samples was performed by XRF at the Washington State University GeoAnalytical lab (https://environment.wsu.edu/facilities/geoanalytical-lab/). The rest of the peridotite samples and the limestone samples were analyzed using an Agilent 720 Axial ICP-OES that was calibrated to natural standards (Table S1) at Lamont Doherty Earth Observatory (LDEO) using lithium metaborate fusion and nitric acid solution. Sample composition and analytical precision are given in table S1.

Polished thin sections of 16 samples were analyzed with a standard petrographic microscope for phase identification where possible. Nine of the sixteen were also quantitatively analyzed using a 5-spectrometer Cameca SX-100 microprobe at AMNH using a 10 μm beam diameter with 15 kV accelerating voltage, 10nA current and 20-30s peak time to determine major element composition of phases using natural standards. Calibration information is shown in Table S2.

Carbonates from carbonate-serpentine veins in seven peridotite samples were separated from the matrix and stained with Alizarin Red S following a modified version of Friedman's protocol (1959) to differentiate between calcite and dolomite. Calcite mineral separates were crushed using a mortar and pestle to form a fine powder for clumped isotope thermometry analysis. Powders were analyzed using a Thermo Finnegan MAT 253 configured to collect masses 44 to 49 isotopologues (cf. Eiler 2007) at Woods Hole Oceanographic Institution. Analyses, standards and data processing for both sample and standards were carried out following the protocols described by Huntington et al. (2009) and Passey et al. (2010). Three different $\Delta 47$ (a measure of isotopologue ^{13}C-^{16}O-^{18}O enrichment compared to a stochastic distribution) temperatures are reported following

calibrations by Bristow et al. (2011), Dennis & Schrag (2010), and Ghosh et al. (2006) for comparison (Table I). All discussion is based on the Bristow et al. $\Delta 47$ calibration. Over the analytical run standards 102-GC-AZ01 and NBS19 averaged $\Delta 47$ 0.728$\pm$0.047‰ and 0.436$\pm$0.014‰ respectively. These values are either within or close to the range of the average values reported by Dennis et al, 2011 inter-laboratory study, 0.713$\pm$ 0.12‰ (1 S.D.) for 102-GC-AZ01 and 0.392$\pm$0.017‰ (1 S.D.) for NBS19. Three of these carbonate separates were dissolved in HNO_3 and analyzed for strontium isotopes ($^{87}Sr/^{86}Sr$) using a ThermoScientific Neptune Plus multi-collector Inductively Coupled Plasma Mass Spectrometer (MC-ICP-MS) in static mode at LDEO, over run repeat analyses of the NBS-987 Sr-standard averaged a ($^{87}Sr/^{86}Sr$) ratio of 0.710252$\pm$0.000024, within the NIST SRM value of 0.710248.

2.4 Results

Mineralogy and textures in Wadi Fins peridotites

All mantle peridotite samples exhibit high degrees of serpentinization. Relict olivine is rare in thin section but appears in a few samples and even in some diffractograms (OM13-19 and OM13-2). It represents almost 20% of the OM13-19 thin section, making this the least altered sample analyzed for this study. All samples in the matrix have mesh textures typical of serpentine replacing olivine (O'Hanley 1996; Wicks, Whittaker, and Zussman 1977). XRD data show that the main serpentine mineral is lizardite with minor occurrences of chrysotile. Relict pyroxenes are present in most thin sections and show various degrees of alteration to serpentine. Olivines and orthopyroxenes have compositions (Tables S5 and S6) similar to those previously reported in the ophiolite (Hanghøj et al. 2010;

Monnier et al. 2006). For samples in which the carbonate content is high enough for XRD identification calcite is the main carbonate phase occurring mostly in veins. Sample OM13-4 is an exception. Here, dolomite occurs in the matrix and is the most abundant carbonate in the sample. Magnesite or brucite were not identified by XRD or microprobe analysis in any sample.

The outcrops in Wadi Fins contain micron to centimeter scale carbonate veins as well as composite fine-grained serpentine-carbonate veins and rare pure serpentine veins. The alteration phases in the peridotites include matrix serpentine and carbonate-serpentine veins. These phases are evident in the outcrops and hand samples as shown in Figure 3. While calcite is the most abundant carbonate in the veins dolomite occurs along vein edges in close proximity with serpentine. Serpentine (XRD lizardite) in the mixed serpentine-carbonate veins is in some cases isotropic in cross-polarized light due to its fine-grained nature in the veins. These serpentines usually have low iron contents (X_{Fe} (molar Fe/[Molar Fe+Mg]=3.8 mol% on average) compared to matrix serpentines with X_{Fe}=8.6 mol% on average. Iron oxides occur in the magnesium rich serpentine veins and reach over 50 μm in diameter. Serpentines in the matrix have iron contents similar to or greater than relict olivine and orthopyroxene in samples OM13-2 and OM13-9 (Figure 4 and table S5 and S6). Iron oxides rarely occur far from veins in the primary serpentine matrix.

Bulk-rock composition

Almost all Wadi Fins samples show significant enrichment in CaO from the carbonate veins. Larger positive CaO anomalies correlate with larger negative anomalies of most

major oxides (MgO, SiO_2, FeO, Al_2O_3, Cr_2O_3). Sample bulk rock compositions are compared to average Oman harzburgite (Godard, Jousselin, and Bodinier 2000; Hanghøj et al. 2010; Monnier et al. 2006) in Figure 5. MnO anomalies correlate with CaO anomalies, because MnO is mainly hosted in carbonate veins (average MnO content in carbonate minerals is 0.6 wt%). Calcium contents in bulk rock compositions lie in the expected path of alteration for Oman harzburgite that has modified by addition of calcite (Figure 6). When projected from calcite the majority of samples are more silica-rich than Oman peridotites (Figure 7). Bulk rock compositions are reported in supplementary table S3.

Carbon, oxygen and Sr isotopes ratios of carbonates veins

$\Delta 47$, δ^{13}C, $\delta^{18}O$ and clumped isotope temperatures for 7 samples, and $^{87}Sr/^{86}Sr$ for three of them, are reported in table 2.1. Measured $\Delta 47$ values of the calcite veins correspond to precipitation temperatures between 25-60 ℃, consistent with vein formation near the surface. δ^{13}C and $\delta^{18}O$ in the calcite veins measured are within the range of observed values of Maastrichtian-Eocene sediments in the area (Figure 8) (Schlüter et al. 2008). $^{87}Sr/^{86}Sr$ ratios of the three measured samples are between 0.70778-0.70790, similar to the Cretaceous limestones (Schlüter et al. 2008) and seawater at the Cretaceous-Paleogene (McArthur, Howarth, and Shields 2012). This similarity suggests that alteration occurred around this time as changes in seawater $^{87}Sr/^{86}Sr$ after the Cretaceous-Paleogene (McArthur, Howarth, and Shields 2012) is not reflected in the carbonate veins hosted in the peridotite.

Bulk rock composition of overlying limestones

The limestones overlying the peridotites are fine-grained. In the unconformity, clastic dikes or "Neptunian veins" of grey limestone intrude the peridotites and contain angular clasts of altered peridotite. Oddly, the clastic dikes appear to root in the unconformity and do not cut the overlying limestone in any outcrop. Above the unconformity, the first few hundred meters of section are mainly composed of limestones. Calcium-rich dolomites occur midsection (∼50 meters above the unconformity), changing back to limestone at the top of the section. All samples have trace amounts of SiO_2, up to 0.35 wt% with an average of 0.13 wt% for samples within 15 meters of the unconformity. Major element compositions of the limestones are reported in supplementary Table S4.

2.5 Reaction path model

Model Setup

The details of the alteration sequence described above were used to constrain a reaction path model of carbonate-saturated seawater reacting with Oman peridotite using EQ3/6 V 8.0 (Wolery and Jarek 2003). For all calculations we used the Klein et al. (2009) EQ3/6 thermodynamic database. This database contains equilibrium constants from 0 to 400 ℃ at 50 MPa, a pressure that we consider within the range expected for the alteration. The model has by three stages. In the first stage, 1 kg of simulated Cretaceous seawater (Table II) is speciated at 25℃ using EQ3. In the second stage, seawater is heated to 60℃ while reacting with one mole of idealized limestone in a closed system. Two idealized limestone compositions were used, one with 100% calcite and a second with 99% calcite and 1% quartz to account to for presence of chert in the Qahlah and Simsina forma-

tions (Nolan et al. 1990). In the third stage, the resulting fluid then reacts with rock with the initial composition of average Oman harzburgite (Hanghøj et al. 2010; Monnier et al. 2006) and dunite (Hanghøj et al. 2010) using EQ6 with special reactant mode in a titration system at 60℃. The special reactant mode in EQ6 restricts the model to an equilibrium system.

Secondary minerals known to form during serpentinization were allowed to precipitate, forming solid solutions in the third stage of the model (Supplementary Table S6). Precipitated minerals in this stage represent the resulting mineralogy produced by the reaction of the input fluid with Oman peridotite. Even though lizardite is the main serpentine mineral in our samples, its thermodynamic properties are not well constrained, so it is not included in the database. Instead, we used chrysotile as the main Mg-serpentine mineral, as its thermodynamic properties are similar to lizardite (Evans 2004). Results of the third stage are reported using mass ratios of water/rock (W/R=kg H_2O/kg of rock reacted) following literature convention (e.g. Klein and Garrido 2011; Klein et al. 2009; Palandri and Reed 2004).

Model Results

We present the results of four model runs with varying the composition of the peridotite and limestone reactants. These 4 runs are: harzburgite with calcite derived fluid, harzburgite with calcite-quartz derived fluid, dunite with calcite derived fluid and dunite with calcite-quartz derived fluid. Figures 9 to 12 summarize the results of these reaction path models.

In all models, mineral appearance and disappearance proceeds in the same order in all

models (Figure 9). Carbonate coexists with serpentine and hematite for W/R> 100 and is the dominant phase at W/R>5000. The amount of carbonate minerals is constant along the reaction path for W/R>100. Below W/R of 30 carbonates are unstable and do not appear in the equilibrium assemblage. Below W/R of 5000 serpentine becomes the dominant phase with minor chlorite, brucite and iron oxides (hematite for W/R above 20 and magnetite below). The amount and presence of brucite depends on the peridotite reactant. Both dunite models have brucite occurring at higher W/R ratios than in harzburgites, consistent with higher Mg/Si ratios in dunite compared to harzburgite.

The fluid composition entering the peridotite differs only in the $SiO_{2(aq)}$ concentration, which is $\sim$5 times higher in the calcite-quartz saturated fluids compared to the calcite saturated fluids. The evolution of the fluid composition evolution is almost identical for the harzburgite and dunite models (Figure 10). All models show an increase in dissolved Al resulting from a drastic increase in pH (Hitch et al. 1980; May, Helmke, and Jackson 1979; Wesolowski 1992). The pH rises to 12 in harzburgite models (Figure 11) at W/R < 100 and up to 11.5 for dunite models at W/R < 20. The increase in dissolved Al at high pH in the models is coeval with both an increase in dissolved Si in the fluid, and steep decreases in Mg and Fe. Fe in all models is only soluble at W/R between 20 to 200. All models show abrupt drops in fO_2 at W/R < 3000 (Figure 11) consistent with oxidation of Fe^{2+} in the solid reaction products, and the production of molecular hydrogen from serpentinization of peridotite (Frost 1985). Solid mass and volume both increase along the entire reaction path. Mass changes in the models (Figure 12) are significant with increases over 50% when the system precipitates carbonates at high W/R. Decreasing W/R stabilizes the mass increases to $\sim$16%, mainly from water in the serpentine minerals. Solid volume

changes follow a similar path, with significant increases at W/R >1000. Decreasing W/R stabilizes the volume increases to ∼40%.

2.6 Discussion

The presence of peridotite laterite ∼12 km from the Wadi Fins location provides evidence that the ophiolite was sub-aerially weathered in a tropical climate (Al-Khirbash 2015; Al-Khirbash et al. 2013; Alsharhan and Nasir 1996) after emplacement of the ophiolite onto the Arabian continental margin and erosion of the crustal section in the area. This alteration stage seemingly limited to breccias and fluvial conglomerates along the unconformity in Wadi Fins, was followed by a marine transgression, and deposition of Maastrichtian and younger sediments – spanning the Cretaceous-Paleogene (K-Pg) boundary – above an unconformity overlying peridotite. δ^{13}C and δ^{18}O in the Qahlah, and Simsina and Jafnayn limestone formations (Schlüter et al. 2008) are similar to values in our carbonate samples (Figure 8 and Table I). ^{87}Sr/^{86}Sr ratios are within error of the values reported for the overlying cretaceous limestones (Schlüter et al. 2008) and values for K-Pg boundary age seawater (McArthur, Howarth, and Shields 2012), providing evidence that pore waters in K-Pg age limestone were the source of the fluid that serpentinized and formed veins in the peridotite. Temperatures during alteration, estimated by clumped isotope thermometry, were around 20-60℃. We infer that the alteration occurred at moderate pressures (300-600 bars) based on limestone unit thickness estimates (Nolan et al. 1990; Racey 1995; Wyns et al. 1992). We also infer that interaction between peridotites and fluids equilibrated with the overlying sediments formed abundant calcite-rich veins and thus resulting in significant CaO enrichments observed in Wadi Fins.

Isochemical serpentinization of olivine-rich rocks requires the formation of a magnesium-rich phase, usually brucite (Evans 1977; Evans et al. 1976) or magnesite when CO_2-rich fluids are present (Kelemen et al. 2011). We interpret the absence of these minerals in our samples, along with higher SiO_2 contents than average Oman peridotites, as an indication of non-isochemical serpentinization in Wadi Fins.

Wadi Fins peridotites have low Al_2O_3/SiO_2 (<0.035), similar to other depleted peridotites in Oman (e.g. Godard, Jousselin, and Bodinier 2000; Hanghøj et al. 2010; Monnier et al. 2006) with lower MgO/SiO_2 ratios (Figure 13). They follow a trend parallel to the terrestrial geochemical fractionation array (Asimow 1999; Baker and Beckett 1999; Jagoutz et al. 1979; Snow and Dick 1995) at lower MgO/SiO_2 ratios.

MgO/SiO_2 below the geochemical fractionation array are commonly interpreted as a result of alteration processes involving magnesium leaching (Monnier et al. 2006; Snow and Dick 1995). The much lower MgO/SiO_2 in our Wadi Fins samples suggest higher degrees of alteration than in the regionally extensive suite of less altered peridotites studied by Godard, Jousselin, and Bodinier 2000; Hanghøj et al. 2010 and Monnier et al. 2006. Extensive leaching of magnesium leaching would result in an appreciable drop in the Mg# (molar Mg/(Mg+Fe)) decreasing MgO/SiO_2. This is not observed in our samples. On the contrary, several samples have bulk rock Mg# significantly higher (up to 93.3) than most Oman peridotites (Avg Mg# 91, Max Mg# 92 e.g. Godard, Jousselin, and Bodinier 2000; Hanghøj et al. 2010; Monnier et al. 2006), and higher than relict primary olivines and pyroxenes in our samples, with Mg# $\sim$91. Higher Mg# can either be explained by removal of iron or addition of magnesium. While we infer minor iron mobility, primarily based on observation of iron oxides along veins, we find unlikely that major amounts of iron

were preferentially leached to produce higher Mg#. Instead, to explain the low MgO/SiO_2 and variable Mg# in our samples, we prefer to invoke silica addition along with minor amounts of Mg gain or loss. Serpentinization of olivine-rich rocks with addition of silica in the fluid will proceed following the simplified reaction:

$$3Mg_2SiO_4 + 2SiO_{2(aq)} + 4H_2O = 2Mg_3Si_2O_5(OH)_4$$

This reaction forms serpentine without a magnesium rich phase such as brucite or magnesite. Limestones right above the unconformity in Wadi Fins contain small amounts of silica, and chert is present in small quantities in the Qahlah and Simsina formations (Nolan et al. 1990; Schlüter et al. 2008) providing a source of silica to the fluid. Reaction path modeling of calcite-quartz derived fluids with harzburgite and dunite result in MgO/SiO_2 ratios (Figure 13) that encompass the whole range observed in Wadi Fins at W/R between ∼3000 and 1000. In contrast, reaction modeling with fluids that were not initially quartz-saturated does not reproduce the observed compositions of our Wadi Fins samples; the lowest MgO/SiO_2 are 1.02 and 0.90 for dunite and harzburgite respectively at W/R ∼12,000. W/R as high as those required (∼3000 to 1000) to reproduce our sample compositions are predicted to result in significant volume and mass increases. Such solid volume increases represent large strains, which would have caused unrealistically high stresses in an elastic rock matrix. Instead, the resulting elastic stresses must have been relaxed by deformation along fractures due to tectonic stresses and/or reaction-driven cracking (Jamtveit, Malthe-Sørenssen, and Kostenko 2008; Kelemen and Hirth 2012; Kelemen and Matter 2008; Macdonald and Fyfe 1985; Rudge, Kelemen, and Spiegelman 2010).

The opening of existing cracks, and/or formation of new fractures, in turn, may have allowed these large volumes of fluid to react with the rocks.

2.7 Conclusions

Alteration of the peridotites in Wadi Fins happened in several stages. The first stage probably began near the axis of the oceanic spreading ridge where the Samail ophiolite crust formed (Coleman 1981; Hopson et al. 1981; Lippard, Shelton, and Gass 1986) before emplacement. After emplacement some alteration of the uppermost section under tropical weathering conditions is indicated by the presence of the peridotite laterite in outcrops ∼12 km to the south of the peridotite outcrops of this study (Al-Khirbash 2015; Al-Khirbash et al. 2013; Alsharhan and Nasir 1996; Wyns et al. 1992). In our field area, breccias and fluvial conglomerates along the unconformity represent this stage of alteration. Sub-aerial weathering was followed by addition of calcium carbonate – mostly in calcite veins – and silica – mostly in serpentine – sourced from the Qahlah and Simsina limestone formations. This alteration took place at 25-60℃, moderate pressures (<500 bar) and high W/R. Reaction path modeling reproduces the mineral assemblage observed in the Wadi Fins samples. At high W/R ratios, carbon and silica are transferred from the fluids into the precipitated minerals. These results reproduce the observed trends in the natural samples, particularly the changes MgO/SiO_2 and Mg#, and mimics the proposed later alteration stage when large volumes of carbonate saturated-seawater circulated through the peridotites, resulting in precipitation of carbonates and serpentine. Results are consistent with previous modeling of peridotite alteration with seawater (e.g. Klein et al. 2009). This alteration setting provides a window into the modification of peridotites by fluids

similar to seawater at low temperatures far from oceanic spreading ridges and provides insights on the behavior of proposed engineered mineral carbonation using seawater as carbon bearing fluid (Kelemen and Matter 2008; Kelemen et al. 2011). In particular, chemical data and modeling support the inference that solid mass and volume both increase during low temperature alteration of peridotite, leading to large elastic stresses that must be accommodated by deformation along fractures induced by tectonic stresses and/or reaction-driven cracking.

References

Al-Khirbash, Salah (2015). "Genesis and mineralogical classification of Ni-laterites, Oman Mountains." In: *Ore Geology Reviews* 65, pp. 199–212. ISSN: 01691368. DOI: 10.1016/j.oregeorev.2014.09.022.

Al-Khirbash, Salah et al. (2013). "Rare earth element mobility during laterization of mafic rocks of the Oman ophiolite." In: *Arabian Journal of Geosciences* 7.12, pp. 5443–5454. ISSN: 1866-7511. DOI: 10.1007/s12517-013-1189-6.

Alsharhan, A.S. and Sobhi Nasir (1996). "Sedimentological and geochemical interpretation of a transgressive sequence: the Late Cretaceous Qahlah Formation in the western Oman Mountains, United Arab Emirates." In: *Sedimentary Geology* 101.3-4, pp. 227–242. ISSN: 00370738. DOI: 10.1016/0037-0738(95)00067-4.

Alt, Jeffrey C. and Wayne C. Shanks (1998). "Sulfur in serpentinized oceanic peridotites: Serpentinization processes and microbial sulfate reduction." In: *Journal of Geophysical Research* 103.November 2015, p. 9917. ISSN: 0148-0227. DOI: 10.1029/98JB00576.

Alt, Jeffrey C. et al. (2013). "The role of serpentinites in cycling of carbon and sulfur: Seafloor serpentinization and subduction metamorphism." In: *Lithos* 178, pp. 40–54. ISSN: 00244937. DOI: 10.1016/j.lithos.2012.12.006.

Asimow, Paul D. (1999). "A model that reconciles major- and trace-element data from abyssal peridotites." In: *Earth and Planetary Science Letters* 169.3, pp. 303–319. ISSN: 0012821X. DOI: 10.1016/S0012-821X(99)00084-9.

Bach, Wolfgang and Frieder Klein (2009). "The petrology of seafloor rodingites: Insights from geochemical reaction path modeling." In: *Lithos* 112.1-2, pp. 103–117. ISSN: 00244937. DOI: 10.1016/j.lithos.2008.10.022.

Baker, Michael B. and John R Beckett (1999). "The origin of abyssal peridotites: a reinterpretation of constraints based on primary bulk compositions." In: *Earth and Planetary Science Letters* 171.1, pp. 49–61. ISSN: 0012-821X. DOI: https://doi.org/10.1016/S0012-821X(99)00130-2.

Barnes, Ivan, James R. O'Neil, and J.J Trescases (1978). "Present day serpentinization in New Caledonia, Oman and Yugoslavia." In: *Geochimica et Cosmochimica Acta* 42.1, pp. 144–145. ISSN: 00167037. DOI: 10.1016/0016-7037(78)90225-9.

Barnes, Jaime D. and Zachary D. Sharp (2006). "Achlorine isotope study of DSDP/ODP serpentinized ultramafic rocks: Insights into the serpentinization process." In: *Chemical Geology* 228.4, pp. 246–265. ISSN: 00092541. DOI: 10.1016/j.chemgeo.2005.10.011.

Bonatti, Enrico, James R. Lawrence, and Noris Morandi (1984). "Serpentinization of oceanic peridotites: temperature dependence of mineralogy and boron content." In: *Earth and Planetary Science Letters* 70.1, pp. 88–94. ISSN: 0012821X. DOI: 10.1016/0012-821X(84)90211-5.

Boschi, Chiara et al. (2013). "Serpentinization of mantle peridotites along an uplifted lithospheric section, Mid Atlantic Ridge at 11° N." In: *Lithos* 178, pp. 3–23. ISSN: 00244937. DOI: 10.1016/j.lithos.2013.06.003.

Boudier, Françoise and Robert G. Coleman (1981). "Cross section through the peridotite in the Samail ophiolite, southeastern Oman Mountains." In: *Journal of Geophysical Research: ...* 86.B4, p. 2573. ISSN: 0148-0227. DOI: 10.1029/JB086iB04p02573.

Boudier, Françoise, Adolphe Nicolas, and Benoit Ildefonse (1996). "Magma chambers in the Oman ophiolite: fed from the top and the bottom." In: *Earth and Planetary Science Letters* 144.1-2, pp. 239–250. ISSN: 0012821X. DOI: 10.1016/0012-821X(96)00167-7.

Braun, Michael Geoffrey and Peter B. Kelemen (2002). "Dunite distribution in the Oman Ophiolite: Implications for melt flux through porous dunite conduits." In: *Geochemistry, Geophysics, Geosystems* 3.11, pp. 1–21. ISSN: 15252027. DOI: 10.1029/2001GC000289.

Bristow, Thomas F et al. (2011). "A hydrothermal origin for isotopically anomalous cap dolostone cements from south China." In: *Nature* 474.7349, pp. 68–71. ISSN: 1476-4687. DOI: 10.1038/nature10096.

Chavagnac, Valerie et al. (2013). "Characterization of hyperalkaline fluids produced by low-temperature serpentinization of mantle peridotites in the Oman and Ligurian ophiolites." In: *Geochemistry, Geophysics, Geosystems* 14.7, pp. 2496–2522. ISSN: 15252027. DOI: 10.1002/ggge.20147.

Clark, Ian D. and Jean-Charles Fontes (1990). "Paleoclimatic reconstruction in northern Oman based on carbonates from hyperalkaline groundwaters." In: *Quaternary Research* 33.3, pp. 320–336. ISSN: 00335894. DOI: 10.1016/0033-5894(90)90059-T.

Coleman, Robert G. (1977). *Ophiolites*. Berlin, Springer–Verlag. ISBN: 3642666752.

Coleman, Robert G. (1981). "Tectonic setting for ophiolite obduction in Oman." In: *Journal of Geophysical Research: Solid Earth* 86.B4, pp. 2497–2508. ISSN: 0148-0227. DOI: 10.1029/JB086iB04p02497.

Coleman, Robert G. and Clifford A. Hopson (1981). "Introduction to the Oman Ophiolite Special Issue." In: *Journal of Geophysical Research: Solid Earth* 86.B4, pp. 2495–2496. ISSN: 01480227. DOI: 10.1029/JB086iB04p02495.

Collier, Martin Lee (2012). "Spatial-Statistical Properties of Geochemical Variability as Constraints on Magma Transport and Evolution Processes at Ocean Ridges." PhD thesis. Columbia University.

Dennis, Kate J. and Daniel P. Schrag (2010). "Clumped isotope thermometry of carbonatites as an indicator of diagenetic alteration." In: *Geochimica et Cosmochimica Acta* 74.14, pp. 4110–4122. ISSN: 00167037. DOI: 10.1016/j.gca.2010.04.005.

Eiler, John M. (2007). ""Clumped-isotope" geochemistry—The study of naturally-occurring, multiply-substituted isotopologues." In: *Earth and Planetary Science Letters* 262.3-4, pp. 309–327. ISSN: 0012821X. DOI: 10.1016/j.epsl.2007.08.020.

Escartín, J., G. Hirth, and B. Evans (1997). "Effects of serpentinization on the lithospheric strength and the style of normal faulting at slow-spreading ridges." In: *Earth and Planetary Science Letters* 151.3-4, pp. 181–189. ISSN: 0012-821X. DOI: 10.1016/S0012-821X(97)81847-X.

Evans, Bernard W. (1977). "Metamorphism of alpine peridotite and serpentinite." In: *Annual Reviews in Earth and Planetary Sciences*, pp. 397–447. ISSN: 0084-6597. DOI: 10.1146/annurev.ea.05.050177.002145.

Evans, Bernard W. (2004). "The Serpentinite Multisystem Revisited: Chrysotile Is Metastable." In: *International Geology Review* 46.6, pp. 479–506. ISSN: 0020-6814. DOI: 10.2747/0020-6814.46.6.479.

Evans, Bernard W. et al. (1976). "Stability of chrysotile and antigorite in the serpentinite multisystem." In: *Schweizerische mineralogische und petrographische Mitteilungen* 56, pp. 79–93.

Falk, Elisabeth S. and Peter B. Kelemen (2015). "Geochemistry and petrology of listvenite in the Samail ophiolite, Sultanate of Oman: Complete carbonation of peridotite during

ophiolite emplacement." In: *Geochimica et Cosmochimica Acta* 160, pp. 70–90. ISSN: 00167037. DOI: 10.1016/j.gca.2015.03.014.

Friedman, Gerald M. (1959). "Identification of Carbonate Minerals by Staining Methods." In: *SEPM Journal of Sedimentary Research* Vol. 29.1, pp. 87–97. ISSN: 1527-1404. DOI: 10.1306/74D70894-2B21-11D7-8648000102C1865D.

Frost, Ronald B. (1985). "On the stability of sulfides, oxides, and native metals in serpentinite." In: *Journal of Petrology* 26.June 1983, pp. 31–63. ISSN: 00223530. DOI: 10.1093/petrology/26.1.31.

Früh-Green, Gretchen L. et al. (2004). "Serpentinization of oceanic peridotites: Implications for geochemical cycles and biological activity." In: *AGU Monograph*. Vol. 144, pp. 119–136. DOI: 10.1029/144GM08.

Ghosh, Prosenjit et al. (2006). "13C–18O bonds in carbonate minerals: A new kind of paleothermometer." In: *Geochimica et Cosmochimica Acta* 70.6, pp. 1439–1456. ISSN: 00167037. DOI: 10.1016/j.gca.2005.11.014.

Godard, Marguerite, David Jousselin, and Jean-Louis Bodinier (2000). "Relationships between geochemistry and structure beneath a palaeo-spreading centre: a study of the mantle section in the Oman ophiolite." In: *Earth and Planetary Science Letters* 180.1-2, pp. 133–148. ISSN: 0012821X. DOI: 10.1016/S0012-821X(00)00149-7.

Gregory, Robert T. and Hugh P. Taylor (1981). "An oxygen isotope profile in a section of Cretaceous oceanic crust, Samail Ophiolite, Oman: Evidence for δ ¹⁸ O buffering of the oceans by deep (>5 km) seawater-hydrothermal circulation at mid-ocean ridges." In: *Journal of Geophysical Research: Solid Earth* 86.B4, pp. 2737–2755. ISSN: 01480227. DOI: 10.1029/JB086iB04p02737.

Guillot, Stéphane et al. (2015). "Tectonic significance of serpentinites." In: *Tectonophysics* 646, pp. 1–19. ISSN: 0040-1951. DOI: 10.1016/J.TECTO.2015.01.020.

Hacker, Bradley R. (1994). "Rapid Emplacement of Young Oceanic Lithosphere: Argon Geochronology of the Oman Ophiolite." In: *Science* 265.5178, pp. 1563–1565. ISSN: 0036-8075. DOI: 10.1126/science.265.5178.1563.

Hacker, Bradley R., Jed L. Mosenfelder, and E Gnos (1996). "Rapid emplacement of the Oman ophiolite: Thermal and geochronologic constraints." In: *Tectonics* 15.6, pp. 1230–1247. ISSN: 02787407. DOI: 10.1029/96TC01973.

Hanghøj, Karen et al. (2010). "Composition and Genesis of Depleted Mantle Peridotites from the Wadi Tayin Massif, Oman Ophiolite; Major and Trace Element Geochemistry, and Os Isotope and PGE Systematics." In: *Journal of Petrology* 51.1-2, pp. 201–227. ISSN: 0022-3530. DOI: 10.1093/petrology/egp077.

Hitch, B. F. et al. (1980). *The solubility of (α-Al(OH)3) in 1 molal NaCl as a function of pH and temperature*. Tech. rep. Oak Ridge National Laboratory Report ORNL-5623.

Hopson, C. A. et al. (1981). "Geologic section through the Samail Ophiolite and associated rocks along a Muscat-Ibra Transect, southeastern Oman Mountains." In: *Journal of Geophysical Research: Solid Earth* 86.B4, pp. 2527–2544. ISSN: 01480227. DOI: 10.1029/JB086iB04p02527.

Huntington, K W et al. (2009). "Methods and limitations of 'clumped' CO2 isotope (Delta47) analysis by gas-source isotope ratio mass spectrometry." In: *Journal of mass spectrometry : JMS* 44.9, pp. 1318–29. ISSN: 1096-9888. DOI: 10.1002/jms.1614.

Jagoutz, E. et al. (1979). "The abundances of major, minor and trace elements in the earth's mantle as derived from primitive ultramafic nodules." In: *Proceedings of the Lunar and Planetary Science Conference 10*, pp. 2031–2050.

Jamtveit, Bjørn, Anders Malthe-Sørenssen, and Olga Kostenko (2008). "Reaction enhanced permeability during retrogressive metamorphism." In: *Earth and Planetary Science Letters* 267.3, pp. 620–627. ISSN: 0012-821X. DOI: https://doi.org/10.1016/j.epsl.2007.12.016.

Kelemen, Peter B., Michael Geoffrey Braun, and Greg Hirth (2000). "Spatial distribution of melt conduits in the mantle beneath oceanic spreading ridges: Observations from the Ingalls and Oman ophiolites." In: *Geochemistry, Geophysics, Geosystems* 1.7, n/a–n/a. ISSN: 15252027. DOI: 10.1029/1999GC000012.

Kelemen, Peter B. and Greg Hirth (2012). "Reaction-driven cracking during retrograde metamorphism: Olivine hydration and carbonation." In: *Earth and Planetary Science Letters* 345-348, pp. 81–89. ISSN: 0012821X. DOI: 10.1016/j.epsl.2012.06.018.

Kelemen, Peter B. and Jürg M. Matter (2008). "In situ carbonation of peridotite for CO2 storage." In: *Proceedings of the National Academy of Sciences* 105.45, pp. 17295–17300. ISSN: 0027-8424. DOI: 10.1073/pnas.0805794105.

Kelemen, Peter B. et al. (2011). "Rates and Mechanisms of Mineral Carbonation in Peridotite: Natural Processes and Recipes for Enhanced, in situ CO 2 Capture and Storage." In: *Annual Review of Earth and Planetary Sciences* 39.1, pp. 545–576. ISSN: 0084-6597. DOI: 10.1146/annurev-earth-092010-152509.

Klein, Frieder, Wolfgang Bach, and Thomas M. McCollom (2013). "Compositional controls on hydrogen generation during serpentinization of ultramafic rocks." In: *Lithos* 178, pp. 55–69. ISSN: 00244937. DOI: 10.1016/j.lithos.2013.03.008.

Klein, Frieder and Carlos J. Garrido (2011). "Thermodynamic constraints on mineral carbonation of serpentinized peridotite." In: *Lithos* 126.3-4, pp. 147–160. ISSN: 00244937. DOI: 10.1016/j.lithos.2011.07.020.

Klein, Frieder et al. (2009). "Iron partitioning and hydrogen generation during serpentinization of abyssal peridotites from 15°N on the Mid-Atlantic Ridge." In: *Geochimica et Cosmochimica Acta* 73.22, pp. 6868–6893. ISSN: 00167037. DOI: 10.1016/j.gca.2009.08.021.

Klein, Frieder et al. (2014). "Magnetite in seafloor serpentinite—Some like it hot." In: *Geology* 42, pp. 135–138. ISSN: 0091-7613. DOI: 10.1130/g35068.1.

Lippard, S.J., A.W. Shelton, and I.G. Gass (1986). "The Ophiolite of Northern Oman." In: *Geological Society Memoir* 11.

Macdonald, A.H. and W.S. Fyfe (1985). "Rate of serpentinization in seafloor environments." In: *Tectonophysics* 116.1-2, pp. 123–135. ISSN: 00401951. DOI: 10.1016/0040-1951(85)90225-2.

Mann, A., S. S. Hanna, and S. C. Nolan (1990). "The post-Campanian tectonic evolution of the Central Oman Mountains: Tertiary extension of the Eastern Arabian Margin." In: *Geological Society, London, Special Publications* 49.1, pp. 549–563. ISSN: 0305-8719. DOI: 10.1144/GSL.SP.1992.049.01.33.

May, Howard M., Philip A. Helmke, and Marion L. Jackson (1979). "Gibbsite solubility and thermodynamic properties of hydroxy-aluminum ions in aqueous solution at 25??C." In: *Geochimica et Cosmochimica Acta* 43.6, pp. 861–868. ISSN: 00167037. DOI: 10.1016/0016-7037(79)90224-2.

McArthur, J M, R J Howarth, and G A Shields (2012). "Chapter 7 - Strontium Isotope Stratigraphy BT - The Geologic Time Scale." In: Boston: Elsevier, pp. 127–144. ISBN: 978-0-444-59425-9. DOI: http://dx.doi.org/10.1016/B978-0-444-59425-9.00007-X.

Mervine, Evelyn M. et al. (2014). "Carbonation rates of peridotite in the Samail Ophiolite, Sultanate of Oman, constrained through 14C dating and stable isotopes." In: *Geochimica et Cosmochimica Acta* 126, pp. 371–397. ISSN: 00167037. DOI: 10.1016/j.gca.2013.11.007.

Mervine, Evelyn M. et al. (2015). "Applications and limitations of U-Th disequilibria systematics for determining ages of carbonate alteration minerals in peridotite." In: *Chemical Geology* 412, pp. 151–166. ISSN: 00092541. DOI: 10.1016/j.chemgeo.2015.07.023.

Monnier, Christophe et al. (2006). "Along-ridge petrological segmentation of the mantle in the Oman ophiolite." In: *Geochemistry, Geophysics, Geosystems* 7.11, n/a–n/a. ISSN: 15252027. DOI: 10.1029/2006GC001320.

Monnin, Christophe et al. (2011). "Characterization of hyperalkaline fluids produced by serpentinization of mantle peridotites in Oman and in Liguria (Northern Italy)." In: *Mineralog. Mag* 75, p. 1490.

Nasir, Sobhi et al. (2007). "Mineralogical and geochemical characterization of listwaenite from the Semail Ophiolite, Oman." In: *Chemie der Erde - Geochemistry* 67.3, pp. 213–228. ISSN: 00092819. DOI: 10.1016/j.chemer.2005.01.003.

Neal, C. and G. Stanger (1985). "Past and present serpentinization of ultramafic rocks: An example from the Semail ophiolite nappe of northern Oman." In: *The Chemistry of Weathering*. Ed. by JI Drewer. Dordrecht, Holland: D. Reidel Publishing Company, 249–275.

Nicolas, Adolphe et al. (2000). "Accretion of Oman and United Arab Emirates ophiolite–Discussion of a new structural map." In: *Marine Geophysical Researches*, pp. 147–179. DOI: 10.1023/A:1026769727917.

Nolan, S. C. et al. (1990). "Maastrichtian to early Tertiary stratigraphy and palaeogeography of the Central and Northern Oman Mountains." In: *Geological Society, London, Special Publications* 49.1, pp. 495–519. ISSN: 0305-8719. DOI: 10.1144/GSL.SP.1992.049.01.31.

O'Hanley, David S. (1996). *Serpentinites: Records of Tectonic and Petrological History*. New York and Oxford: Oxford University Press, p. 227. ISBN: 0-19-508254-0.

Palandri, James L and Mark H Reed (2004). "Geochemical models of metasomatism in ultramafic systems: serpentinization, rodingitization, and sea floor carbonate chimney precipitation." In: *Geochimica et Cosmochimica Acta* 68.5, pp. 1115–1133. ISSN: 00167037. DOI: 10.1016/j.gca.2003.08.006.

Pallister, JS and RJ Knight (1981). "Rare-earth element geochemistry of the Samail Ophiolite near Ibra, Oman." In: *Journal of Geophysical Research: Solid ...* 86.B4, p. 2673. ISSN: 0148-0227. DOI: 10.1029/JB086iB04p02673.

Passey, Benjamin H. et al. (2010). "High-temperature environments of human evolution in East Africa based on bond ordering in paleosol carbonates." In: *Proceedings of the National Academy of Sciences of the United States of America* 107.25, pp. 11245–9. ISSN: 1091-6490. DOI: 10.1073/pnas.1001824107.

Paukert, Amelia N. et al. (2012). "Reaction path modeling of enhanced in situ CO2 mineralization for carbon sequestration in the peridotite of the Samail Ophiolite, Sultanate

of Oman." In: *Chemical Geology* 330-331, pp. 86–100. ISSN: 00092541. DOI: 10.1016/j.chemgeo.2012.08.013.

Racey, Andrew (1995). "Lithostratigraphy and Larger Foraminiferal (Nummulitid) Biostratigraphy of the Tertiary of Northern Oman." In: *Micropaleontology* 41, p. 1. ISSN: 00262803. DOI: 10.2307/1485849.

Rioux, Matthew et al. (2012). "Rapid crustal accretion and magma assimilation in the Oman-U.A.E. ophiolite: High precision U-Pb zircon geochronology of the gabbroic crust." In: *Journal of Geophysical Research* 117.B7, B07201. ISSN: 0148-0227. DOI: 10.1029/2012JB009273.

Rioux, Matthew et al. (2013). "Tectonic development of the Samail ophiolite: High-precision U-Pb zircon geochronology and Sm-Nd isotopic constraints on crustal growth and emplacement." In: *Journal of Geophysical Research: Solid Earth* 118.5, pp. 2085–2101. ISSN: 21699313. DOI: 10.1002/jgrb.50139.

Rudge, John F, Peter B. Kelemen, and Marc Spiegelman (2010). "A simple model of reaction-induced cracking applied to serpentinization and carbonation of peridotite." In: *Earth and Planetary Science Letters* 291.1, pp. 215–227. ISSN: 0012-821X. DOI: https://doi.org/10.1016/j.epsl.2010.01.016.

Sánchez-Murillo, Ricardo et al. (2014). "Geochemical evidence for active tropical serpentinization in the Santa Elena Ophiolite, Costa Rica: An analog of a humid early Earth?" In: *Geochemistry, Geophysics, Geosystems* 15, pp. 1783–1800. ISSN: 15252027. DOI: 10.1002/2013GC005213.

Schlüter, M. et al. (2008). "Evolution of a Maastrichtian–Paleocene tropical shallow-water carbonate platform (Qalhat, NE Oman)." In: *Facies* 54.4, pp. 513–527. ISSN: 0172-9179. DOI: 10.1007/s10347-008-0150-8.

Schwarzenbach, Esther M., Esteban Gazel, and Mark J. Caddick (2014). "Hydrothermal processes in partially serpentinized peridotites from Costa Rica: evidence from native copper and complex sulfide assemblages." In: *Contributions to Mineralogy and Petrology* 168. ISSN: 0010-7999. DOI: 10.1007/s00410-014-1079-2.

Schwarzenbach, Esther M. et al. (2012). "Sulfur geochemistry of peridotite-hosted hydrothermal systems: Comparing the Ligurian ophiolites with oceanic serpentinites." In: *Geochimica et Cosmochimica Acta* 91, pp. 283–305. ISSN: 00167037. DOI: 10.1016/j.gca.2012.05.021.

Searle, Michael P. and G. M. Graham (1982). ""Oman Exotics"—Oceanic carbonate build-ups associated with the early stages of continental rifting." In: *Geology* 10.1, p. 43. ISSN: 0091-7613. DOI: 10.1130/0091-7613(1982)10<43:OECBAW>2.0.CO;2.

Seyfried, William E., D.I. Foustoukos, and Qi Fu (2007). "Redox evolution and mass transfer during serpentinization: An experimental and theoretical study at 200°C, 500bar with implications for ultramafic-hosted hydrothermal systems at Mid-Ocean Ridges." In: *Geochimica et Cosmochimica Acta* 71.15, pp. 3872–3886. ISSN: 00167037. DOI: 10.1016/j.gca.2007.05.015.

Snow, Jonathan E. and Henry J.B. Dick (1995). "Pervasive magnesium loss by marine weathering of peridotite." In: *Geochimica et Cosmochimica Acta* 59.20, pp. 4219–4235. ISSN: 00167037. DOI: 10.1016/0016-7037(95)00239-V.

Stanger, G. (1985). "Silicified serpentinite in the Semail nappe of Oman." In: *Lithos* 18, pp. 13–22. ISSN: 00244937. DOI: 10.1016/0024-4937(85)90003-9.

Streit, Elisabeth, Peter B. Kelemen, and John Eiler (2012). "Coexisting serpentine and quartz from carbonate-bearing serpentinized peridotite in the Samail Ophiolite, Oman." In: *Contributions to Mineralogy and Petrology* 164.5, pp. 821–837. ISSN: 00107999. DOI: 10.1007/s00410-012-0775-z.

Thompson, Geoffrey and William G. Melson (1970). "Boron contents of serpentinites and metabasalts in the oceanic crust: Implications for the boron cycle in the oceans." In: *Earth and Planetary Science Letters* 8.1, pp. 61–65. ISSN: 0012821X. DOI: 10.1016/0012-821X(70)90100-7.

Tilton, G. R., C. a. Hopson, and J. E. Wright (1981). "Uranium-lead isotopic ages of the Samail Ophiolite, Oman, with applications to Tethyan ocean ridge tectonics." In: *Journal of Geophysical Research* 86.B4, p. 2763. ISSN: 0148-0227. DOI: 10.1029/JB086iB04p02763.

Warren, Clare J et al. (2005). "Dating the geologic history of Oman's Semail ophiolite: insights from U-Pb geochronology." In: *Contributions to Mineralogy and Petrology* 150.4, pp. 403–422. ISSN: 1432-0967. DOI: 10.1007/s00410-005-0028-5.

Wesolowski, David J. (1992). "Aluminum speciation and equilibria in aqueous solution: I. The solubility of gibbsite in the system Na-K-Cl-OH-Al(OH)4from 0 to 100°C." In: *Geochimica et Cosmochimica Acta* 56.3, pp. 1065–1091. ISSN: 00167037. DOI: 10.1016/0016-7037(92)90047-M.

Wicks, Frederick J., EJW Whittaker, and J Zussman (1977). "Model for serpentine textures after olivine." In: *Canadian mineralogist* 15, pp. 446–458.

Wolery, T J and R L Jarek (2003). "EQ3/6, version 8.0—software user's manual." In: *Civilian Radioactive Waste Management System, Management & Operating Contractor. Sandia National Laboratories, Albuquerque, New Mexico.*

Wyns, R. et al. (1992). *Explanatory notes to the geological map of the Tiwi Quadrangle, Sultanate of Oman. Geoscience map, scale 1:100,000, sheet NF 40-8B*. Sultanate of Oman: Ministry of Petroleum and Minerals, Directorate General of Minerals, p. 66.

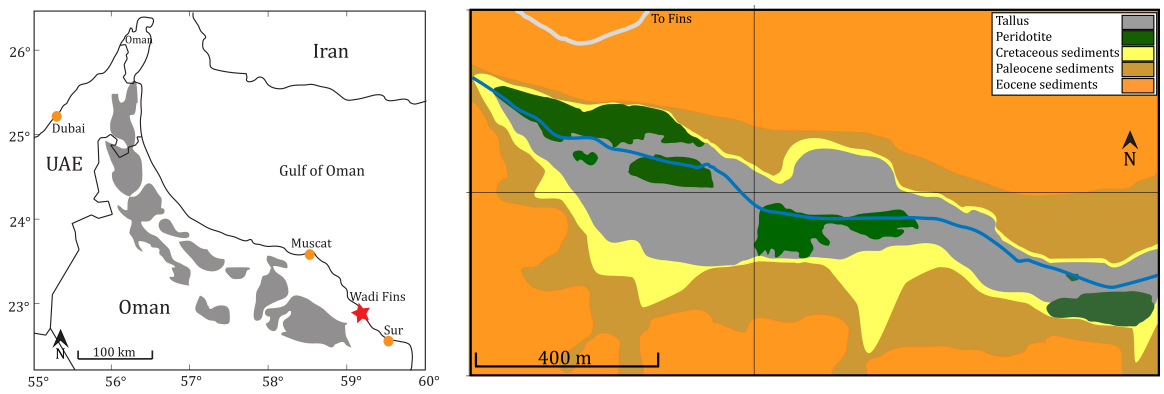

Figure 2.1: (Left) Map of the Samail ophiolite after Hanghøj et al. (2010). Red star shows location of Wadi Fins. (Right) Geologic map of Wadi Fins compiled from (Wyns et al. 1992b), Google Earth data and field observations. Map area is between UTM coordinates 2,532,838 to 2,533,636 m N and 721,824 to 722,551 m E in zone 40 Q

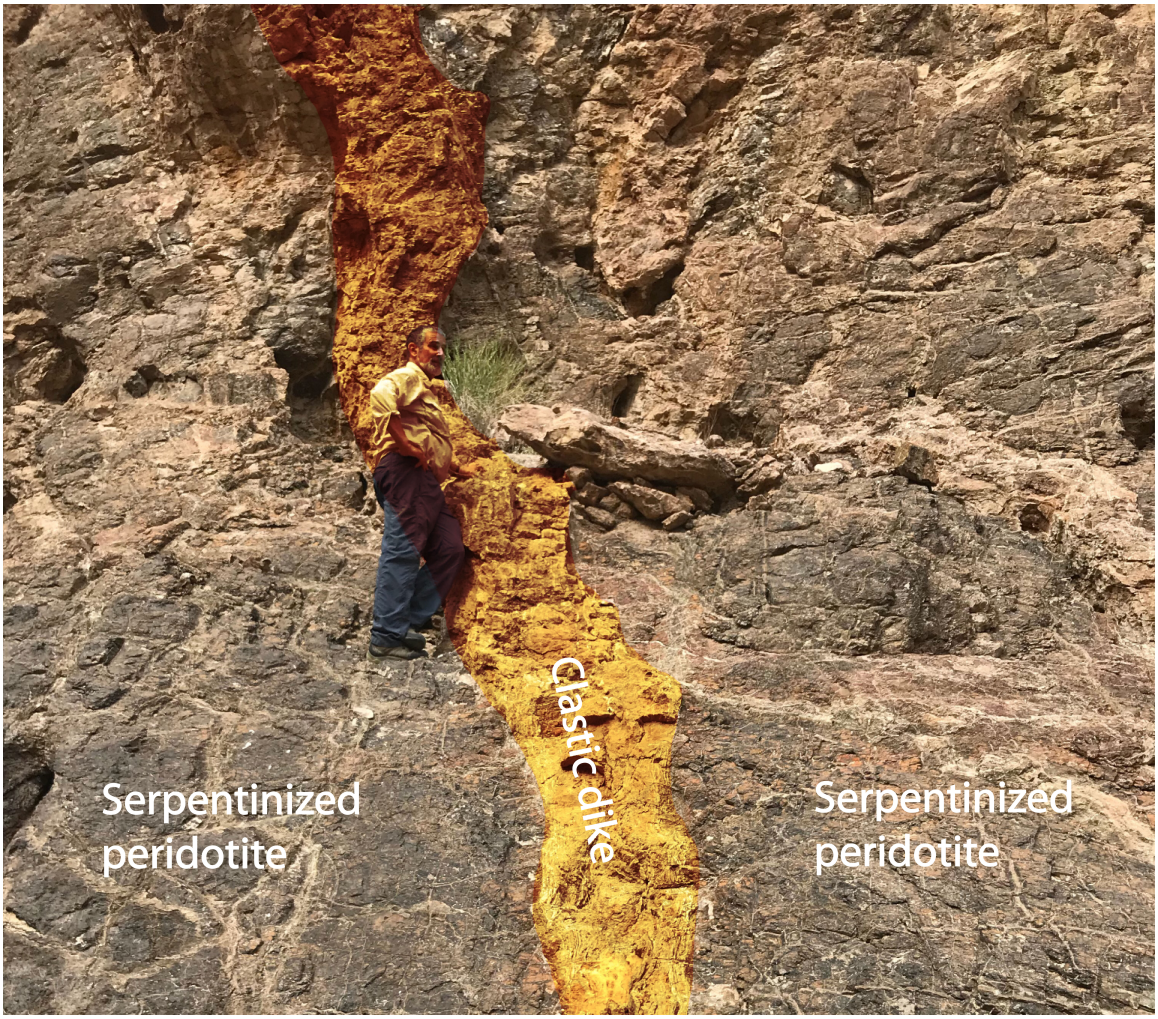

Figure 2.2: Clastic dike of limestone (highlighted in yellow) intruding the peridotite in Wadi Fins. A person is shown for scale

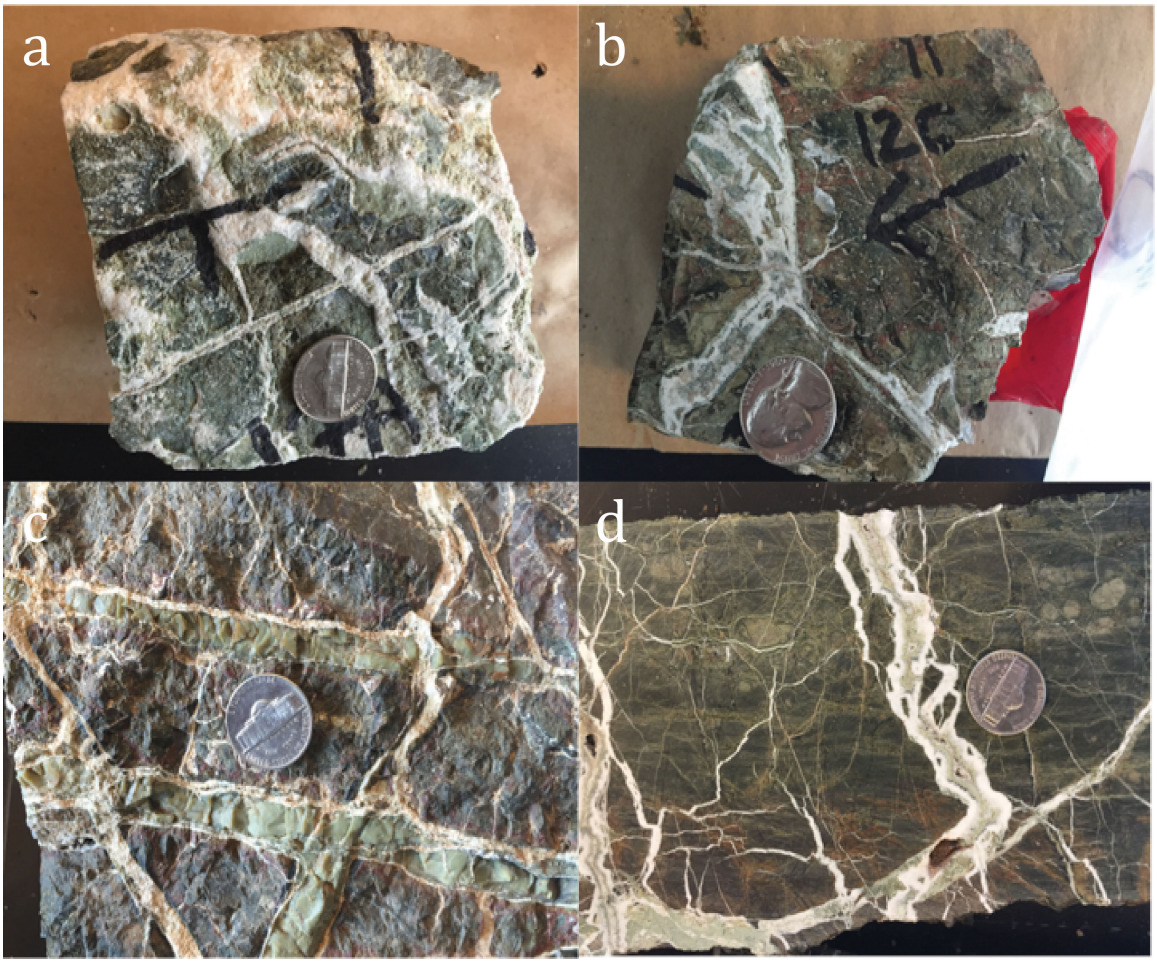

Figure 2.3: Examples of serpentine-carbonate veins crosscutting serpentine matrix. (a) OM13-17A, (b) OM13-12C, (c) OM13-15 in which the prominent waxy-green vein below coin is isotropic serpentine and (d) OM13-13. Serpentine in the veins is magnesium rich and contains small magnetite crystals. Coin for scale (D=2.1 cm). Veins >0.5cm are composite serpentine-carbonate.

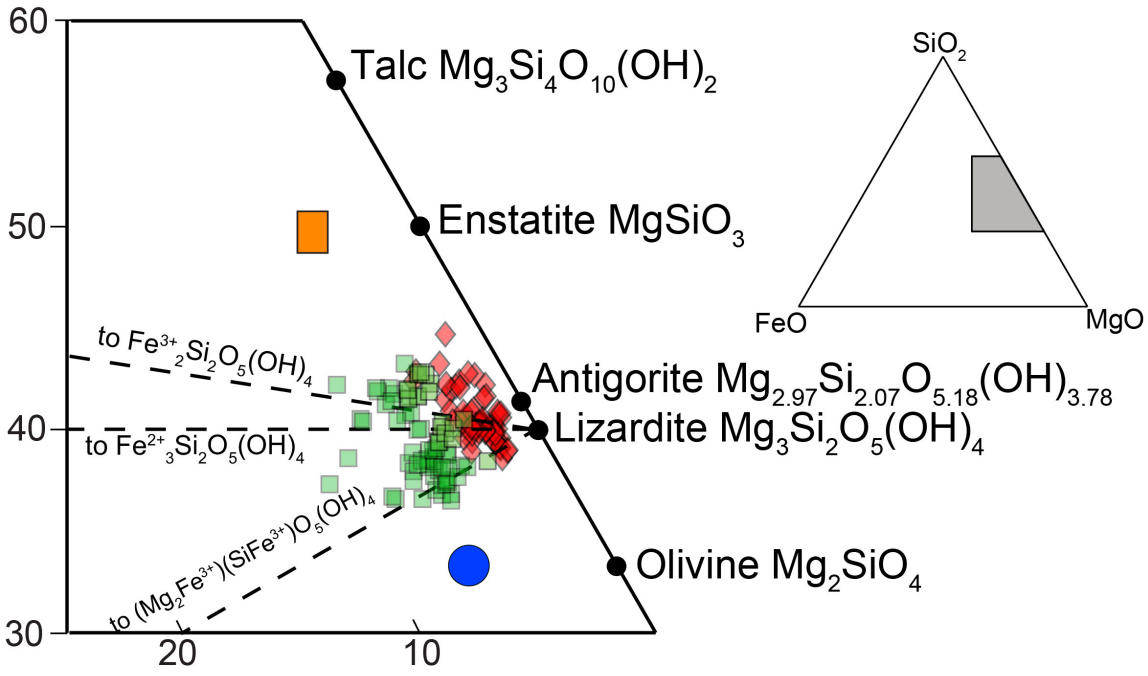

Figure 2.4: Projection of electron microprobe analysis of matrix serpentines (green), vein serpentines (red), relict olivines (blue), and pyroxenes (orange) onto a ternary MgO-SiO2-FeO diagram (molar proportions). All Fe as FeO.

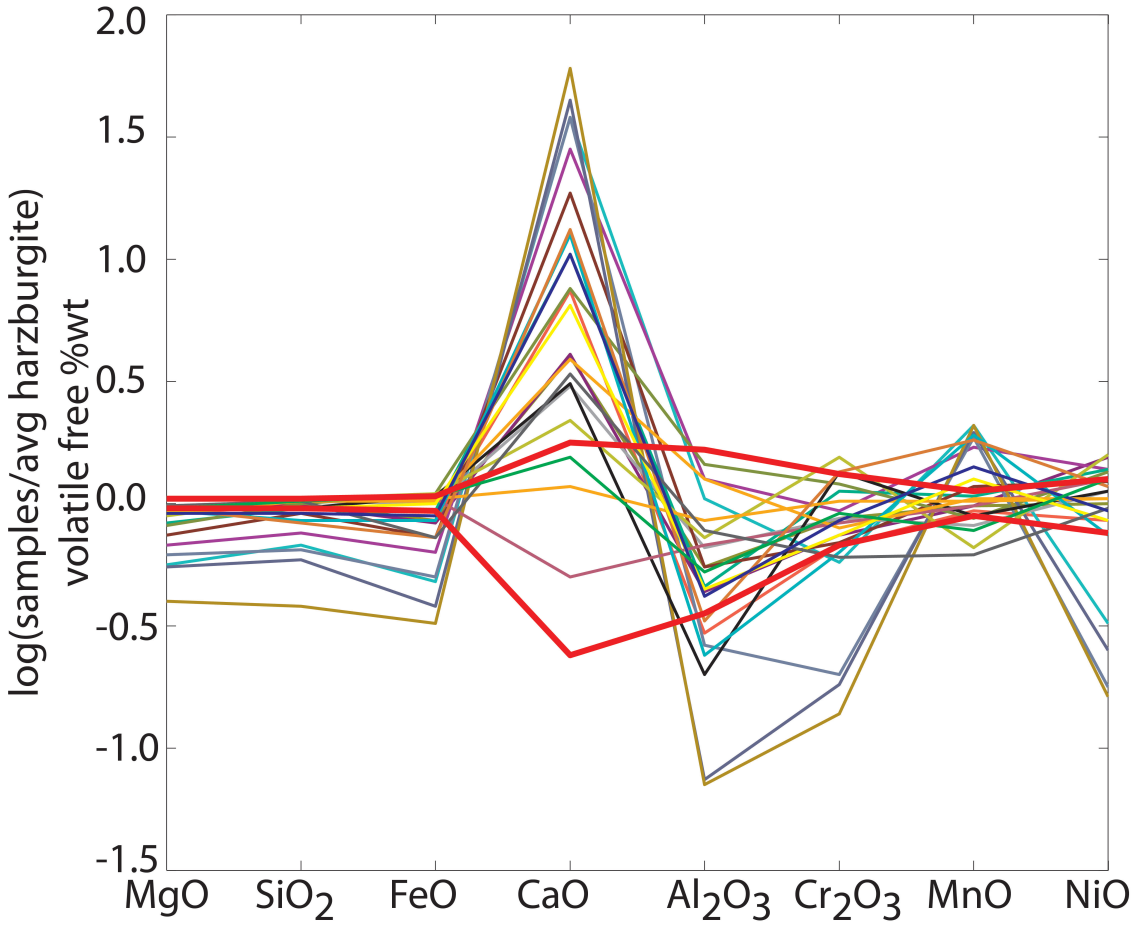

Figure 2.5: Major element data compared to average Oman harzburgite. Data are projected from loss-on-ignition (LOI) and the volatile-free composition is ratioed to average Oman harzburgite (Godard et al., 2000; Hanghøj et al., 2010; Monnier et al., 2006) A value of zero ($\log_{10}$ of 1) is identical in composition of average Oman harzburgite. Positive values indicate enrichments relative to the protolith, while negative values indicate depletions relative to the protolith. Red thick lines are 2σ deviations from average Oman harzburgite average (Godard et al., 2000; Hanghøj et al., 2010; Monnier et al., 2006).

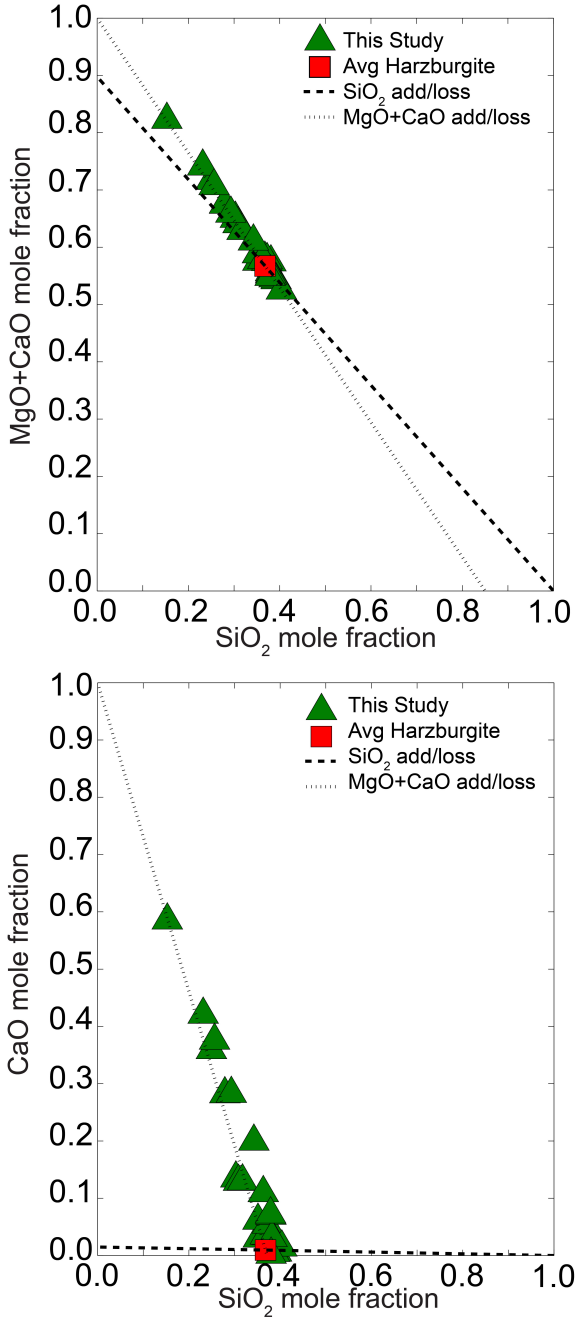

Figure 2.6: (Top) Volatile-free molar MgO+CaO versus molar SiO_2. (Bottom) Volatile-free molar CaO versus molar SiO_2. Dashed and dotted grey lines show expected composition if the composition of average Oman harzburgite composition is perturbed only by loss or addition of Mg+Ca or Si. (Average harzburgite from Godard et al., 2000; Hanghøj et al., 2010 and Monnier et al., 2006).

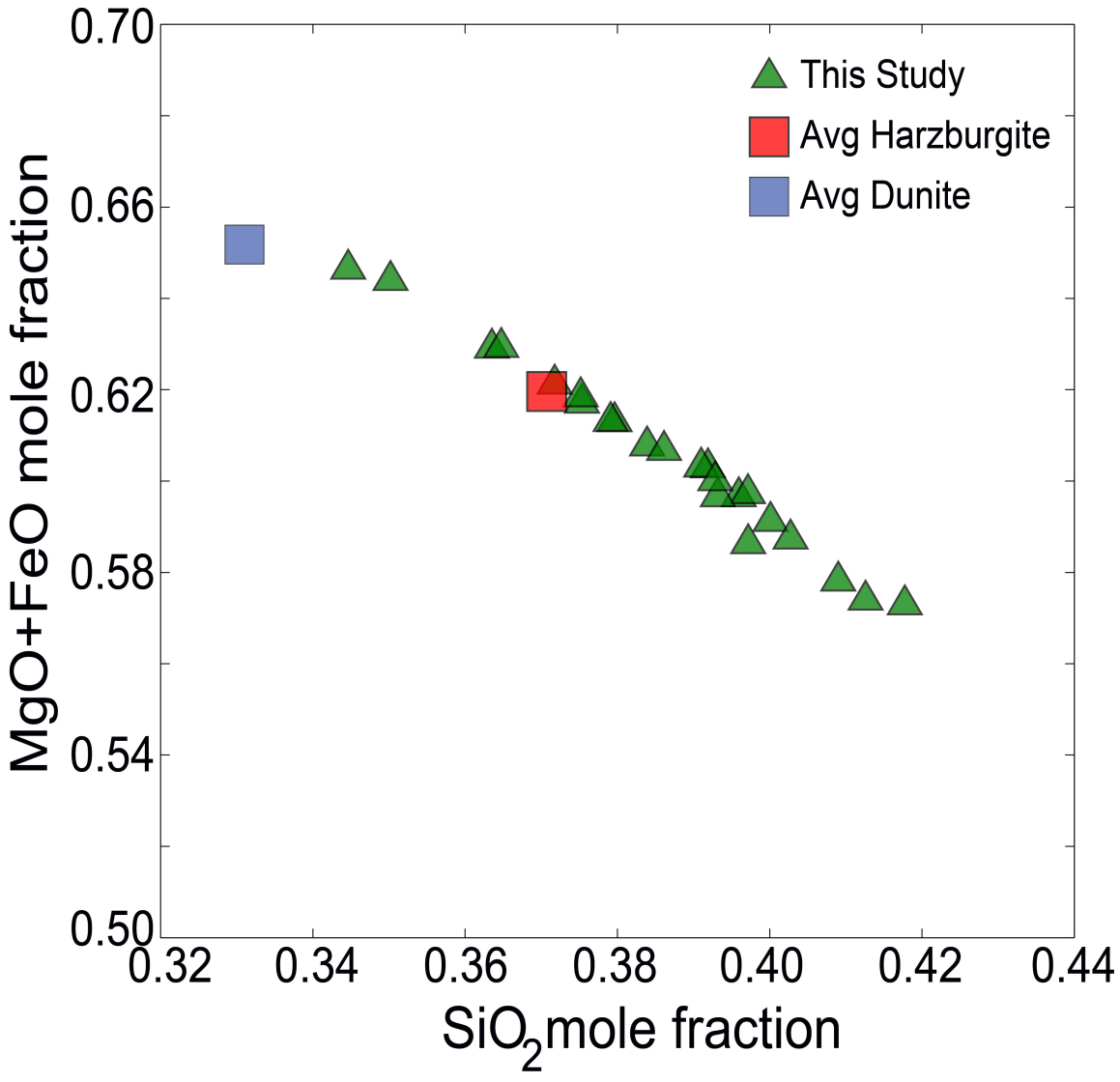

Figure 2.7: Volatile-free, calcite-free MgO+FeO vs SiO_2 (projected from CaO+LOI). (Average harzburgite and average dunite from Godard et al., 2000; Hanghøj et al., 2010; Monnier et al., 2006).

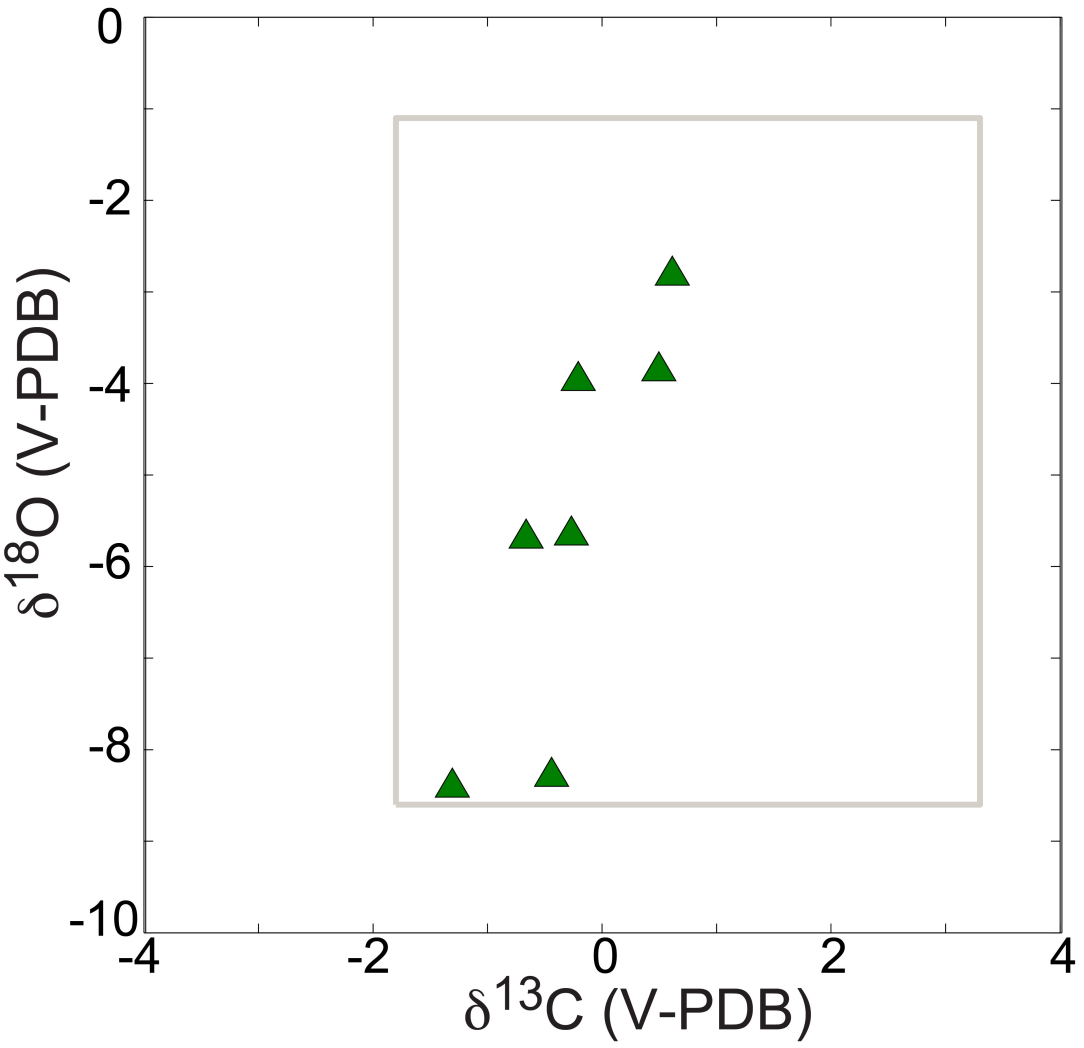

Figure 2.8: Stable isotope δ^{13}C vs. δ^{18}O of Wadi Fins carbonate veins in green with range observed in the overlying limestone units from Schlüter et al., 2008 in grey.

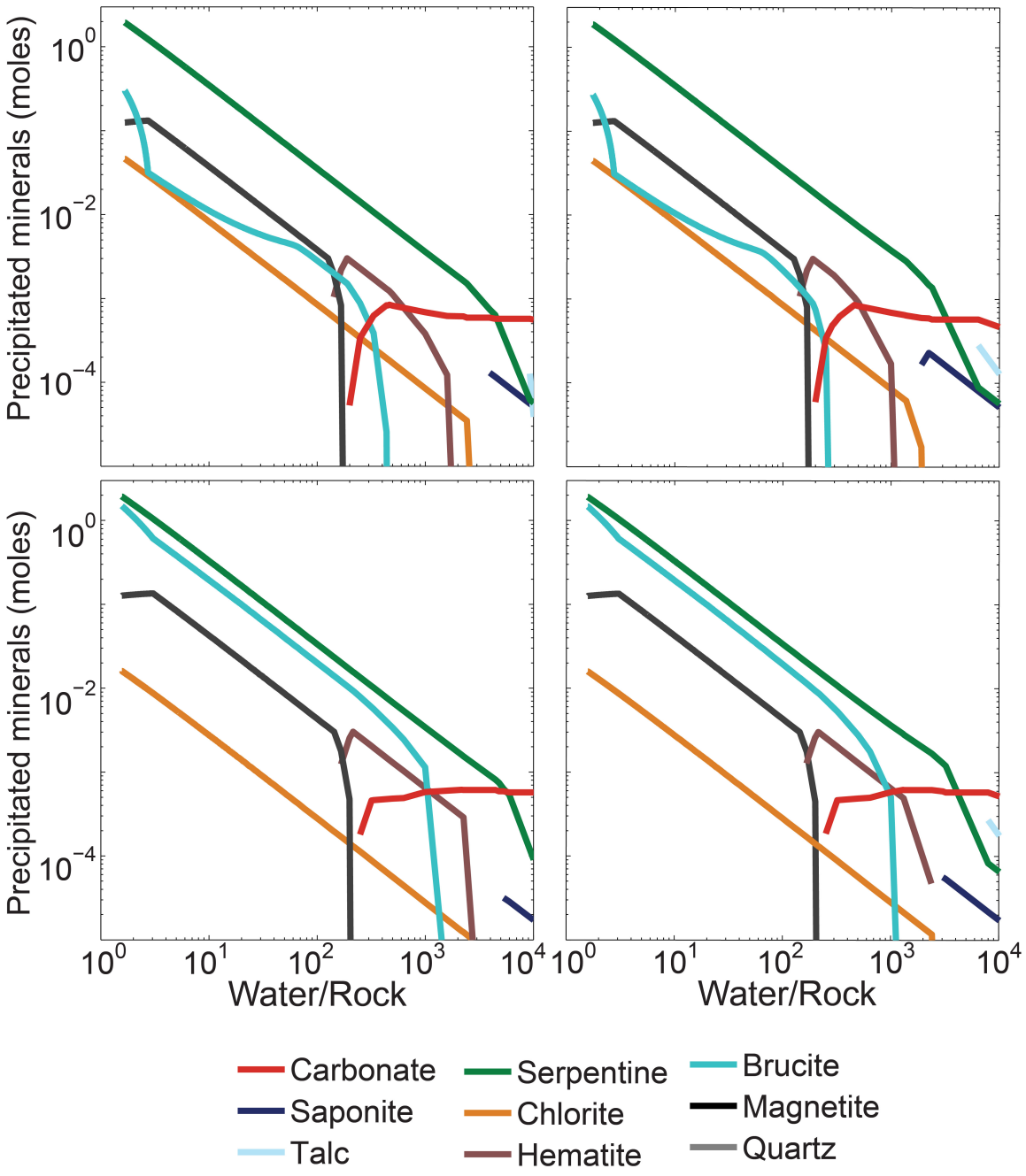

Figure 2.9: Mineral reaction products for reaction path models. Top left harzburgite with calcite-saturated fluid; top right harzburgite with calcite-quartz saturated fluid. Bottom left dunite with calcite-saturated-fluid; bottom right dunite with calcite-quartz saturated fluid.

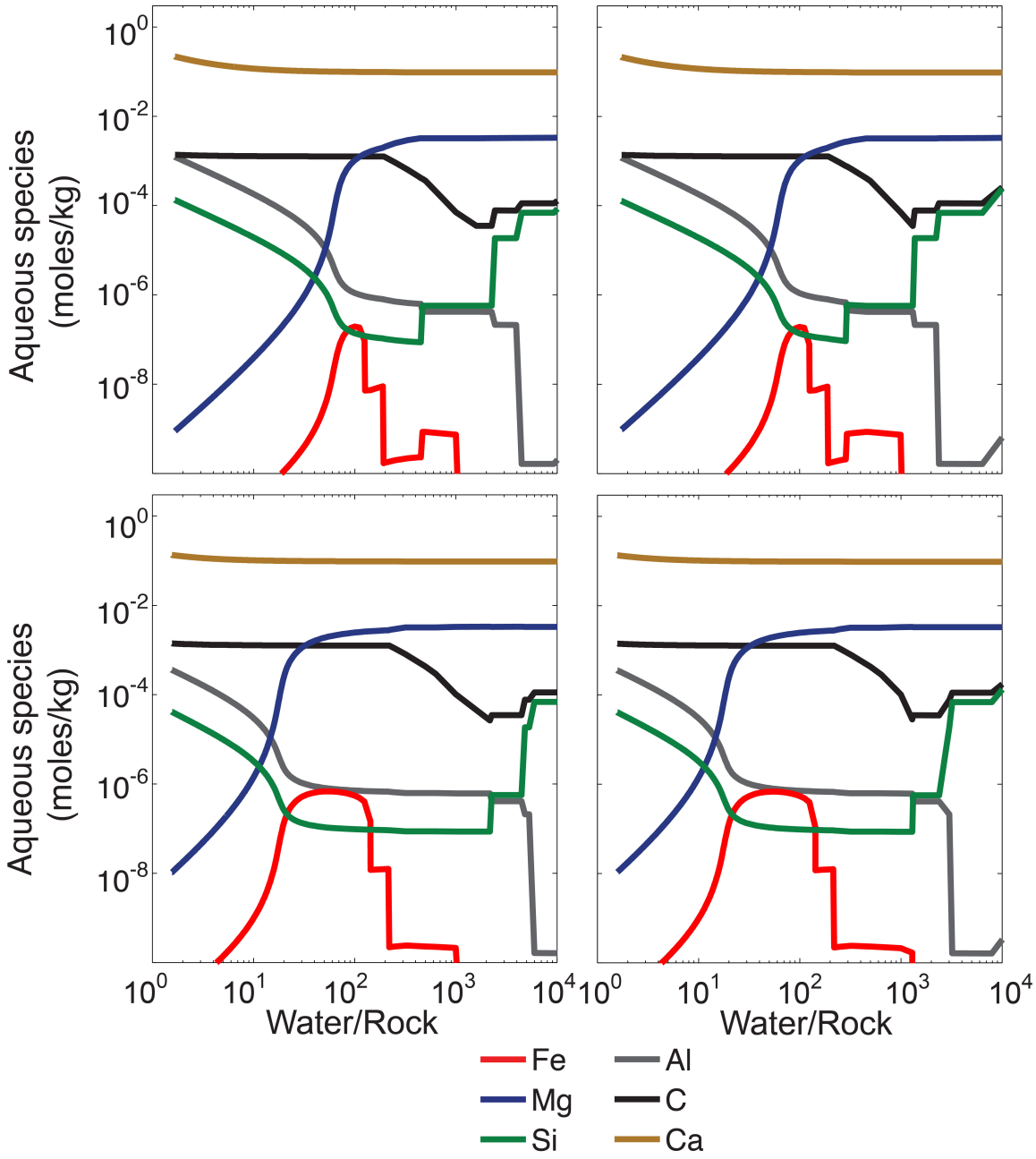

Figure 2.10: Fluid chemistry of reaction path models. Top left harzburgite with calcite-saturated fluid; top right harzburgite with calcite-quartz-saturated fluid. Bottom left dunite with calcite-saturated fluid; bottom right dunite with calcite-quartz saturated fluid.

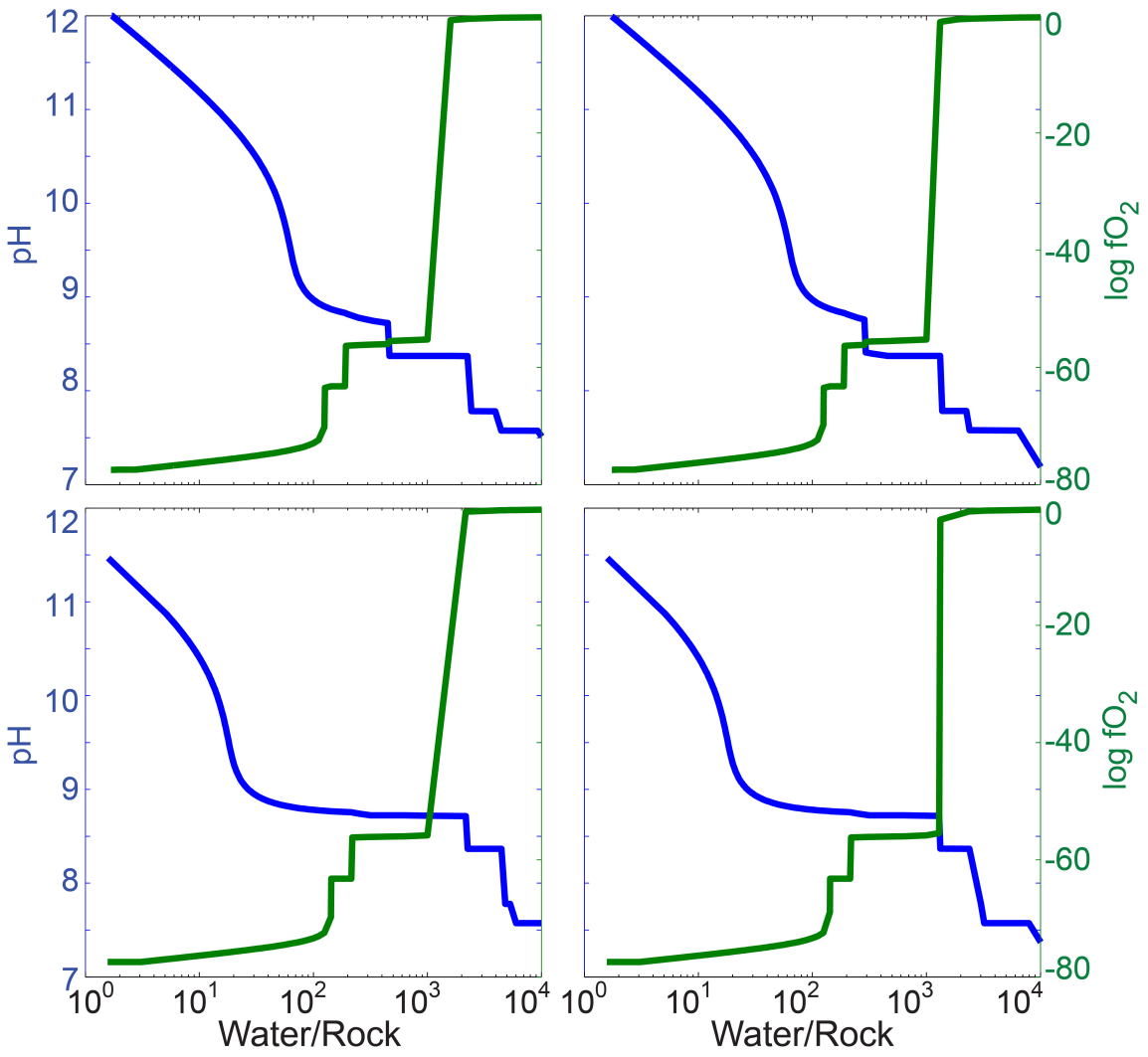

Figure 2.11: Reaction path model oxygen fugacity and pH as a function of W/R. Top left harzburgite with calcite-saturated fluid; top right harzburgite with calcite-quartz-saturated fluid. Bottom left dunite with calcite-saturated fluid; bottom right dunite with calcite-quartz-saturated fluid

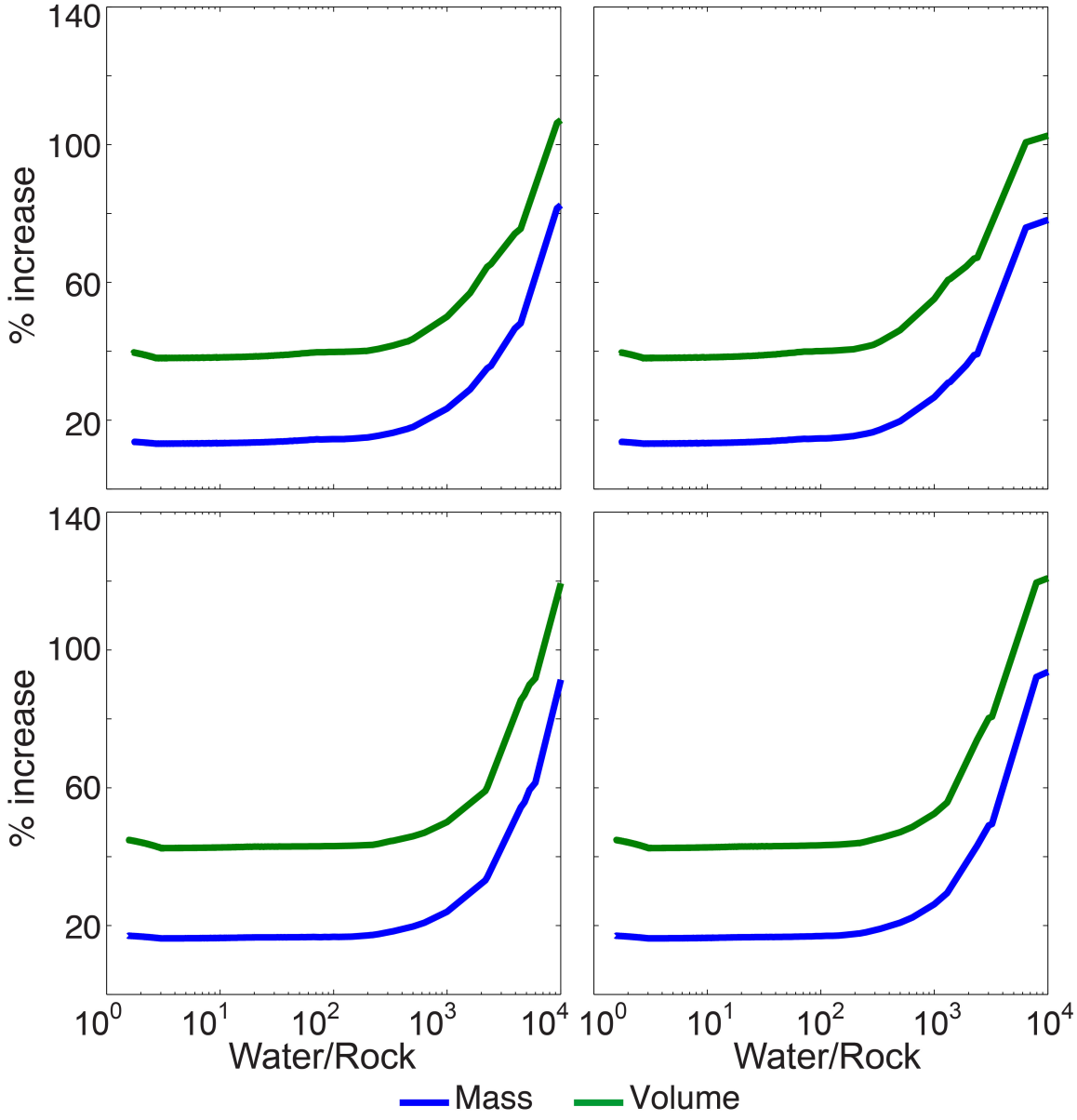

Figure 2.12: Reaction path model mass and volume changes as a function of W/R Top left harzburgite with calcite-saturated fluid; top right harzburgite with calcite-quartz saturated fluid. Bottom left dunite with calcite-saturated fluid; bottom right dunite with calcite-quartz-saturated fluid.

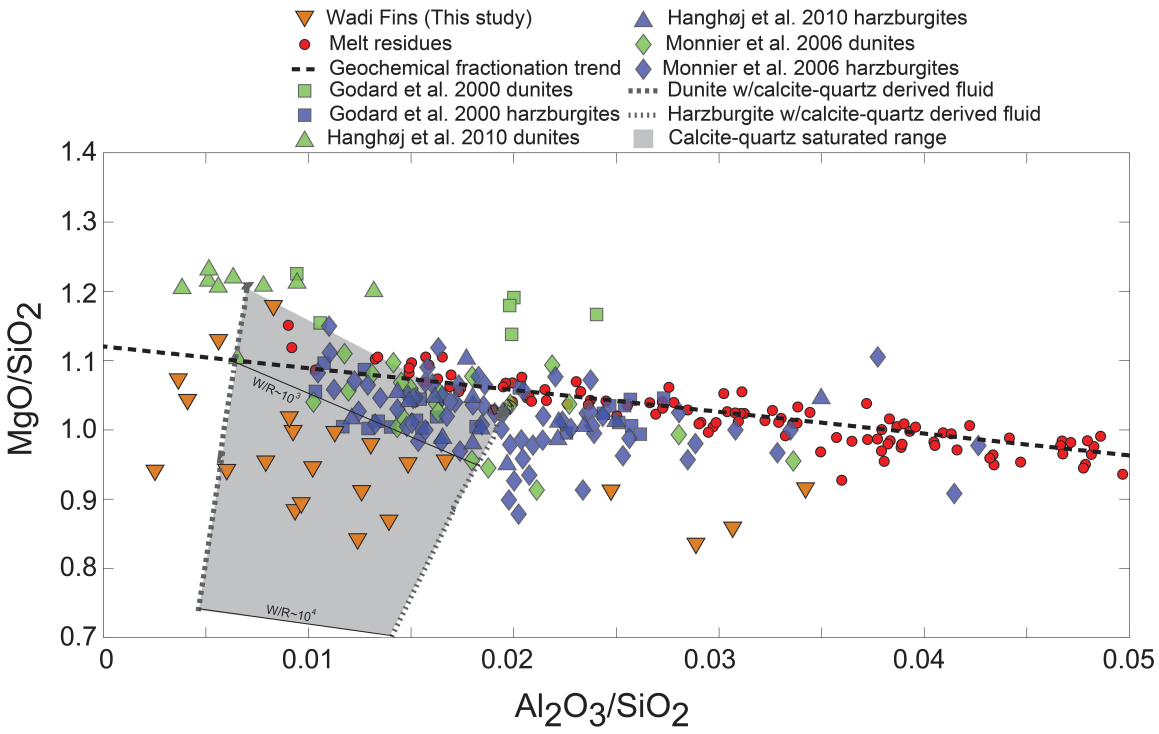

Figure 2.13: Whole rock MgO/SiO_2 vs Al_2O_3/SiO_2 for Wadi Fins samples, Oman peridotites (Godard et al., 2000; Hanghøj et al., 2010; Monnier et al., 2006) and peridotite melt residues (Asimow, 1999; Baker & Beckett, 1999). Geochemical fractionation is a linear fit of melt residues (e.g. Jagoutz, 1979, Snow and Dick, 1995). Reaction path model results for harzburgite and dunite protoliths are shown for reference (lines). Grey shaded polygon encompass the range of model results for reaction of harzburgite and dunite with calcite-quartz saturated fluids. Tie lines show W/R for the reaction paths.

Table 2.1: Stable Isotope, $\Delta 47$ and clump temperatures for selected carbonates

Sample	^{13}C ‰V-PDB	^{18}O ‰V-PDB	$\Delta 47$ ‰	T °C (Ghosh et al, 2006)	T °C (Dennis & Schrag 2010)	T °C (Bristow et al 2011)	^{87}Sr/^{86}Sr
OM13-1	-0.664±0.020	-5.693±0.006	0.612±0.012	46±3	66±7	56±4	0.707785±0.000010
OM13-11	-0.267±0.032	-5.659±0.194	0.628±0.010	42±2	57±5	50±3	NA
OM13-13	-1.307±0.065	-8.412±0.141	0.716±0.015	22±3	18±6	25±4	0.707895±0.000023
OM13-14A	-0.441±0.033	-8.296±0.144	0.649±0.021	37±5	47±10	44±6	0.707950±0.000012
OM13-15	-0.207±0.018	-3.970±0.143	0.660±0.005	34±1	41±3	40±2	NA
OM13-17A	0.613±0.175	-2.820±0.317	0.658±0.010	34±2	42±4	41±3	NA
OM13-3	0.497±0.092	-3.864±0.095	0.641±0.012	38±3	50±6	46±4	NA

Uncertainties are reported as standard deviation of the replicates of each sample divided by $\sqrt{n-1}$

Table 2.2: Initial fluid composition used in the models

Component	mmol/kg
Na^+	464
Cl^-	546
HCO_3^-	1.56
Ca^{2+}	69.2
Mg^{2+}	29.6
K^+	9.8
SiO_2, aq	0.11
Fe^{2+}	0.0000015
Al^{3+}	0.000037
O_2, aq	0.25
pH	7.8

Ca^{2+}, Mg^{2+} and HCO_3^- from Hansen and Wollman 2003. HCO_3^- from equilibrium with pCO_2 3x present. All other from Klein et al, 2009

3 Major element mobility during serpentinization, oxidation and weathering of mantle peridotite at low temperatures

This chapter has been submitted for publication in Philosophical Transactions of the Royal Society A

Abstract

Mantle peridotite in Wadi Fins in eastern Oman exhibits three concentric alteration zones with oxide and sulfide mineralogy recording gradients in fO_2 and fS_2 of more than 20 orders of magnitude over 15-20 cm. The black cores of samples (5 cm in diameter) exhibit incomplete, nearly isochemical serpentinization, with relict primary mantle minerals (olivine, opx and cpx) along with sulfide assemblages (pentlandite/heazlewoodite/bornite) recording low fO_2 and fS_2. In addition to the black cores, two alteration zones are evident from their coloration in outcrop and hand samples: green and red. These zones exhibit non-isochemical alteration characterized by intergrowths of stevensite/lizardite. All three reaction zones are cut by calcite ± serpentine veins, which are most abundant in the outer, red zones, sometimes are flanked by narrow red and/or green zones where they cut the black zones, and thus may be approximately coeval with all three alteration zones. These zones record progressively higher oxygen fugacities (fO_2) recorded by Ni-rich sulfides and iron oxides/hydroxides. These alteration zones lost 20-30% of their initial magnesium content, together with mobilization of iron over short distances from inner green zones into outer red zones, where iron is reprecipitated in goethite intermixed with silicates due to higher fO_2. Thermodynamic modeling at 60 ℃ and 50 MPa (estimated alteration conditions), reproduces sulfide assemblages, fO_2 changes and Mg and Fe mobility.

3.1 Introduction

Alteration of mantle peridotite is an important part of the global geochemical cycle. Peridotite minerals, mainly olivine ($(Mg,Fe)_2SiO_4$) and pyroxenes ($(Ca,Mg,Fe)_2Si_2O_6$), are far from equilibrium in Earth's near surface conditions, and are altered by aqueous fluids to form hydrated silicates (serpentinization), carbonates (carbonation) and oxides. Serpentinization of seafloor peridotites is a significant sink for water, carbon and sulfur (Alt and Shanks 1998; Alt et al. 2013; Barnes and Sharp 2006). Carbonation of peridotites is an important part of the present carbon cycle (e.g. Alt et al. 2013; Kelemen and Manning 2015; Schwarzenbach et al. 2013), and could be accelerated to achieve significant capture and storage of anthropogenic carbon emissions (Kelemen and Matter 2008; Lackner et al. 1995; Seifritz 1990).

In many cases, serpentinization and carbonation of mantle peridotite are inferred to be nearly isochemical, except for addition of water and carbon dioxide (e.g. Kelemen et al. 2011; O'Hanley 1996 and references therein), though in detail there could be small changes in major element concentrations (e.g. Malvoisin 2015). Reaction pathways for serpentinization vary, depending on temperature, pressure, fluid composition, fluid/rock (W/R) ratios, and the primary mineralogy of the protolith. Serpentinization at relatively low time integrated water-rock ratios produces strongly reducing conditions (Frost 1985; McCollom and Bach 2009; Schwarzenbach, Gazel, and Caddick 2014). The resulting fluids are among the most reduced on Earth, saturated in metal alloys such as awaruite (Ni_2Fe to Ni_3Fe), wairauite (CoFe) and native copper (Cu), and sulfides such as heazlewoodite (Ni_3S_2) and polydymite (Ni_3S_4) (e.g. Klein et al. 2009; Schwarzenbach, Gazel, and Cad-

dick 2014). As fluid-rock ratios increase, the alteration system becomes fluid-dominated, resulting in more oxidizing and alkaline conditions that produce opaque mineral assemblages recording variable oxygen fugacity (e.g. Alt and Shanks 1998; Eckstrand 1975; Frost 1985; Klein et al. 2009; Schwarzenbach et al. 2012).

This paper describes the alteration sequence and geochemistry of a suite of pervasively altered mantle peridotites that record variable fO_2 over short distances (10-15cm) in Wadi Fins in a southeastern exposure of the Samail ophiolite in the Sultanate of Oman. We first describe and present data on the mineralogy and chemistry observed in the Wadi Fins rocks, and then use these data to constrain temperature, oxygen fugacity and fluid fluxes during alteration to provide insights on pervasive alteration processes of mantle peridotites relevant to multiple geological settings.

3.2 Geological Setting

The Samail ophiolite along the northeast coast of Oman is among the largest and best exposed sections of oceanic crust and its underlying mantle in the world (Coleman 1977; Lippard and Shelton 1986). It was thrust over adjacent oceanic lithosphere soon after magmatic formation of oceanic crust at a submarine spreading ridge, and then onto the margin of the Arabian subcontinent in the late Cretaceous (Hacker and Mosenfelder 1996; Nicolas et al. 2000; Rioux et al. 2013; Tilton, Hopson, and Wright 1981; Warren et al. 2005).

The mantle section of the ophiolite is mainly composed of highly depleted, residual mantle peridotites (mostly harzburgites, e.g. (Godard, Jousselin, and Bodinier 2000; Hanghøj et al. 2010; Monnier et al. 2006), together with 5 to 15% dunite (Boudier and Coleman 1981; Braun and Kelemen 2002; Kelemen, Braun, and Hirth 2000), together with

refertilized lherzolites near the basal thrust (Khedr et al. 2014). These peridotites are pervasively serpentinized, with serpentine (± brucite) composing $\sim$ 30 wt% in "fresh" rock to nearly 100% (Boudier, Baronnet, and Mainprice 2010; Obeso and Kelemen 2018). Alteration occurred throughout the history of the ophiolite, beginning near the axis of the oceanic spreading ridges where the Samail ophiolite crust formed (e.g. Gregory and Taylor 1981) and continuing to the present day (e.g Clark and Fontes 1990; Kelemen and Matter 2008; Mervine et al. 2014; Neal and Stanger 1985).

The mantle peridotites were exposed by sub-aerial erosion in the late Cretaceous. They are locally capped by Late Cretaceous (Maastrichtian) laterites (Al-Khirbash 2015; Nolan et al. 1990), and elsewhere by fluvial conglomerates rich in peridotite cobbles. This was followed by a marine transgression, which deposited shallow marine carbonates over a broad region in the Arabian peninsula, including the Qahlah, Simsina and Jafnayn formations (Nolan et al. 1990). The carbonate cover is particularly extensive in the southeastern section of the ophiolite (Nolan et al. 1990; Schlüter et al. 2008). In this area, outcrops of peridotite are rare and occur only on the bottom of deep canyons like Wadi Tiwi and Wadi Fins where erosion has cut down through the Late Cretaceous unconformity. In Wadi Fins (Figure 1), peridotites below the unconformity were altered at low temperatures ($\sim$60℃ or less) and pressures (50 MPa based on thickness of the overlying sediments) (Obeso and Kelemen 2018). Serpentinizing fluids were derived from the overlying limestones, providing a source of water, calcium, carbon and silica to the rocks, sufficient to reduce bulk rock MgO/SiO_2 ratios, and form an extensive network of carbonate and serpentine-carbonate veins (Obeso and Kelemen 2018).

3.3 Analytical Methods

Analyzed samples were collected during the 2013 and 2015 field seasons in Wadi Fins, Oman (UTM 40Q 722503E 2533160N). All samples were collected from an outcrop close to the Cretaceous unconformity (Figure 1). This outcrop exhibits concentric halos of alteration with sharp oxidation gradients and an extensive network of carbonate veins (Figure 2). Hand samples were subdivided and powdered in alumina into 4 parts following the visually evident reaction fronts (Figure 2). Part 1: partially serpentinized cores (black cores); part 2: metasomatically modified peridotite (green zones), part 3: oxidized peridotite (red zones) and part 4: carbonate veins.

Powdered samples were analyzed by X-Ray diffraction (XRD) at Lamont Doherty Earth Observatory using an Olympus Terra portable XRD. Diffractograms were analyzed using Match! Software to identify main minerals.

Major element concentrations and loss on ignition (LOI) of the bulk rocks were measured at LDEO using an Agilent 720 Axial ICP-OES. Concentrations of Fe_2O_3 were determined from ICP-OES data together with FeO concentrations determined by titration. Trace elements were analyzed at LDEO using a VG PlasmaQuad ExCell quadrupole ICP-MS following HNO_3-HF digestion. Standards and analytical precision are given in tables S1 (ICP-OES) and S2 (ICP-MS).

Polished thin sections were analyzed with a standard petrographic microscope for mineral identification where possible. These thin sections were quantitatively analyzed using a 5-spectrometer Cameca SX-100 electron microprobe (EMP) at American Museum of Natural History (AMNH). Calibration information is reported in Table S3. For small

opaque minerals that were impossible to identify in reflected light, chemical compositions from EMP were essential for phase identification.

3.4 Petrology and Mineralogy

Bulk rock chemical compositions for partially serpentinized cores (black cores), metasomatically modified peridotite (green zones), and oxidized peridotite (red zones) are shown in Table 1.

Black cores

The cores of samples OM15-5, OM15-6 and OM15-7 show relict primary minerals (olivine, pyroxene and spinel) both in thin section and in difractograms, along with abundant serpentine. The major element compositions of the sample cores compared to the average (±2σ) composition of Oman harzburgite (Hanghøj et al., 2010) are shown in figure 3 using a volatile-free constant mass isocon (Grant 1986). Isocons are designed to detect concentration changes from the original rock during metasomatism. The isocon on these diagrams is a line that goes through the origin and through concentrations of major/minor elements that are thought to have no relative gain or loss of mass. FeO and SiO_2 are slightly enriched in the cores (∼4% relative) close to the upper limits of natural variability (average±2σ) reported by previous studies (Godard, Jousselin, and Bodinier 2000; Hanghøj et al. 2010; Monnier et al. 2006). This enrichment is complemented by a small depletion (∼5% relative) in MgO, with concentrations close to the lower bound of variability. All other major elements are within expected variability (Figure 3). Most trace elements measured are similar to the composition of highly depleted harzburgites and are within variability (average±2σ) reported in the ophiolite (Godard, Jousselin, and Bodinier

2000; Hanghøj et al. 2010; Monnier et al. 2006), except for Rb (∼270 ppb) with concentrations approximately ten times higher than the average of published compositions (∼30 ppb).

Electron microprobe (EMP) analyses of orthopyroxene, clinopyroxene and spinel exhibit small deviations from the composition of these minerals in other Oman harzburgites. Both orthopyroxene and clinopyroxene have low Al and Cr concentrations as well as low Cr (molar Cr/(Cr +Al)) compared to other Oman locations (Figure 4). Spinels have high Mg# (molar Mg/(Mg+Fe_{tot})) and low Cr#, with compositions toward the fertile end of spinels observed in the ophiolite (Figure 4). Average serpentine (Mg#89.1±2.8 1σ) is slightly enriched in iron compared to precursor olivine (average Mg#90.4±0.3) and orthopyroxene (average Mg#90.1±0.3) (Figure 5). paque mineralogy in the cores is dominated by Cr-spinels, plus trace quantities of sulfide minerals. Iron oxides were not detected in OM15-6, while in OM15-5 and OM15-7 magnetite is observed in thin section in trace quantities. Ni-rich pentlandite with an average stoichiometry of $(Fe_{3.1}Ni_{5.9})S_8$ was identified in all samples and is the most abundant sulfide (Figure 6) . Such high nickel contents are associated with pentlandite/heazlewoodite assemblages (Harris and Nickel 1972). End-member heazlewoodite is observed in one sample, suggesting that intergrowths of these two minerals are present in our samples. Multiple Cu bearing sulfides occur in the black cores, including chalcocite (Cu_2S), bornite (Cu_5FeS_4), and Cu-bearing pentlandites: samaniite ($Cu_2Fe_5Ni_2S_8$) and sugakiite ($Cu(Fe,Ni)_8S_8$). An obvious mixing trend in Figure 6 between pentlandite and chalcocite, suggests that these minerals are finely intergrown in these samples. Most sulfides occur along veins filled with serpentine, rather than in spatial association with primary minerals.

Green Zones

The transition from partially serpentinized peridotites (black cores) to the green zones in thin section is very sharp (Figure 2), as it is in hand samples and outcrops. Primary minerals are almost completely altered to serpentine. There are abundant bastites (serpentine pseudomorphs replacing pyroxene) as well as fine-grained serpentine with characteristic mesh textures intergrown with a fine-grained mineral with high birefringence likely talc. Thin sections show a relatively high abundance of microcrystalline, equant to slightly elongated diopside compared to the black cores. Diffractograms of all samples are noisy with high backgrounds at low 2θ and some poorly-defined, broad peaks suggesting low crystallinity (Supplementary Figure 1). A small broad peak at 8.8° 2θ in samples OM15-5 and OM15-7 and a larger peak at 6.2° in OM15-6 confirms the presence of clay minerals: montmorillonite and stevensite (Mg-montmorillonite) coexisting with lizardite. The proportions of these end-members are very uniform and close to 1:1 (Figure 7), which may reflect alternating serpentine and stevensite layers on the scale of the unit cell (Faust and Fahey 1962).

The bulk rock composition of the green zone samples (Figure 3 and Table 1) shows enrichments of SiO_2 (∼16%), CaO (∼150%) and Al_2O_3 (∼80%), and depletion of MgO (∼20%) and FeO (∼17%), compared to the black cores, if constant, volatile-free mass is assumed. The high abundance of diopside in thin section and the relative enrichment in CaO suggest that some of the observed diopside is secondary in origin. Some EMP analyses of serpentine are nearly stoichiometric, and with similar iron contents as serpentines in the cores Mg (avg 88±4.5) similar to serpentines in the black cores. Several EMP analyses with low

total oxides (73 to 88wt%) with molar (Mg+Fe)/Si close to 1 probably represent serpentine intergrown stevensite. This assemblage has previously been described as “deweylite” (Beinlich et al. 2012; Faust and Fahey 1962). Sr, Rb, and U are enriched in the green zones by a factor of 10 compared to the black cores.

Sulfides occur in trace quantities in the green zones. The sulfide assemblages (Figure 6) have high Ni/Fe compared to those in the black cores, and have low metal/sulfur ratios. Sulfides include godlevskite (Ni_9S_8), millerite (NiS), and siegenite $(Ni,Co)_3S_4$. Cu-pentlandite and chalcopyrite ($CuFeS_2$) are the main Cu bearing sulfides identified in the green zones, and are in close proximity to the black cores. Heazlewoodite is not observed in the green zones.

Red Zones

Like the transition from black cores to green zones, the transition from green to red zones is also sharp in outcrop, hand sample and thin section (figure 2). The red, oxidized zones are characterized by the occurrence of goethite (FeO(OH)), lizardite and stevensite as the main minerals identified by XRD. With the assumption of constant volatile-free mass, when compared to the black zones, bulk rock composition (Figure 3 and Table 1) does not show significant enrichments in SiO_2 or CaO, unlike the green zones. The isocon diagram does show a significant enrichment in FeO ($\sim$50% relative) and Al_2O_3 ($\sim$80% relative) and depletion of MgO ($\sim$20% relative) compared to the black cores, if constant, volatile-free mass is assumed. Goethite is so finely intergrown with the stevensite/lizardite matrix that no pure microprobe analyses were obtained. Instead, analyses form a mixing line from the stevensite/lizardite assemblages towards goethite (Figure 7).

Serpentines in the red zones are significantly more iron rich that the cores and the green zones (Avg Mg#74±11). Sr and Rb have an enrichment of 10x compared to the black cores, as in the green zones. U in red zones of samples OM15-5 and OM15-7 is enriched up to ∼600x relative to the cores. Only Ni sulfides, godlevskite, millerite and siegenite, were identified in the red zones.

Carbonate and Serpentine veins

Veins of carbonate ± serpentine are a striking feature of the outcrops (Figure 2). These are similar to the veins described by de Obeso and Kelemen (2018), from outcrops a few hundred meters east (downstream) from the sample locality described in this paper. The wider carbonates veins (∼1-2 cm) have carbonate, mainly calcite, with minor dolomite bands (∼100μm) along contacts with altered peridotite. The oxidized, red zones described above usually surround these wider veins. Smaller (<1 cm thick) veins composed of pure carbonate minerals (mainly calcite with minor dolomite close to contacts with peridotite) extend from the wider veins into the green zones and less-altered black cores. The branching and cross-cutting veins form right angle intersections in outcrop, creating a pattern of hierarchical fractures which has been associated with volume change during serpentinization and carbonation (Iyer et al. 2008; Kelemen and Hirth 2012; O'Hanley 1992).

3.5 Thermodynamic modelling

Model Setup

Using the petrological and mineralogical constraints described above we used a modified version of de Obeso and Kelemen (2018) EQ3/6 model of hydrous fluids reacting with

peridotite (Wolery and Jarek 2003). The model is run at 50 MPa and 60 ℃, the maximum alteration temperature estimated for Wadi Fins based on clumped isotope data (Obeso and Kelemen 2018). In addition to major oxides we included Ni, S and Cu in the model system. For all calculations we used a modified version of Klein et al. EQ3/6 thermodynamic database (Klein et al. 2009). We added stevensite ($Mg_3Si_4O_10(OH)_2{\cdot}6(H_2O)$) to the database using logKs reported in Supplementary Table 9. The same database was used to built phase diagrams for the Fe-Ni-Cu-O-S system at 60℃ using Geochemist Workbench 12.0.2. Secondary minerals allowed to precipitate along the reaction path are listed in Supplementary Table 10.

The model has five main stages. In the first, 1 kg of simulated Cretaceous seawater (Supplementary Table 11) is speciated at 25℃ using EQ3. In the second stage, the speciated seawater is heated to 60℃ and then equilibrates with calcite and quartz in a closed system, to approximate pore water in the SiO_2-bearing limestones overlying peridotites in the area. Assumptions regarding source fluid composition are based on the $^{87}Sr/^{86}Sr$ of the calcite veins in our samples. $^{87}Sr/^{86}Sr$ is higher than in the limestone immediately above the unconformity, and higher than in seawater during the time of formation of the unconformity (Obeso and Kelemen 2018), and instead corresponds approximately to the Sr isotope ratio in seawater at the Cretaceous-Paleocene boundary, and in overlying limestones of that age tens of meters above the unconformity (McArthur, Howarth, and Shields 2012; Schlüter et al. 2008) . In the third stage, the resulting fluid reacts with rock with the composition of OM15-6 core using EQ6 with special reactant mode in a titration system at 60℃. (We also ran models in reaction path mode, which yielded very similar results). The fourth stage models an open system in which the most evolved fluids from the

third stage react with secondary minerals precipitated over the reaction path, to simulate fluids flowing through black cores and back into more altered rocks, while reacting with the alteration phases that were precipitated along the Stage 3 reaction path. Results from the third and fourth stages of the model are reported as a function of water-rock mass ratios (W/R), following literature convention (Klein et al. 2009; Palandri and Reed 2004). The evolved fluids from stage 4 are finally mixed with initial seawater in stage 5.

Model Results

The results from Stage 3 of model are shown in Figure 8. Serpentine is the most abundant mineral along the entire reaction path. Fe^{3+} is incorporated into serpentine down to a water rock ratio of about 4. As W/R decreases, diopside and stevensite precipitate while some Fe^{2+} is incorporated into serpentine. Calcite is predicted in the equilibrium mineral assemblage at W/R > 500, along with stevensite and serpentine. W/R < 10 is characterized by precipitation of serpentine, magnesite, secondary diopside and minor stevensite. Sulfide and oxide minerals follow changing fO_2 and fS_2 as W/R increases (Figure 12). At W/R > 800, sulfur is oxidized and is present as dissolved sulfate rather than sulfide minerals, and fS_2 is very low. Millerite is predicted to precipitate when W/R is between 800 and 10. Chalcopyrite forms at W/R > 3, whereas bornite is precipitated at lower W/R. Pentlandite coexisting with heazlewoodite and bornite is replaced by awaruite at W/R close to 1.

Fe is almost completely insoluble at high W/R, where fO_2 is high. In contrast, iron is mobile in the system at W/R between 1000 and 10, and particularly between 1000 and 100. Fe and Mg are about four orders of magnitude more soluble, and SiO_2 is two orders

of magnitude more soluble, above W/R of 10, compared to their solubility at lower W/R. W/R ratios below 10 are characterized by nearly constant fluid composition.

Stage 4 is characterized by the conversion of serpentine to stevensite. Up to 10% of the Stage 3 serpentine reacts to stevensite at W/R close to 5 (Figure 10), and - compared to the final fluid from Stage 3 - the Stage 4 fluid is enriched in Fe (16%) and Mg (64%) and depleted in SiO_2 (20%). Further reaction of the Stage 3 final fluid with stevensite and serpentine result in formation of progressively more stevensite at the expense of serpentine, enriching the Stage 4 mineral assemblage in SiO_2 (3 μmol of serpentine per kg of water). The final Stage 4 fluid, enriched in Fe and Mg (relative to stage 3 evolved fluid), precipitates all its Fe as goethite when mixed with seawater in stage 5.

3.6 Discussion

Petrogenesis of the Wadi Fins protolith

Wadi Fins harzburgites are residues of partial melting and melt extraction, similar to harzburgites from other areas of the ophiolite (Godard, Jousselin, and Bodinier 2000; Hanghøj et al. 2010; Monnier et al. 2006) and as depleted as the most depleted abyssal peridotites (Bodinier and Godard 2007; Dick 1989; Godard et al. 2008; Johnson and Dick 1992; Johnson, Dick, and Shimizu 1990; Niu 2004; Paulick et al. 2006). However, spinel Cr#'s in Wadi Fins lie within the low end of the field defined by spinels from the Oman harzburgites, some with values as low as Cr#=15 (Figure 4). Cr in opx and cpx are also relatively low, averaging 11 in cpx and 7 in opx. By comparison, pyroxene Cr#'s in typical Samail harzburgites range from 9 to 30 in cpx (Avg. 18) and 8 to 22 in opx (Avg. 16). While the low Cr#'s in these minerals are similar to those in fertile basal lherzolites (11

to 25 in spinel (Avg. 15), 8 to 11 in cpx (Avg. 9) and 6 to 11 in opx (Avg. 8)) (Khedr et al. 2014), average concentrations of Al and Cr in cpx and opx from Wadi Fins are lower than any previously reported concentrations in Samail harzburgites (Supplementary Tables 5 and 6). Temperatures estimated using the Brey Kohler (1990) Ca in orthopyroxene and two pyroxene thermometers, and the Witt-Eicksen Seck (1991) Al in orthopyroxene thermometer, suggest that Wadi Fins harzburgites equilibrated at temperatures ∼800℃ (Table 2). Closure temperatures and cooling rates in harzburgites in the Wadi Tayin massif of the Samail ophiolite, the nearest large massif to Wadi Fins, decrease systematically with depth away from the paleo-Moho (Dygert, Kelemen, and Liang 2017; Hanghøj et al. 2010) This observation, together with low equilibration temperatures in Wadi Fins and low Cr, suggest that these harzburgites cooled slowly deep in the mantle section, allowing for extensive Al transfer from pyroxenes to spinel. Growth of additional spinel during subsolidus cooling and re-equilibration provided a sink for both Al and Cr from pyroxenes.

Low W/R serpentinization recorded in the black cores

Serpentinization reactions combine ultramafic rocks with hydrous fluid, commonly forming serpentine, brucite, magnetite and hydrogen (review by Moody (1976) and references therein). However, in detail the mineral products depend on the original protolith, water to rock ratios (W/R), temperature, pressure and fluid composition (e.g. Bach et al. 2004; Frost 1985; Frost and Beard 2007; Klein et al. 2009, 2014; Schwarzenbach, Gazel, and Caddick 2014). At W/R ratios close to 1, Fe^{2+} in mantle silicates is oxidized to form magnetite or Fe^{3+}-rich serpentine, producing very low oxygen fugacities (fO_2) in the fluid,

leading to dissociation of H_2O to form H_2 (e.g. Klein et al. 2009; Neal and Stanger 1983; Sleep et al. 2004). While olivine is actively serpentinizing fO_2 is buffered to extremely low values such this reaction Frost and Beard 2007.

In his classic paper, Frost (1985) proposed that sulfide-oxide assemblages in Fe-Ni-S-O-H system record the redox conditions during serpentinization. This approach was further developed and applied by Klein and Bach (2009). More recently, Schwarzenbach et al. (2014) added copper-bearing sulfides to constrain redox conditions in the Cu-Fe-S-O-H system. Based on this prior work, the Fe-Ni-Cu sulfide assemblages in the cores of Wadi Fins samples, pentlandite-heazlewoodite (Figure 6), are characteristic of serpentinization at low W/R. Stage 3 modeling predicts mineral assemblages consistent with the sulfide assemblages in the black cores (heazlewoodite-pentlandite-bornite; Figure 9) at W/R less than 3. Phase equilibrium constraints and model calculations indicate that these assemblages formed at extremely low fO_2, at or near the dissociation limit for H_2O to H_2, together with fS_2 just above the limits for stability of native metals (awaruite and copper). The lack of native copper and awaruite in the cores is consistent with low alteration temperatures, as their stability fields in fO_2 vs fS_2 space shift to lower fugacities at low temperature, compared to those calculated at higher temperatures in previous studies.

Non-isochemical behavior and increased fO_2 in green and red zones

Serpentinization is commonly inferred to be nearly isochemical except for the addition of water (e.g. O'Hanley 1996; Shervais, Kolesar, and Andreasen 2005 and references therein), though this is not always accurate in detail (Malvoisin 2015; Merino 2013; Merino and Canals 2011; Monnier et al. 2006). Addition of H_2O, without substantial removal of

other components, together with decreasing density as the mineralogy is transformed from olivine + pyroxene to serpentine ± brucite, clays, iron oxides, requires substantial volume increases when compared to the original rock (Coleman and Keith 1971; Macdonald and Fyfe 1985). Nearly isochemical alteration is inferred for the partially serpentinized, black cores in Wadi Fins, because their Mg/Si/Fe ratios are similar to average Samail harzburgites and residual peridotites worldwide (e.g. Coleman and Keith 1971; Falk and Kelemen 2015). This inference is consistent with the results of our Stage 3 thermodynamic models at low W/R, which predict mineral assemblages similar to the black cores, insignificant changes in anhydrous rock composition and volatile-free mass, together with very large increases in the solid volume.

The green and red zones in Wadi Fins correspond to a completely different alteration process, at higher W/R. We can constrain W/R using uranium concentrations. Black cores have U concentrations similar to Oman harzburgites. In contrast, U concentrations increase dramatically, up to 10x core values in the green zones, and up to 600x core values in the red zones (Table 1). This increase correlates with changes in Fe^{3+}/Fe_{Tot} (Figure 11). If almost all of the U is derived from the seawater end-member (Deschamps et al. 2013), with $\sim$ 3 ppb U similar to modern seawater (Owens et al., 2011), then a W/R ratio of 200 or more is necessary to enrich the red zones in Wadi Fins.

The mineralogy and compositions of the green and red zones are not that of a peridotite serpentinized under nearly isochemical conditions, as shown in the isocon diagrams (Figure 3). These diagrams suggest pervasive metasomatism, leading to silica-rich and iron-rich compositions in the green and red zones, respectively. This might reflect transitional stages between partially serpentinized peridotites and laterites, such as those

observed in Wadi Tiwi (Al-Khirbash 2015).

The proportion of SiO_2 increases sharply (from 45 to 53 wt%, volatile-free) from the black cores to the green zones, and drops back sharply in the red zones to SiO_2 concentrations similar to those in the black cores. On the other hand FeO concentration decreases from the black cores to the green zones (from $\sim$ 9 to 7 wt%, volatile-free) and then increases sharply in the oxidized, red zones (to 14 wt% volatile free). Assuming immobile Al_2O_3 in the isocons for our samples results in a total loss of volatile-free mass of approximately 40% relative. Such a large mass decrease is not supported by field observations or textures at any scale, and is inconsistent with our thermodynamic modeling. Instead, assumptions of constant SiO_2 and constant volatile-free mass in the isocon for the red zones yield almost identical results, suggesting that SiO_2 is relatively immobile. Therefore we favor the assumption of quasi-constant, volatile-free mass, or immobile SiO_2, rather than immobile Al_2O_3. The assumption of constant SiO_2 yields MgO depletion of $\sim$25% relative in the green zones and 20% relative in the red zones, compared to the black cores. This is consistent with our Stage 4 models, in which MgO is leached out of the rock as serpentine reacts with final Stage 3 fluids to form stevensite.

When compared with the black zones, FeO has a depletion of $\sim$25% relative in the green zones and an enrichment of $\sim$50% relative in the red zones. Our Stage 4 model suggests that this may be derived from mobility of Fe. At low fO_2, Fe^{2+} is dissolved from the green zones, transported into the red zones, and precipitated as Fe^{3+} in goethite due to increasing fO_2, as fluids from the cores and green zones mix with oxidizing fluids.

Further evidence for iron mobility in Wadi Fins can be drawn from the intergrowth of goethite with serpentine in the red zones (Figure 7), as well as the presence of iron oxides

in the carbonate veins (E. Cooperdock, personal communication). Overall, the remobilization of FeO and leaching of MgO represent a 9% decrease in volatile-free mass (3% mass increase including volatiles) and a 15% increase in solid volume, compared to the protolith represented by the black cores. For comparison a 100% serpentinized harzburgite under isochemical conditions keeps volatile-free mass constant (∼13% mass increase from water) and requires a ∼45% increase in solid volume (Coleman and Keith 1971). Magnesium loss from highly altered peridotites has been previously inferred from the products of marine weathering (Milliken, Lynch, and Seifert 1996; Snow and Dick 1995) and has been suggested as a potential mechanism for formation of "deweylite" assemblages (Beinlich et al. 2010).

Peridotites in this area exhibit clear signs of major element mobility during open system weathering resulting in Mg loss and the formation of 1:1 stevensite:lizardite mixtures in the green and red zones, coupled with nearly isochemical alteration of the black cores that preserve partially serpentinized peridotite compositions and mineral assemblages. Variable W/R results in significant changes in mineralogy and fO_2 in different alteration zones (Figures 9 and 12). Black cores record highly reducing conditions at W/R $\sim$ 1, whereas the green and red zones record much higher W/R and fO_2. This change in fO_2 is evident based on equilibria involving sulfide minerals in the different zones (Figures 7) and from the results of thermodynamic modeling (Figures 9).

3.7 Conclusions

Altered mantle peridotites in Wadi Fins contain three distinct alteration zones that record a gradient of ∼20 orders of magnitude in fO_2 and fS_2 in sulfide/oxide min-

eralogy of over a distance of 15-20 cm. The black cores are characterized by pentlandite/heazlewoodite/bornite assemblages, recording very low oxygen fugacities. Such low fO_2 is associated with serpentinization at low W/R (Alt and Shanks 1998; Frost 1985). The black cores contain relict primary mantle minerals plus alteration products associated with low temperature, nearly isochemical serpentinization. The green zones surrounding the black cores show pervasive alteration resulting in relatively high SiO_2 concentration and a depletion of MgO and FeO, forming mixtures of stevensite and lizardite. These mixtures are present in the red zones, intergrown with goethite. Thermodynamic modeling suggests that iron and magnesium were mobilized from the green zones following serpentinization while reacting with reduced core fluids with iron precipitating when the fluids become oxidized. These mass transfer reactions combine to produce a volatile-free mass loss of 9%, together with a 15% increase in the solid volume, in the green and red zones compared to the black cores. This volume change is significantly less than calculated for isochemical serpentinization of harzburgite (constant volatile-free mass and 45% volume increase). We suspect that the marked zoning seen in this area, which is unusual in the mantle section of the Samail ophiolite, is due to the proximity of the Cretaceous unconformity. The rocks we've studied may be viewed as transitional in some ways between typical, partially serpentinized mantle peridotites in ophiolites and oceanic drill core, on the one hand, and laterites on the other.

References

Al-Khirbash, Salah (2015). "Genesis and mineralogical classification of Ni-laterites, Oman Mountains." In: *Ore Geology Reviews* 65, pp. 199–212. ISSN: 01691368. DOI: 10.1016/j.oregeorev.2014.09.022.

Alt, Jeffrey C. and Wayne C. Shanks (1998). "Sulfur in serpentinized oceanic peridotites: Serpentinization processes and microbial sulfate reduction." In: *Journal of Geophysical Research* 103.November 2015, p. 9917. ISSN: 0148-0227. DOI: 10.1029/98JB00576.

Alt, Jeffrey C. et al. (2013). "The role of serpentinites in cycling of carbon and sulfur: Seafloor serpentinization and subduction metamorphism." In: *Lithos* 178, pp. 40–54. ISSN: 00244937. DOI: 10.1016/j.lithos.2012.12.006.

Bach, Wolfgang et al. (2004). "Seawater-peridotite interactions: First insights from ODP Leg 209, MAR 15°N." In: *Geochemistry, Geophysics, Geosystems* 5.9, n/a–n/a. ISSN: 15252027. DOI: 10.1029/2004GC000744.

Barnes, Jaime D. and Zachary D. Sharp (2006). "Achlorine isotope study of DSDP/ODP serpentinized ultramafic rocks: Insights into the serpentinization process." In: *Chemical Geology* 228.4, pp. 246–265. ISSN: 00092541. DOI: 10.1016/j.chemgeo.2005.10.011.

Beinlich, Andreas et al. (2010). "CO2 sequestration and extreme Mg depletion in serpentinized peridotite clasts from the Devonian Solund basin, SW-Norway." In: *Geochimica et Cosmochimica Acta* 74.24, pp. 6935–6964. ISSN: 00167037. DOI: 10.1016/j.gca.2010.07.027.

Beinlich, Andreas et al. (2012). "Massive serpentinite carbonation at Linnajavri, N-Norway." In: *Terra Nova* 24.6, pp. 446–455. ISSN: 09544879. DOI: 10.1111/j.1365-3121.2012.01083.x.

Bodinier, J.-L. and Marguerite Godard (2007). "Orogenic, Ophiolitic, and Abyssal Peridotites." In: *Treatise on Geochemistry*, pp. 1–73. DOI: 10.1016/B0-08-043751-6/02004-1.

Boudier, Françoise, Alain Baronnet, and David Mainprice (2010). "Serpentine Mineral Replacements of Natural Olivine and their Seismic Implications: Oceanic Lizardite versus Subduction-Related Antigorite." In: *Journal of Petrology* 51.1-2, pp. 495–512. ISSN: 1460-2415. DOI: 10.1093/petrology/egp049.

Boudier, Françoise and Robert G. Coleman (1981). "Cross section through the peridotite in the Samail ophiolite, southeastern Oman Mountains." In: *Journal of Geophysical Research: ...* 86.B4, p. 2573. ISSN: 0148-0227. DOI: 10.1029/JB086iB04p02573.

Braun, Michael Geoffrey and Peter B. Kelemen (2002). "Dunite distribution in the Oman Ophiolite: Implications for melt flux through porous dunite conduits." In: *Geochemistry, Geophysics, Geosystems* 3.11, pp. 1–21. ISSN: 15252027. DOI: 10.1029/2001GC000289.

Brey, G P and T Kohler (1990). "Geothermobarometry in 4-phase lherzolites .2. New thermobarometers, and practical assessment of existing thermobarometers." In: *Journal of Petrology* 31.6, pp. 1353–1378. ISSN: 0022-3530. DOI: 10.1093/petrology/31.6.1353.

Clark, Ian D. and Jean-Charles Fontes (1990). "Paleoclimatic reconstruction in northern Oman based on carbonates from hyperalkaline groundwaters." In: *Quaternary Research* 33.3, pp. 320–336. ISSN: 00335894. DOI: 10.1016/0033-5894(90)90059-T.

Coleman, Robert G. (1977). "Geologic, Tectonic, and Petrologic Nature of Four Ophiolites." In: *Ophiolites: Ancient Oceanic Lithosphere?* Berlin, Heidelberg: Springer Berlin Heidelberg, pp. 159–198. ISBN: 978-3-642-66673-5. DOI: 10.1007/978-3-642-66673-5{_}8.

Coleman, Robert G. and T. E. Keith (1971). "A Chemical Study of Serpentinization — Burro Moutain, California." In: *Journal of Petrology* 12.2, pp. 311–328.

Deschamps, Fabien et al. (2013). "Geochemistry of subduction zone serpentinites: A review." In: *Lithos* 178, pp. 96–127. ISSN: 00244937. DOI: 10.1016/j.lithos.2013.05.019.

Dick, Henry J.B. (1989). "Abyssal peridotites, very slow spreading ridges and ocean ridge magmatism." In: *Geological Society, London, Special Publications* 42.1, 71 LP –105. DOI: 10.1144/GSL.SP.1989.042.01.06.

Dygert, Nick, Peter B. Kelemen, and Yan Liang (2017). "Spatial variations in cooling rate in the mantle section of the Samail ophiolite in Oman: Implications for formation of lithosphere at mid-ocean ridges." In: *Earth and Planetary Science Letters* 465, pp. 134–144. ISSN: 0012-821X. DOI: 10.1016/J.EPSL.2017.02.038.

Eckstrand, O R (1975). "The Dumont serpentinite; a model for control of nickeliferous opaque mineral assemblages by alteration reactions in ultramafic rocks." In: *Economic Geology* 70.1, pp. 183–201. DOI: 10.2113/gsecongeo.70.1.183.

Falk, Elisabeth S. and Peter B. Kelemen (2015). "Geochemistry and petrology of listvenite in the Samail ophiolite, Sultanate of Oman: Complete carbonation of peridotite during ophiolite emplacement." In: *Geochimica et Cosmochimica Acta* 160, pp. 70–90. ISSN: 00167037. DOI: 10.1016/j.gca.2015.03.014.

Faust, George and Joseph Fahey (1962). "The Serpentine-Group Minerals: Geological Survey Professional Paper 384-A." In: p. 99.

Frost, Ronald B. (1985). "On the stability of sulfides, oxides, and native metals in serpentinite." In: *Journal of Petrology* 26.June 1983, pp. 31–63. ISSN: 00223530. DOI: 10.1093/petrology/26.1.31.

Frost, Ronald B. and James S. Beard (2007). "On silica activity and serpentinization." In: *Journal of Petrology* 48.0, pp. 1351–1368. ISSN: 00223530. DOI: 10.1093/petrology/egm021.

Godard, Marguerite, David Jousselin, and Jean-Louis Bodinier (2000). "Relationships between geochemistry and structure beneath a palaeo-spreading centre: a study of the mantle section in the Oman ophiolite." In: *Earth and Planetary Science Letters* 180.1-2, pp. 133–148. ISSN: 0012821X. DOI: 10.1016/S0012-821X(00)00149-7.

Godard, Marguerite et al. (2008). "Geochemistry of the highly depleted peridotites drilled at ODP Sites 1272 and 1274 (Fifteen-Twenty Fracture Zone, Mid-Atlantic Ridge): Implications for mantle dynamics beneath a slow spreading ridge." In: *Earth and Planetary Science Letters* 267.3-4, pp. 410–425. ISSN: 0012-821X. DOI: 10.1016/J.EPSL.2007.11.058.

Grant, James A (1986). "The isocon diagram; a simple solution to Gresens' equation for metasomatic alteration." In: *Economic Geology* 81.8, pp. 1976–1982. DOI: 10.2113/gsecongeo.81.8.1976.

Gregory, Robert T. and Hugh P. Taylor (1981). "An oxygen isotope profile in a section of Cretaceous oceanic crust, Samail Ophiolite, Oman: Evidence for δ ¹⁸ O buffering of the oceans by deep (>5 km) seawater-hydrothermal circulation at mid-ocean ridges." In: *Journal of Geophysical Research: Solid Earth* 86.B4, pp. 2737–2755. ISSN: 01480227. DOI: 10.1029/JB086iB04p02737.

Hacker, Bradley R. and Jed L. Mosenfelder (1996). "Metamorphism and deformation along the emplacement thrust of the Samail ophiolite, Oman." In: *Earth and Planetary Science Letters* 144.3-4, pp. 435–451. ISSN: 0012821X. DOI: 10.1016/S0012-821X(96)00186-0.

Hanghøj, Karen et al. (2010). "Composition and Genesis of Depleted Mantle Peridotites from the Wadi Tayin Massif, Oman Ophiolite; Major and Trace Element Geochemistry, and Os Isotope and PGE Systematics." In: *Journal of Petrology* 51.1-2, pp. 201–227. ISSN: 0022-3530. DOI: 10.1093/petrology/egp077.

Harris, D C and E H Nickel (1972). "Pentlandite compositions and associations in some mineral deposits." In: *The Canadian Mineralogist* 11.4, pp. 861–878.

Iyer, K. et al. (2008). "Reaction-assisted hierarchical fracturing during serpentinization." In: *Earth and Planetary Science Letters* 267.3-4, pp. 503–516. ISSN: 0012821X. DOI: 10.1016/j.epsl.2007.11.060.

Johnson, Kevin T.M. and Henry J.B. Dick (1992). "Open system melting and temporal and spatial variation of peridotite and basalt at the Atlantis II Fracture Zone." In: *Journal*

of Geophysical Research: Solid Earth 97.B6, pp. 9219–9241. ISSN: 0148-0227. DOI: 10.1029/92JB00701.

Johnson, Kevin T.M., Henry J.B. Dick, and Nobumichi Shimizu (1990). "Melting in the oceanic upper mantle: An ion microprobe study of diopsides in abyssal peridotites." In: *Journal of Geophysical Research: Solid Earth* 95.B3, pp. 2661–2678. ISSN: 0148-0227. DOI: 10.1029/JB095iB03p02661.

Kelemen, Peter B., Michael Geoffrey Braun, and Greg Hirth (2000). "Spatial distribution of melt conduits in the mantle beneath oceanic spreading ridges: Observations from the Ingalls and Oman ophiolites." In: *Geochemistry, Geophysics, Geosystems* 1.7, n/a–n/a. ISSN: 15252027. DOI: 10.1029/1999GC000012.

Kelemen, Peter B. and Greg Hirth (2012). "Reaction-driven cracking during retrograde metamorphism: Olivine hydration and carbonation." In: *Earth and Planetary Science Letters* 345-348, pp. 81–89. ISSN: 0012821X. DOI: 10.1016/j.epsl.2012.06.018.

Kelemen, Peter B. and Craig E. Manning (2015). "Reevaluating carbon fluxes in subduction zones, what goes down, mostly comes up." In: *Proceedings of the National Academy of Sciences* 112.30, E3997–E4006. DOI: 10.1073/pnas.1507889112.

Kelemen, Peter B. and Jürg M. Matter (2008). "In situ carbonation of peridotite for CO2 storage." In: *Proceedings of the National Academy of Sciences* 105.45, pp. 17295–17300. ISSN: 0027-8424. DOI: 10.1073/pnas.0805794105.

Kelemen, Peter B. et al. (2011). "Rates and Mechanisms of Mineral Carbonation in Peridotite: Natural Processes and Recipes for Enhanced, in situ CO 2 Capture and Storage." In: *Annual Review of Earth and Planetary Sciences* 39.1, pp. 545–576. ISSN: 0084-6597. DOI: 10.1146/annurev-earth-092010-152509.

Khedr, Mohamed Zaki et al. (2014). "Chemical variations of abyssal peridotites in the central Oman ophiolite: Evidence of oceanic mantle heterogeneity." In: *Gondwana Research* 25.3, pp. 1242–1262. ISSN: 1342-937X. DOI: 10.1016/J.GR.2013.05.010.

Klein, Frieder and Wolfgang Bach (2009). "Fe-Ni-Co-O-S phase relations in peridotite-seawater interactions." In: *Journal of Petrology* 50.1, pp. 37–59. ISSN: 00223530. DOI: 10.1093/petrology/egn071.

Klein, Frieder et al. (2009). "Iron partitioning and hydrogen generation during serpentinization of abyssal peridotites from 15°N on the Mid-Atlantic Ridge." In: *Geochimica et Cosmochimica Acta* 73.22, pp. 6868–6893. ISSN: 00167037. DOI: 10.1016/j.gca.2009.08.021.

Klein, Frieder et al. (2014). "Magnetite in seafloor serpentinite—Some like it hot." In: *Geology* 42, pp. 135–138. ISSN: 0091-7613. DOI: 10.1130/g35068.1.

Lackner, Klaus S. et al. (1995). "Carbon dioxide disposal in carbonate minerals." In: *Energy* 20.11, pp. 1153–1170. ISSN: 03605442. DOI: 10.1016/0360-5442(95)00071-N.

Lippard, S.J. and A.W. Shelton (1986). "Chapter 4 Ophiolite Detachment, Emplacement and Subsequent Deformation." In: *Geological Society, London, Memoirs* 11.1, pp. 140–165. ISSN: 0435-4052. DOI: 10.1144/GSL.MEM.1986.011.01.04.

Macdonald, A.H. and W.S. Fyfe (1985). "Rate of serpentinization in seafloor environments." In: *Tectonophysics* 116.1-2, pp. 123–135. ISSN: 00401951. DOI: 10.1016/0040-1951(85)90225-2.

Malvoisin, Benjamin (2015). "Mass transfer in the oceanic lithosphere: Serpentinization is not isochemical." In: *Earth and Planetary Science Letters* 430, pp. 75–85. ISSN: 0012821X. DOI: 10.1016/j.epsl.2015.07.043.

McArthur, J M, R J Howarth, and G A Shields (2012). "Chapter 7 - Strontium Isotope Stratigraphy BT - The Geologic Time Scale." In: Boston: Elsevier, pp. 127–144. ISBN: 978-0-444-59425-9. DOI: http://dx.doi.org/10.1016/B978-0-444-59425-9.00007-X.

McCollom, Thomas M. and Wolfgang Bach (2009). "Thermodynamic constraints on hydrogen generation during serpentinization of ultramafic rocks." In: *Geochimica et Cosmochimica Acta* 73.3, pp. 856–875. ISSN: 00167037. DOI: 10.1016/j.gca.2008.10.032.

Merino, E (2013). "Kinetic-rheological insights uncovered by the self-accelerating brucite-for-periclase replacement-but only if adjusted on volume. The blind spot of geochemists." In: *AGU Fall Meeting Abstracts*. Vol. 1, p. 2317.

Merino, E and A Canals (2011). "Spontaneous transition of replacive to displacive growth of dolomite in burial dolomitization, and of serpentine in serpentinization." In: *AGU Fall Meeting Abstracts*. Vol. 1, p. 4.

Mervine, Evelyn M. et al. (2014). "Carbonation rates of peridotite in the Samail Ophiolite, Sultanate of Oman, constrained through 14C dating and stable isotopes." In: *Geochimica et Cosmochimica Acta* 126, pp. 371–397. ISSN: 00167037. DOI: 10.1016/j.gca.2013.11.007.

Milliken, K L, F L Lynch, and K E Seifert (1996). "Marine weathering of serpentinites and serpentinite breccias, Sites 897 and 899, Iberia Abyssal Plain." In: *PROCEEDINGS-OCEAN DRILLING PROGRAM SCIENTIFIC RESULTS*. NATIONAL SCIENCE FOUNDATION, pp. 529–540. ISBN: 0884-5891.

Monnier, Christophe et al. (2006). "Along-ridge petrological segmentation of the mantle in the Oman ophiolite." In: *Geochemistry, Geophysics, Geosystems* 7.11, n/a–n/a. ISSN: 15252027. DOI: 10.1029/2006GC001320.

Moody, Judith B. (1976). "Serpentinization: a review." In: *Lithos* 9.2, pp. 125–138. ISSN: 00244937. DOI: 10.1016/0024-4937(76)90030-X.

Neal, C. and G. Stanger (1983). "Hydrogen generation from mantle source rocks in Oman." In: *Earth and Planetary Science Letters* 66, pp. 315–320. DOI: 10.1016/0012-821X(83)90144-9.

Neal, C. and G. Stanger (1985). "Past and present serpentinization of ultramafic rocks: An example from the Semail ophiolite nappe of northern Oman." In: *The Chemistry of Weathering*. Ed. by JI Drewer. Dordrecht, Holland: D. Reidel Publishing Company, 249–275.

Nicolas, Adolphe et al. (2000). "Accretion of Oman and United Arab Emirates ophiolite–Discussion of a new structural map." In: *Marine Geophysical Researches*, pp. 147–179. DOI: 10.1023/A:1026769727917.

Niu, Yaoling (2004). "Bulk-rock Major and Trace Element Compositions of Abyssal Peridotites: Implications for Mantle Melting, Melt Extraction and Post-melting Processes Beneath Mid-Ocean Ridges." In: *Journal of Petrology* 45.12, pp. 2423–2458. ISSN: 1460-2415. DOI: 10.1093/petrology/egh068.

Nolan, S. C. et al. (1990). "Maastrichtian to early Tertiary stratigraphy and palaeogeography of the Central and Northern Oman Mountains." In: *Geological Society, London, Special Publications* 49.1, pp. 495–519. ISSN: 0305-8719. DOI: 10.1144/GSL.SP.1992.049.01.31.

O'Hanley, David S. (1992). "Solution to the volume problem in serpentinization." In: *Geology* 20.8, p. 705. ISSN: 0091-7613. DOI: 10.1130/0091-7613(1992)020<0705:STTVPI>2.3.CO;2.

O'Hanley, David S. (1996). *Serpentinites: Records of Tectonic and Petrological History*. New York and Oxford: Oxford University Press, p. 227. ISBN: 0-19-508254-0.

Obeso, Juan Carlos de and Peter B. Kelemen (2018). "Fluid rock interactions on residual mantle peridotites overlain by shallow oceanic limestones: Insights from Wadi Fins, Sultanate of Oman." In: *Chemical Geology*. ISSN: 0009-2541. DOI: 10.1016/J.CHEMGEO.2018.09.022.

Palandri, James L and Mark H Reed (2004). "Geochemical models of metasomatism in ultramafic systems: serpentinization, rodingitization, and sea floor carbonate chim-

ney precipitation." In: *Geochimica et Cosmochimica Acta* 68.5, pp. 1115–1133. ISSN: 00167037. DOI: 10.1016/j.gca.2003.08.006.

Paulick, H. et al. (2006). "Geochemistry of abyssal peridotites (Mid-Atlantic Ridge, 15°20′N, ODP Leg 209): Implications for fluid/rock interaction in slow spreading environments." In: *Chemical Geology* 234.3-4, pp. 179–210. ISSN: 00092541. DOI: 10.1016/j.chemgeo.2006.04.011.

Rioux, Matthew et al. (2013). "Tectonic development of the Samail ophiolite: High-precision U-Pb zircon geochronology and Sm-Nd isotopic constraints on crustal growth and emplacement." In: *Journal of Geophysical Research: Solid Earth* 118.5, pp. 2085–2101. ISSN: 21699313. DOI: 10.1002/jgrb.50139.

Schlüter, M. et al. (2008). "Evolution of a Maastrichtian–Paleocene tropical shallow-water carbonate platform (Qalhat, NE Oman)." In: *Facies* 54.4, pp. 513–527. ISSN: 0172-9179. DOI: 10.1007/s10347-008-0150-8.

Schwarzenbach, Esther M., Esteban Gazel, and Mark J. Caddick (2014). "Hydrothermal processes in partially serpentinized peridotites from Costa Rica: evidence from native copper and complex sulfide assemblages." In: *Contributions to Mineralogy and Petrology* 168. ISSN: 0010-7999. DOI: 10.1007/s00410-014-1079-2.

Schwarzenbach, Esther M. et al. (2012). "Sulfur geochemistry of peridotite-hosted hydrothermal systems: Comparing the Ligurian ophiolites with oceanic serpentinites." In: *Geochimica et Cosmochimica Acta* 91, pp. 283–305. ISSN: 00167037. DOI: 10.1016/j.gca.2012.05.021.

Schwarzenbach, Esther M. et al. (2013). "Serpentinization and carbon sequestration: A study of two ancient peridotite-hosted hydrothermal systems." In: *Chemical Geology* 351, pp. 115–133. ISSN: 00092541. DOI: 10.1016/j.chemgeo.2013.05.016.

Seifritz, W (1990). "CO2 disposal by means of silicates." In: *Nature* 345, p. 486.

Shervais, John W., Peter Kolesar, and Kyle Andreasen (2005). "A Field and Chemical Study of Serpentinization—Stonyford, California: Chemical Flux and Mass Balance." en. In: *International Geology Review* 47.1, pp. 1–23. ISSN: 0020-6814. DOI: 10.2747/0020-6814.47.1.1.

Sleep, Norman H. et al. (2004). "H2-rich fluids from serpentinization: geochemical and biotic implications." In: *Proceedings of the National Academy of Sciences of the United States of America* 101, pp. 12818–12823. ISSN: 0027-8424. DOI: 10.1073/pnas.0405289101.

Snow, Jonathan E. and Henry J.B. Dick (1995). "Pervasive magnesium loss by marine weathering of peridotite." In: *Geochimica et Cosmochimica Acta* 59.20, pp. 4219–4235. ISSN: 00167037. DOI: 10.1016/0016-7037(95)00239-V.

Tilton, G. R., C. a. Hopson, and J. E. Wright (1981). "Uranium-lead isotopic ages of the Samail Ophiolite, Oman, with applications to Tethyan ocean ridge tectonics." In: *Journal of Geophysical Research* 86.B4, p. 2763. ISSN: 0148-0227. DOI: 10.1029/JB086iB04p02763.

Warren, Clare J et al. (2005). "Dating the geologic history of Oman's Semail ophiolite: insights from U-Pb geochronology." In: *Contributions to Mineralogy and Petrology* 150.4, pp. 403–422. ISSN: 1432-0967. DOI: 10.1007/s00410-005-0028-5.

Witt-Eickschen, G. and H. A. Seck (1991). "Solubility of Ca and Al in orthopyroxene from spinel peridotite: an improved version of an empirical geothermometer." In: *Contributions to Mineralogy and Petrology* 106.4, pp. 431–439. ISSN: 00107999. DOI: 10.1007/BF00321986.

Wolery, T J and R L Jarek (2003). "EQ3/6, version 8.0—software user's manual." In: *Civilian Radioactive Waste Management System, Management & Operating Contractor. Sandia National Laboratories, Albuquerque, New Mexico.*

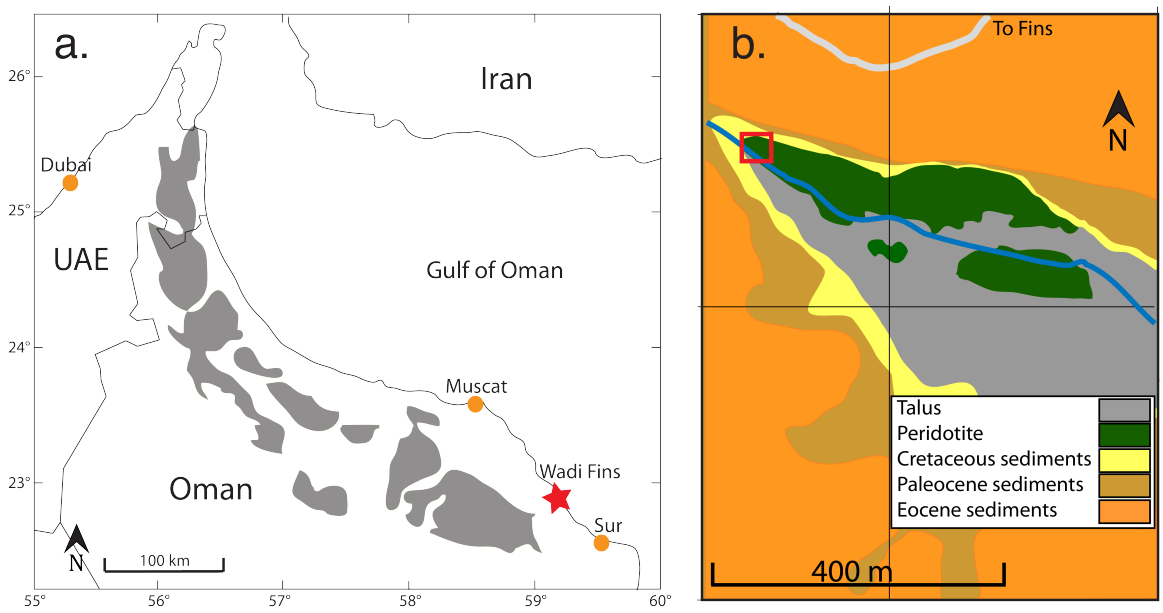

Figure 3.1: (a) Map of the Samail ophiolite after Hanghøj et al. (2010). Red star shows location of Wadi Fins. (b) Geologic map of Wadi Fins compiled from (Wyns et al. 1992b), Google Earth data, and field observations. Red square marks location of samples described in this study. Map area is between UTM coordinates 2,532,838 to 2,533,636 m N and 721,824 to 722,181 m E in zone 40 Q

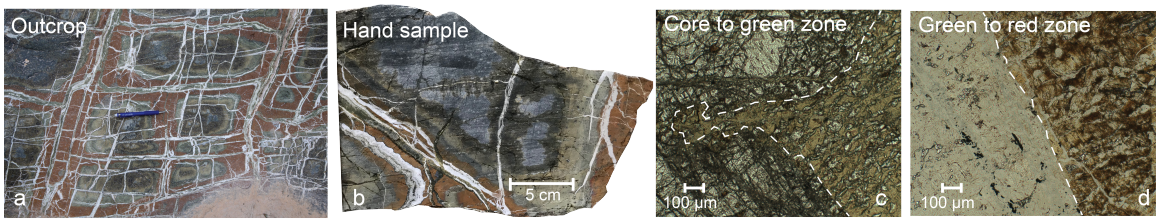

Figure 3.2: Contacts between alteration zones in Wadi Fins, Oman. (a) Peridotite outcrop close to the unconformity with overlying limestones, with sharp reactive fronts in a concentric pattern, and a spatially associated carbonate vein network. Pen for scale. (b) OM15-7 hand sample. (c) Photomicrograph of contact between core and green zone in sample OM15-7 (d) Photomicrograph of contact between green and red zone in sample OM15-7. Photomicrographs in plain polarized light. Dashed white lines emphasize contacts between zones.

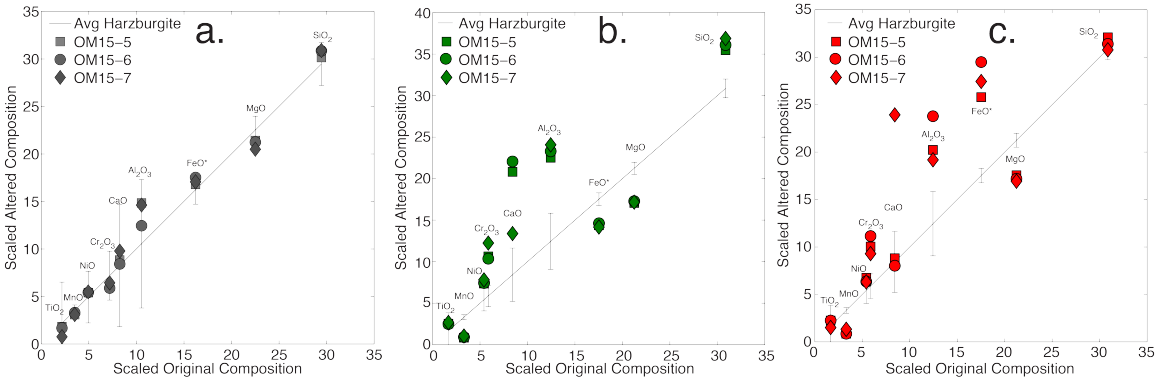

Figure 3.3: Isocon diagram for black cores (a) using average Oman harzburgite (Godard, Jousselin, and Bodinier 2000; Hanghøj et al. 2010; Monnier et al. 2006) as the protolith. Green zones (b) and red zones (c) using OM15-6 core as protolith. Elements were scaled to plot within recommended isocon limits. From left to right: TiO_2 (x100), MnO (x27), NiO (x17) Cr_2O_3 (x17), Al_2O_3 (x12), CaO (x8), FeO* (x2), SiO_2 (x0.66), MgO (x0.5). All data are plotted on a volatile-free basis.

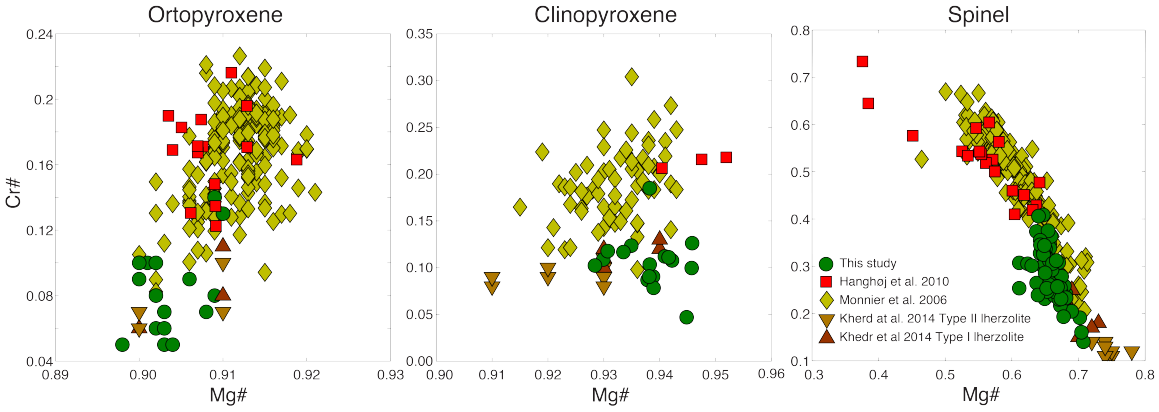

Figure 3.4: Primary mineral Cr# vs Mg# for Wadi Fins partially serpentinized cores and peridotites from other areas of the ophiolite. .

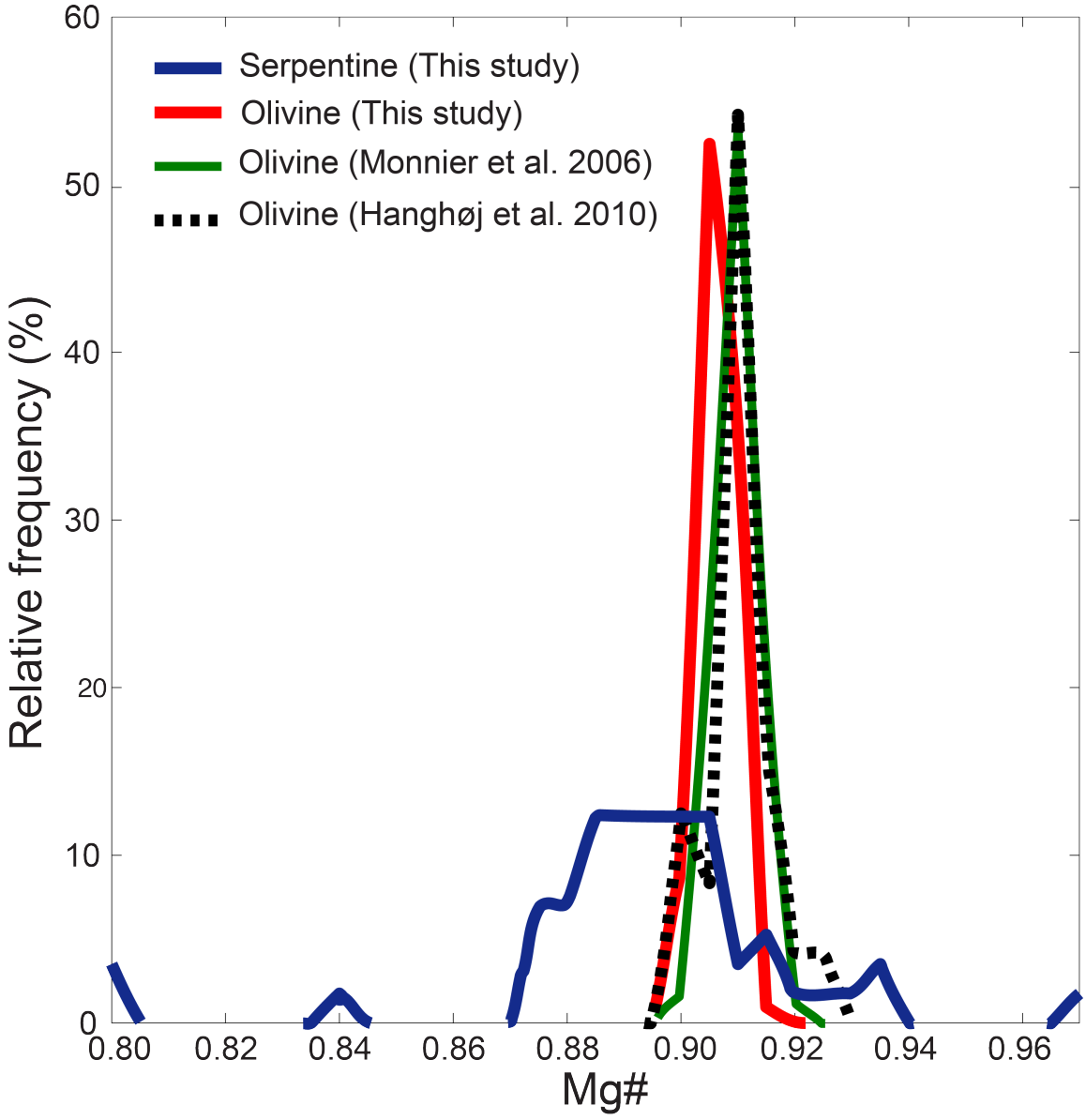

Figure 3.5: Frequency of Mg# in serpentine (blue, n=57) and olivine (red, n=103) from partially serpentinized black cores and literature olivine data: Monnier et al. 2006 (Green, n=171) and Hanghøj et al. 2010 (Black, n=106).

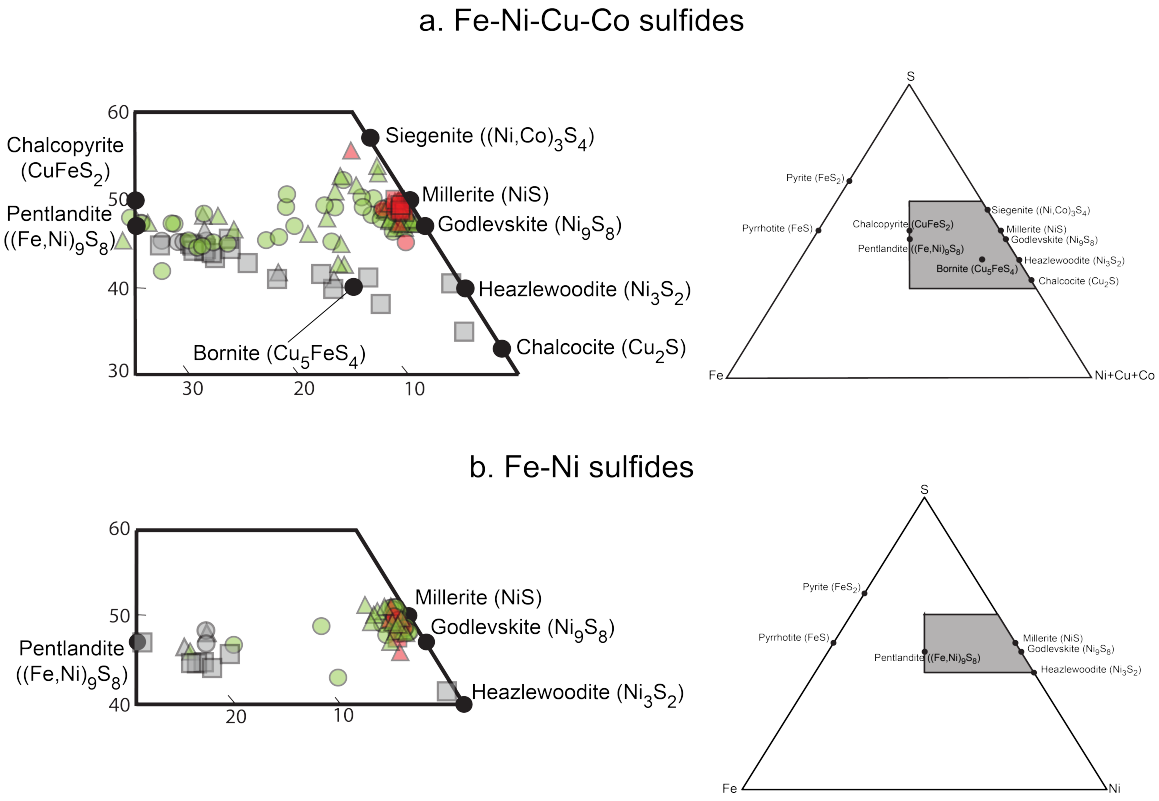

Figure 3.6: Mole fraction ternary diagram of sulfide composition in cores (gray), green zones (green) and red zones (red) in samples OM15-5 (circles), OM15-6 (squares) and OM15-7 (triangles).

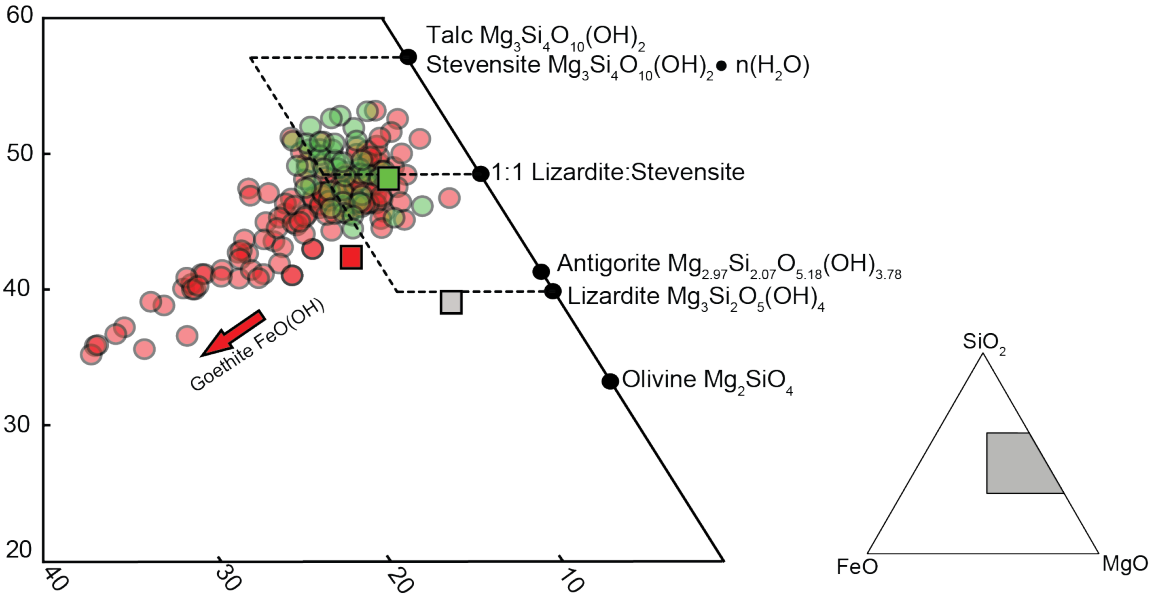

Figure 3.7: Mole fraction Fe-Si-Mg ternary diagram of serpentine and stevensite compositions in green zones and red zones in circles. Squares are whole rock averages (cores in gray).

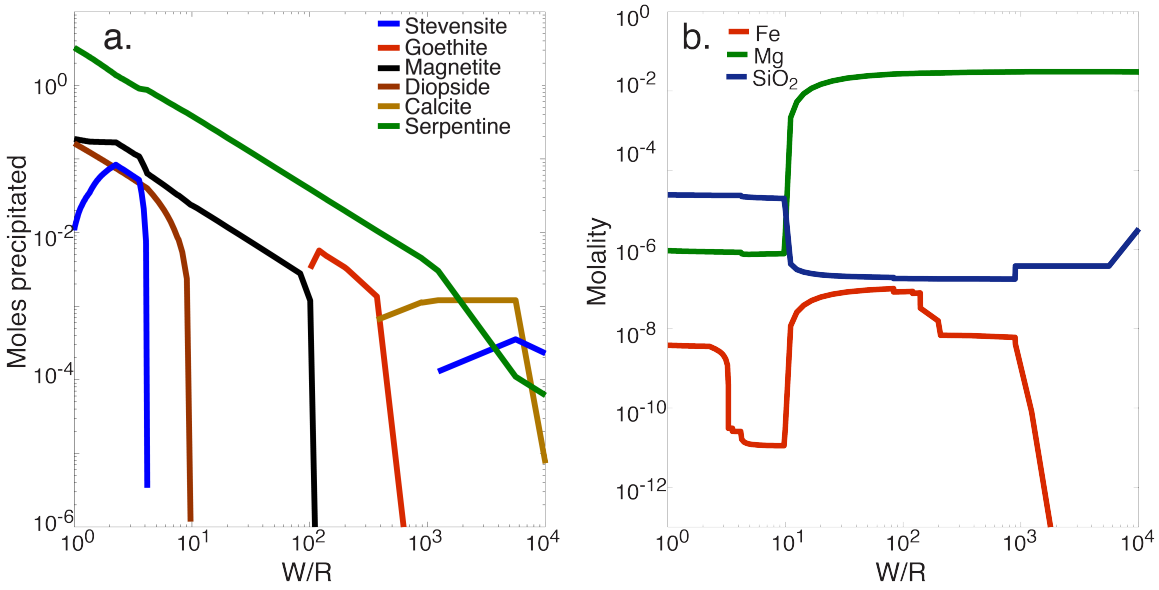

Figure 3.8: Stage 3 model results. a) Secondary mineralogy and b) fluid composition as a function of water/rock (W/R).

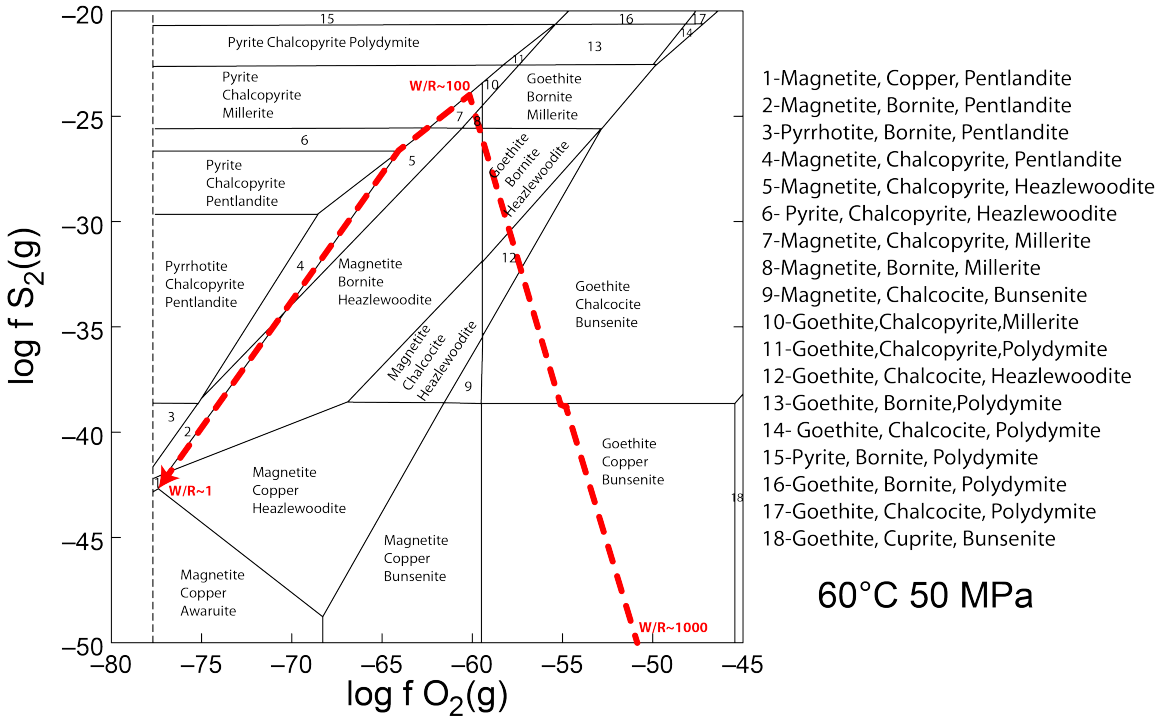

Figure 3.9: Log fO_2-log fS_2 diagram for calculated sulfide and oxide stabilities at 60℃ and 50 MPa in the system Fe-Ni-Cu-O-S. The phase diagram assumes H_2O activity to be one. All equilibrium constants come from a GWB database customized for sulfide, oxide and alloy minerals constructed using the EQ3/6 database. Red arrow shows results of Stage 3 thermodynamic modeling, pointing towards lower water/rock (W/R).

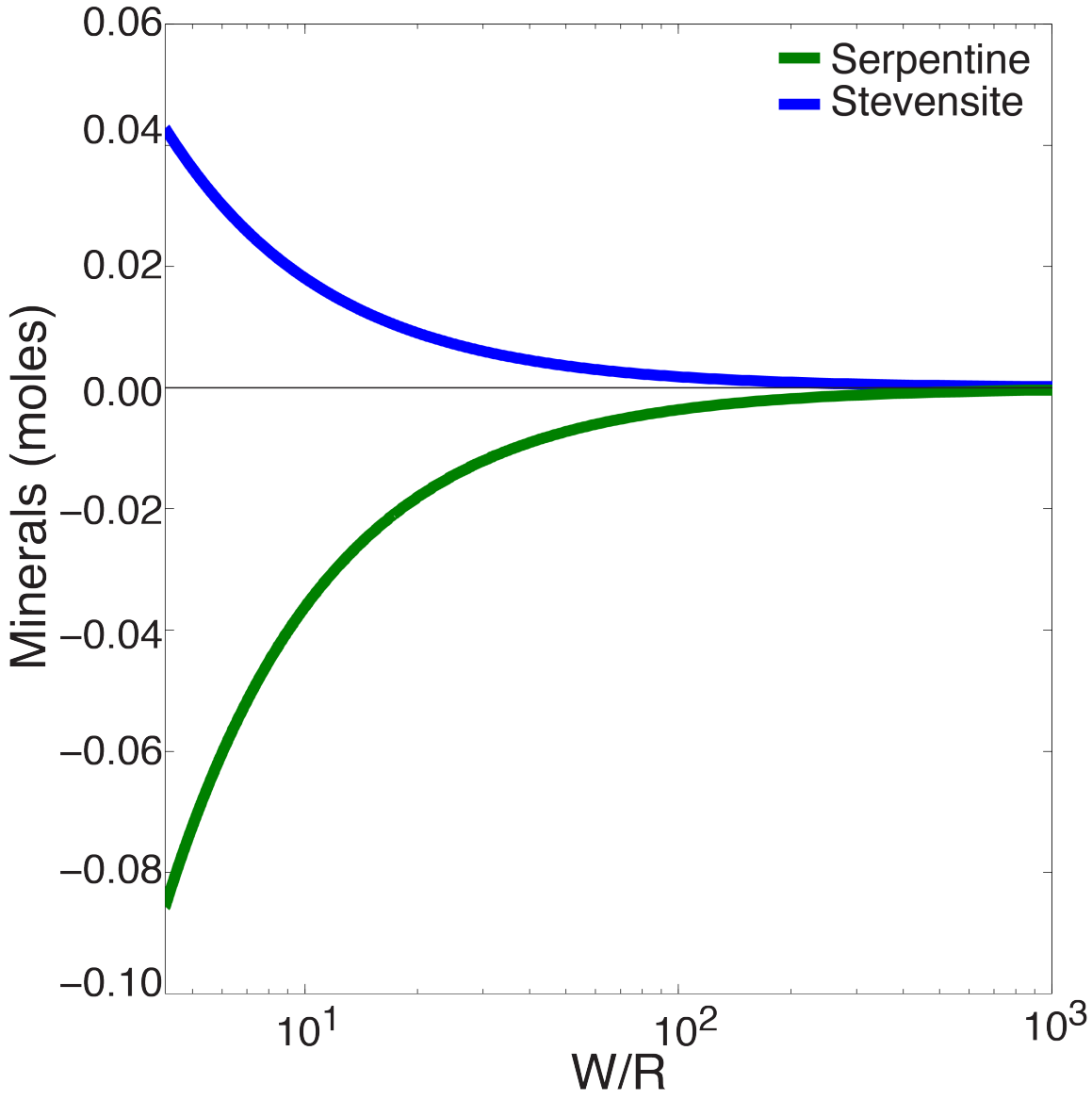

Figure 3.10: Stage 4 model results, illustrating serpentine consumption and stevensite precipitation as a function of water/rock (W/R). (Fe from serpentine is also converted to magnetite in the model reaction).

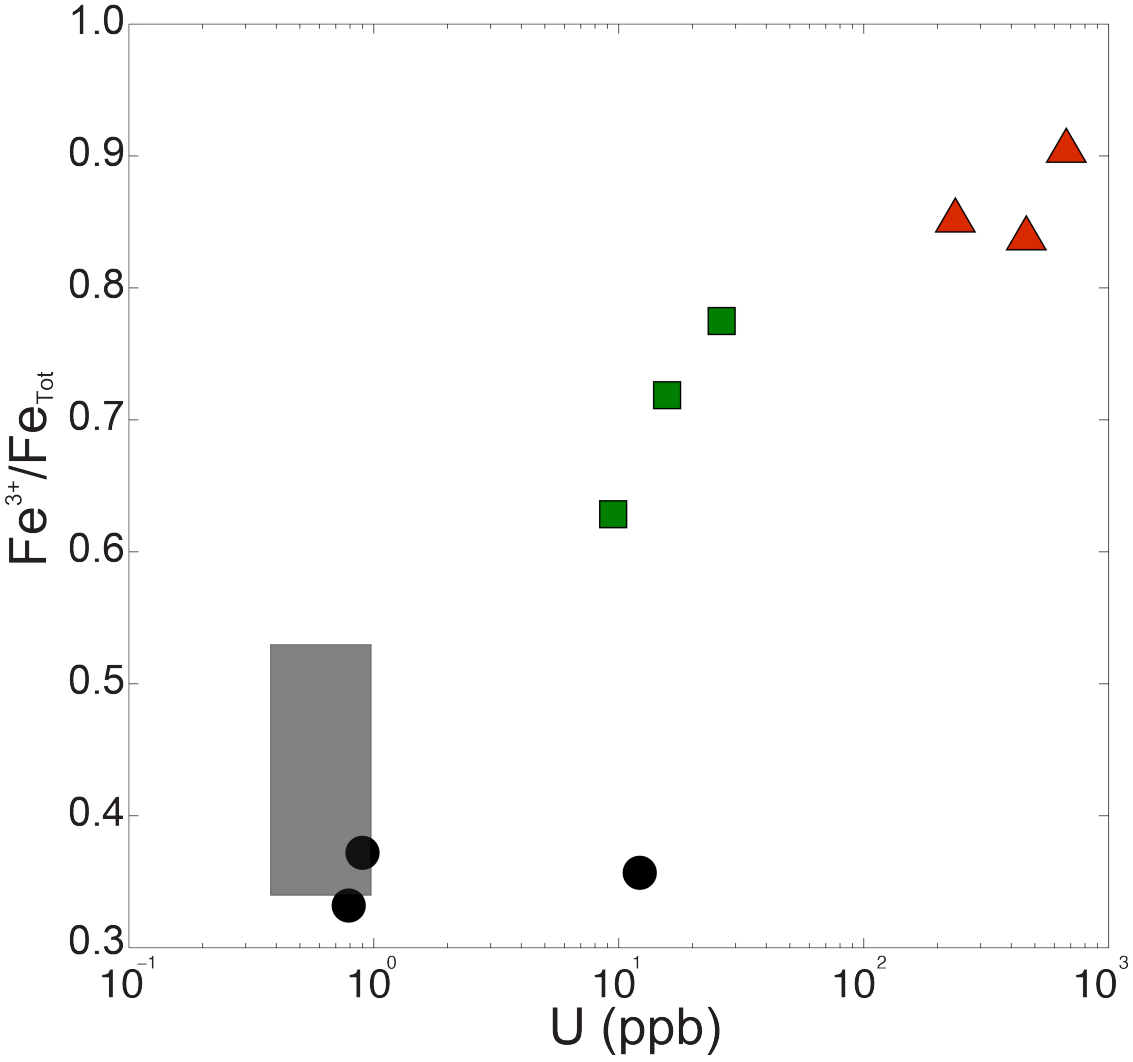

Figure 3.11: Uranium concentrations vs Fe3+/FeTot in Wadi Fins peridotites. Black circles: black cores; green squares: green zones; red circles: red zones. Symbols are larger than analytical uncertainty. Gray square illustrates range of U concentration and Fe3+/FeTot reported by Godard et al. (2000).

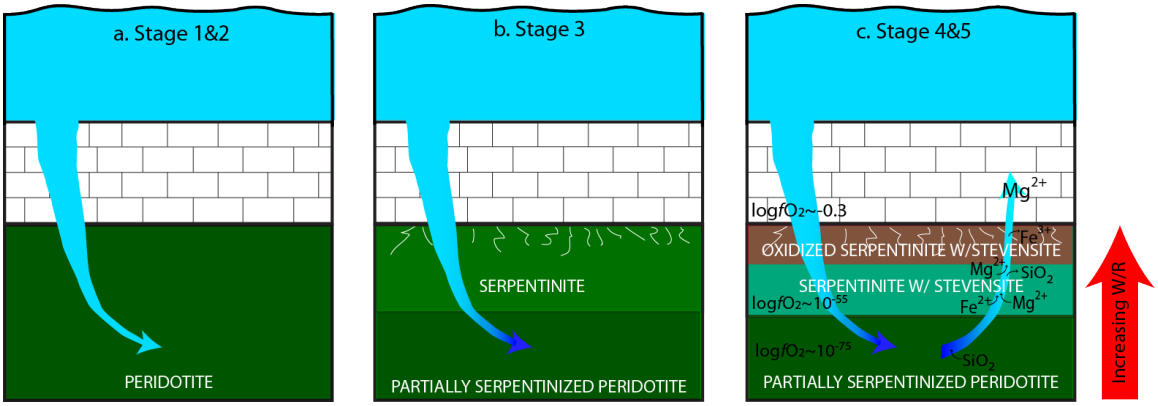

Figure 3.12: Conceptual figure of alteration process of Wadi Fins peridotites. Seawater infiltrates the overlying limestones (a), fluid moves through the peridotite at variable water/rock (W/R) partially serpentinizing the rock at low W/R (b). Reduced fluid moves away from the partially serpentinized peridotite forming stevensite, leaching Mg and precipitating goethite upon mixture with oxidized fluid (c).

Table 3.1: Bulk rock compositions of Wadi Fins altered peridotites

		OM15-5	OM15-5	OM15-5	OM15-6	OM15-6	OM15-6	OM15-7	OM15-7	OM15-7
	Detection limits	Red Zone	Green Zone	Core	Red Zone	Green Zone	Core	Red Zone	Green Zone	Core
SiO_2 (wt%)	0.04	39.99	44.81	41.33	39.21	45.54	43.56	38.18	46.43	42.49
TiO_2 (wt%)	0.010	0.02	0.02	0.02	0.02	0.02	0.02	0.01	0.02	0.01
Al_2O_3 (wt%)	0.09	1.40	1.58	1.13	1.65	1.63	0.98	1.32	1.68	1.12
FeO* tot (wt%)	0.07	10.71	6.05	7.67	12.28	6.15	8.25	11.35	5.94	7.82
MnO (wt%)	0.02	0.03	0.03	0.10	0.03	0.03	0.12	0.04	0.03	0.10
MgO (wt%)	0.06	29.18	28.75	39.13	28.60	29.08	39.96	28.00	28.81	37.54
CaO (wt%)	0.07	0.92	2.19	1.01	0.83	2.32	0.99	2.47	1.40	1.12
Na_2O (wt%)	0.01	0.05	0.04	0.01	0.03	0.03	bdl	0.05	0.09	0.01
K_2O (wt%)	0.01	0.06	0.10	0.02	0.05	0.09	bdl	0.03	0.06	0.01
Cr_2O_3 (wt%)	0.00	0.49	0.53	0.33	0.55	0.51	0.33	0.45	0.60	0.35
LOI (wt%)		16.91	15.77	8.55	16.74	16.14	5.92	17.1	16.31	8.23
Total		99.74	99.87	99.29	99.98	101.53	100.12	99.02	101.38	98.78
Mg#		0.83	0.89	0.90	0.81	0.89	0.90	0.81	0.90	0.90
FeO (wt%)^	0.1	1.9	2.4	5.3	2	1.5	5.5	1.2	1.8	5.1
Fe_2O_3 (wt%)‡		9.79	4.06	2.63	11.42	5.16	3.05	11.28	4.60	3.02
Fe^{3+}/Fe_{Tot}		0.84	0.63	0.33	0.85	0.77	0.36	0.90	0.72	0.37
Cr#		0.19	0.18	0.16	0.18	0.17	0.18	0.19	0.19	0.17
		OM15-5	OM15-5	OM15-5	OM15-6	OM15-6	OM15-6	OM15-7	OM15-7	OM15-7
Trace elements	Detection limits	Red Zone	Green Zone	Core	Red Zone	Green Zone	Core	Red Zone	Green Zone	Core
B (ppm)	1	40	38	151	39	45	117	37	37	146
Co (ppm)	8	112	133	110	98	139	114	102	138	113
Ni (ppm)	23	2591	2865	2275	2448	2889	2357	2414	3029	2322
Cu (ppm)	5	18	21	15	14	23	22	18	27	14
Zn (ppm)	3	40	48	31	44	42	32	40	44	32
Rb (ppm)	0.05	2	2	0.3	1	2	0.4	1	2	0.3
Sr (ppm)	4	118	110	14	113	132	10	129	124	15
Mo (ppb)	43	313	148	138	262	155	128	283	161	128
Cs (ppb)	5	107	97	37	99	105	38	74	79	34
Ba (ppb)	289	1591	2381	bdl	2748	3543	646	4784	4483	bdl
Gd (ppb)	12	16	19	16	19	19	bdl	14	19	12
Dy (ppb)	16	49	57	42	58	69	33	46	54	34
Er (ppb)	7	48	59	43	65	69	35	51	63	37
Tm (ppb)	9	9	11	bdl	12	13	bdl	bdl	11	bdl
Yb (ppb)	22	78	94	63	95	107	52	76	92	61
Lu (ppb)	3	16	16	12	18	19	10	14	18	12
W (ppb)	12	106	32	278	39	22	16	58	13	27
Pb (ppb)	46	64	bdl	101	bdl	bdl	bdl	bdl	bdl	bdl
Th (ppb)	0.27	0.35	1.41	0.52	0.37	0.93	4.19	0.38	0.31	0.29
U (ppb)	0.68	461	9	0.79	237	26	12	672	16	0.90

bdl= Below detection limits of the instrument

FeO* = Oxide total Fe, assuming oxidation state of all Fe to be 2+

^ Determined by titration

‡ Calculated by mass balance from ICP-OES and titration data.

Table 3.2: Equilibration temperatures of Wadi Fins peridotites

	Ca in Opx Brey & Kohler			Al in Opx Witt-Eicksen & Seck			Two pyroxene (BKN)	
Sample	T °C	1σ	n	T °C	1σ	n	T °C	n
OM15-6	814.5	42.3	7	778.3	58.9	6	845.3	5
OM15-7	788.8	30.3	9	731.8	44.1	9	880.9	9
OM15-5	861.7	79.8	5	886.1	156.2	4	NA	NA

4 Carbon mineralization accompanying serpentinization in the Oman ophiolite: A magnesium isotope perspective

Abstract

Alteration of mantle peridotite in the Samail ophiolite forms secondary minerals, mainly serpentine and Mg-rich carbonates. Magnesium accounts for approximately 25 to 30% of peridotite mass and its mobility can be used to trace this alteration. We report the first set of Mg isotope measurements from peridotites and their alteration products in Oman. Our results show that partially serpentinized peridotites have Mg isotope ratios that are indistinguishable from the estimates for the average mantle and bulk silicate earth (δ^{26}Mg =-0.25‰±0.04) However, more extensive peridotite alteration leads to large shifts in isotopic compositions. Our suite of alteration products from the mantle section has a range of δ^{26}Mg spanning ∼4.5‰, which is over 60% of the observed range of δ^{26}Mg on Earth. Isochemical serpentinization at low W/R does not fractionate Mg isotopes. We report serpentine veins with heavy δ^{26}Mg (up to 0.96‰) and propose a mechanism for its formation that requires high W/R and co-precipitation with Mg-carbonates with light isotopic compositions as observed in massive veins of magnesite δ^{26}Mg =-3.3‰ and dolomite δ^{26}Mg =-1.91‰. This complementary enrichment-depletion, and the finite ^{14}C ages of the carbonates suggest that both serpentinization and carbonation are ongoing processes during peridotite weathering in Oman. Rates of calcite precipitation in travertines inferred from $\Delta^{26}Mg_{cal-fl}$ suggest that travertine formation in Oman sequesters a total of 10^6-10^7 kg CO_2/yr.

4.1 Introduction

Alteration of ultramafic rocks is ubiquitous in near surface occurrences, both on land and below the seafloor. Mantle minerals like olivine and pyroxene are unstable at near surface conditions and undergo hydration (serpentinization) and carbonation when fluids percolate in the rocks. These reactions result in the formation of serpentine minerals, carbonates, brucite, magnetite and other Fe-oxides and hydroxides. Serpentinization and carbonation reactions are often nearly isochemical, apart from the addition of H_2O and CO_2 (e.g., Coleman and Keith 1971) with both observations and thermodynamic modeling revealing minor increases in major element ratios such as Si/Mg (e.g. $\leq$ 10% for low temperature reaction with seawater, (Malvoisin 2015, Figure 3; Monnier et al. 2006; Snow and Dick 1995). Recent studies (Obeso and Kelemen 2018, de Obeso and Kelemen, submitted) show that depending on alteration conditions, mass transfer can lead to larger changes in major element chemistry. In Oman, while partially serpentinized harzburgites record a $\sim$ 2% decrease in MgO/SiO_2 compared to comparable, fresh residual mantle peridotites (Monnier et al. 2006), there are examples of heavily altered harzburgite that lost up to 30% of their original Mg (de Obeso and Kelemen, submitted).

Magnesium isotope studies of peridotites show that the composition of the mantle and bulk silicate earth (BSE) is relatively uniform with a δ^{26}Mg= -0.25‰±0.04 (2σ), (Teng 2017; Teng et al. 2010). Liu et al. (2017) report δ^{26}Mg of -0.12‰±0.13 (2σ) for altered seafloor peridotites. There are a limited number of studies on magnesium isotope compositions of ophiolite peridotites. Peridotites from the Purang ophiolite (Tibet) have compositions within uncertainty of mantle compositions δ^{26}Mg=-0.20‰±0.10 (2σ) (Su et al. 2015) while

peridotites from the Feragen and Linnajavri ultramafic bodies have mantle-like Mg isotope ratios (Beinlich et al. 2014).

Given that most peridotites have similar Mg isotope compositions, fractionation of Mg during serpentinization and carbonation has been a topic of research in recent years, as isotopic differences from fresh peridotite could be used to constrain alteration processes. Prior work with natural samples concluded that serpentinization does not fractionate Mg isotopes. Beinlich et al. (2014) showed that coexisting olivine and serpentine in hydrothermally altered peridotites in three different localities in Norway have indistinguishable Mg isotope ratios, and concluded that serpentinization does not fractionate Mg isotopes at the inferred alteration temperature (∼275℃). They also report that carbonation following serpentinization resulted in formation of δ^{26}Mg-enriched talc and δ^{26}Mg-depleted magnesite. Liu et al. (2017) investigated a suite of abyssal peridotites and concluded that heavy isotopic compositions in highly altered samples were a result of low temperature formation of clay minerals rather than serpentinization.

Experimental work has produced conflicting results. Wimpenny et al. (2010) performed San Carlos olivine dissolution experiments at low temperature (∼25℃). They observed an initial, preferential release of light isotopes from olivine to fluid evolving to olivine-like composition with time, and suggest that chrysotile preferentially removed light Mg from solution. More recently Ryu et al. (2016) synthetized lizardite from solution and reported that it was enriched in heavy isotopes relative to the fluid at 90 and 250℃. Following a molecular dynamics approach Wang et al., (2019) also conclude that lizardite crystallization preferentially removes heavy Mg from the fluid.

In this paper we analyzed magnesium isotope compositions of samples from the man-

tle section of the Samail ophiolite in Oman. These are the first measurements of magnesium isotopes from the Samail ophiolite. Their variation sheds light on serpentinization and associated carbon mineralization at low temperatures. The initial isotopic composition of Oman peridotites (average δ^{26}Mg -0.25‰±0.14 2σ) is indistinguishable from average mantle. In some serpentine samples, this composition has been modified, suggesting that high extents of alteration can shift δ^{26}Mg and that there is ongoing serpentinization during alteration of the Samail ophiolite mantle section.

4.2 Geological background and sample selection

The Samail ophiolite in eastern Oman is the best-exposed block of oceanic crust and mantle in the world (Figure 1). The mantle section of the ophiolite is composed of highly depleted harzburgites together with ∼5-15% dunite (Braun 2004; Braun and Kelemen 2002; Collier 2012). These peridotites exhibit different degrees of alteration ranging from ∼30% serpentinized in "fresh" rocks to instances of completely serpentinized (Godard, Jousselin, and Bodinier 2000; Hanghøj et al. 2010; Monnier et al. 2006) and/or completely carbonated peridotites (Falk and Kelemen 2015; Nasir et al. 2007; Stanger 1985). Alteration occurred through out the history of the ophiolite, beginning near axis of the spreading center (Gregory and Taylor 1981), continuing during obduction and emplacement (Falk and Kelemen 2015), and extending to the present (e.g Clark and Fontes 1990; Kelemen and Matter 2008; Mervine et al. 2014; Monnin et al. 2011; Streit, Kelemen, and Eiler 2012).

Previous studies of the low-temperature modern alteration system in Oman propose a three-step alteration process (e.g. Barnes, LaMarche, and Himmelberg 1967; Barnes, O'Neil, and Trescases 1978; Chavagnac et al. 2013b; Kelemen et al. 2011; Neal and Stanger

1985; Noël et al. 2018; Paukert et al. 2012). The first step is characterized by the formation of Mg^{2+}-$HCO3^{-}$ rich waters as meteoric waters react with peridotite near the surface. This so-called "Type I" water percolates into the peridotite formation (Step 2) leading to the precipitation of Mg-rich carbonates, brucite and serpentine. These reactions remove carbon and Mg^{2+} from the fluid and dissolve Ca^{2+}, as it is incompatible in the alteration minerals. The resulting fluids, known as "Type II" waters, have low Mg and C, high Ca and pH, and very low oxygen fugacities (Clark and Fontes 1990; Neal and Stanger 1983; Paukert et al. 2012). The third step involves the return of these hyperalkaline "Type II" fluids to the surface, where the disequilibrium with the atmosphere leads to rapid uptake of atmospheric CO_2 and precipitation of calcite (Chavagnac et al. 2013a; Clark and Fontes 1990; Kelemen and Matter 2008; Kelemen et al. 2011; Mervine et al. 2014; Neal and Stanger 1985; Paukert et al. 2012). Secondary minerals from the three stages have different aqueous Mg2+-mineral fractionation properties (Beinlich et al. 2014; Gao et al. 2018; Liu et al. 2017; Pinilla et al. 2015; Wang et al. 2019; Wimpenny et al. 2014) allowing the use of Mg isotopes as tracers of alteration.

All samples used in this study come from the southern massifs of the ophiolite, within its mantle section (Figure 1). Previously described samples analyzed for this study can be separated into silicate and carbonate bearing groups. Silicate samples include relatively fresh harzburgites (n=6, average $\sim$ 40% relict mantle minerals) and dunites (n=4, $\sim$23%) from Hanghøj et al. (2010), highly serpentinized harzburgites (n=2, 37 and 14%) and dunites (n=1, 0%) from de Obeso and Kelemen (2018), serpentinized harzburgites (n=3, $\sim$40%), high Si harzburgite (n=3, 0%) and oxidized harzburgite (n=3, 0%) from de Obeso and Kelemen (submitted). We also include four samples not previously described: serpen-

tine veins (n=2), serpentinite (n=1) and a "waxy silicate vein" from a serpentinized body with Mg/Si$\sim$1 (n=1).

Carbonate samples include two groups: completely carbonated peridotites, also known as listvenites, from Falk Kelemen (2015), further classified as dolomite listvenites (n=2) and magnesite listvenites (n=2). We also analyzed massive carbonate veins from serpentinized peridotite outcrops, further classified as magnesite veins (n=2) and dolomite veins (n=1) (Kelemen et al. 2011). The three carbonate vein samples have ^{14}C contents corresponding to ages of 32ka, 37ka, and 40ka (Kelemen et al. 2011). Two travertine samples from Kelemen et al. (2011) are also included. These travertines are composed mainly of calcite with ^{14}C ages of 1630 and 18,450 years. We also include two carbonate vein samples not previously described: a massive magnesite vein and a huntite vein. Major element compositions and locations for the new samples are reported in table S1.

4.3 Methods

Samples not previously described (4 silicates and 2 carbonates) were processed in Lamont Doherty Earth Observatory (LDEO). Samples were chipped using a jaw crusher and powdered using an alumina puck mill. Major element analyses and loss on ignition (LOI) of the bulk rocks was performed using lithium metaborate fusion and nitric acid solution. Analysis of these solutions used an Agilent 720 Axial ICP-OES calibrated with rock standards (Table S2).

For Mg isotopic analyses powders of all 37 samples and three USGS rock standards (BCR-2, BHVO-2, BIR-1A) were digested using a conventional HNO_3:HF (3:1) digestion procedure at LDEO. Sample OM17-magnesite was processed in multiple digestion batches

to check reproducibility (n=5). Once digested, all samples were diluted to ∼5 ppm Mg in 0.2% HNO_3. These solutions were processed using a Thermo Dionex 5000+ ion chromatography (IC) system at Princeton University to separate Mg from the silicate/carbonate matrix. As described in more detail in Husson et al. (2015), the procedure was as follows: the automated IC system runs samples through an in-line CS16 cation exchange column that separates various cations and measures peak intensities using changes in conductivity. Collection windows were specified to collect pure Mg cuts. 200 microliters (μL) of solution were run through the column. Mg cuts were dried, treated with concentrated HNO_3, re-dried and re-dissolved in 2% HNO_3 for isotope analysis.

Isotopic analyses were carried out at Princeton University on a Thermo Fisher Scientific Neptune Plus MC-ICP-MS. Sample-standard-sample bracketing was used to correct for instrumental mass fractionation (Galy et al. 2001) and values were normalized to an internal standard. Magnesium isotope ratios are reported using delta notation. Long-term external reproducibility is estimated by comparing Mg standard Cambridge-1 against DSM-3 standard. Measured δ^{26}Mg values for Cambridge-1 yields an average of −2.59±0.05‰ (2σ, n=7), indistinguishable from suggested value -2.623±0.030‰ (2σ) (Galy et al. 2003; Teng et al. 2015). Reported errors for each sample depend on the number of times the sample has been separated and analyzed. For a single separation and analysis, we report the long-term external reproducibility of Cambridge-1 (δ^{26}Mg 2σ=±0.09‰). For multiple chromatographic separations and analysis (n>1) we report the standard error of the mean (SE).

4.4 Results

δ^{26}Mg and δ^{25}Mg results are presented in Table 1. All samples analyzed fall on an isotopic mass-dependent fractionation line in three-isotope space with slope of 0.5196±0.0024 (R^2=0.9992) indistinguishable from the value of 0.5210 estimated for equilibrium fractionation (Young and Galy 2004). Given the linear relationship in three-isotope space, in further discussion we only use δ^{26}Mg. The range of δ^{26}Mg in the samples analyzed is shown in Figure 2. The observed range for samples of this study is ∼4.6‰ (-3.39‰ to 1.19‰), extending over 60% of the terrestrial range (∼7.5‰, from -5.6‰ to 1.8‰) (Teng 2017).

Silicates

δ^{26}Mg values in partially serpentinized harzburgites (-0.25‰±0.14, 2σ) and dunites (-0.24‰±0.10, 2σ) are indistinguishable from average mantle (Figure 3). We exclude three samples from the Wadi Fins area (OM15-5-4, OM15-6-4 and OM15-7-4), described by de Obeso and Kelemen (submitted) from the harzburgite average as they report significant Mg leaching from these outcrop. These samples are heavier than mantle values (average δ^{26}Mg of -0.09‰±0.01, 2σ), and their completely hydrated (OM15-5-2, OM15-6-2 and OM15-7-2) and oxidized (OM15-5-3, OM15-6-3 and OM15-7-3) counterparts in the same outcrop are significantly heavier (average δ^{26}Mg of 0.73‰±0.04 for hydrated samples and 0.86‰±0.17 for oxidized samples, 2σ). These values are the heaviest ever reported for ultramafic rocks.

Mineral separates from veins in the Wadi Fins area are also significantly heavier than mantle values. Two serpentine veins (OM13-17A WP and OM13-15B) have δ^{26}Mg of

0.45‰ and 0.96‰ respectively, and a "waxy vein" (OM15-5-5) with molar Mg/Si of 1 has a heavier isotopic composition, δ^{26}Mg=1.19‰.

Carbonates

Magnesite listvenites (OM09-11 and OM10-26, both with δ^{26}Mg of -0.33‰) are within error of mantle values suggesting nearly isochemical carbonation as inferred from major element ratios by Falk and Kelemen (2015). Dolomite listvenites (OM10-14 and OM10-15) are significantly lighter (δ^{26}Mg of -1.46‰ and -0.89‰). The formation of dolomite listvenites is interpreted as a 1:1 Mg:Ca molar replacement (Falk and Kelemen 2015), and their isotopic compositions suggest that heavy Mg is lost during reaction with a Ca bearing fluid.

Two massive magnesite veins (OM07-39, OM17 Magnesite) are by far the lightest samples analyzed for this study, with δ^{26}Mg from -3.39‰ to -3.14‰. (Five replicate analyses of one of these veins yield an average of -3.38‰±0.02, 2σ). The dolomite (OM07-27) and huntite (BA1B 11-2 17-27cm) veins also have light isotopic compositions compared to mantle values (δ^{26}Mg =-1.91‰ and δ^{26}Mg=-3.04‰ respectively), though they are heavier than the massive magnesites. Travertines (OM07-18 and OM07-34A) precipitated from "Type II" waters are heavier than other carbonates, with δ^{26}Mg of -1.14‰ and -0.89‰.

4.5 Discussion

Results from typical, partially serpentinized harzburgites and dunites (Figure 3) show that the magnesium isotopic composition in the mantle section of the Samail ophiolite is indistinguishable to that the Earth's mantle and BSE (δ^{26}Mg=0.25‰±0.04 ,Teng 2017). Therefore any deviations from mantle values, in the more altered rocks, should be ex-

plained by fractionation during serpentinization, carbonation and weathering of the peridotites.

Isochemical serpentinization of olivine-rich rocks requires the formation of a magnesium-rich phase, usually brucite (Evans 1977; Evans et al. 1976) or magnesite when CO_2-rich fluids are present (Frost 1985; Kelemen et al. 2011) following the simplified reactions:

$$3Mg_2SiO_4 + 6H_2O = 2Mg_3Si_2O_5(OH)_4 + Mg(OH_2)$$

$$4Mg_2SiO_4 + 4H_2O + 2CO_2 = 2Mg_3Si_2O_5(OH)_4 + 2MgCO_3$$

These reactions conserve MgO/SiO_2 of residual mantle peridotite protoliths, formed by melting and melt extraction. All analyzed harzburgites in this study plot below the geochemical fractionation line for the residual mantle (Asimow 1999; Baker and Beckett 1999) indicative of either Mg-loss or Si-addition during alteration (Figure 4). In order to account for departures from the geochemical fractionation we define:

$$\Delta\Big(\frac{MgO}{SiO_2}\Big) = \Big(-3.15 * \Big(\frac{Al_2O_3}{SiO_2}\Big)_{sample} + 1.12\Big) + \Big(\frac{MgO}{SiO_2}\Big)_{sample}$$

Samples with $\Delta(MgO/SiO_2)<0.12$ show δ^{26}Mg indistinguishable from mantle values. As $\Delta(MgO/(SiO_2)$ increases, whole rocks begin to deviate to heavier Mg isotope ratios (Figure 5). This suggests that significant Mg leaching is required to produce bulk rock deviations from mantle isotope ratios. Serpentine veins from Wadi Fins (δ^{26}Mg of 0.96‰

and 0.46‰) show significant enrichments in heavy Mg isotopes. These serpentines are depleted in Fe (Mg# 97-98) compared to ambient peridotite (Mg#90) and formed in high water/rock pathways. They record preferential Mg mobility during alteration at temperatures between 25-60℃ (Obeso and Kelemen 2018), which produced fluids with Mg isotope ratios compositions heavier than the mantle protolith . Considering that previous studies on partially serpentinized samples (Beinlich et al. 2014; Liu et al. 2017) did not observe significant Mg-isotope fractionation during serpentinization, we propose a mechanism in which the observed enrichment in the serpentine veins is related with co-precipitation of carbonates along with serpentine, as occurs along the reaction path outlined by Barnes and O'Neil, (1969) and modeled by subsequent workers (Bruni et al. 2002; Paukert et al. 2012).

Carbon mineralization accompanying serpentinization

Equilibrium isotope fractionation of Mg isotopes during peridotite alteration products is temperature dependent (Li et al. 2015; Pinilla et al. 2015; Ryu et al. 2016; Schott et al. 2016; Wang et al. 2019) making temperature estimates important for understanding alteration. For our calculations we used 30℃, approximately the modern day annual average temperature in the northern Oman mountains (Weyhenmeyer et al. 2002). This temperature is consistent with other temperature constraints established in studies that described the samples used in this study. De Obeso and Kelemen, (2018) estimated alteration in Wadi Fins between 25-60℃ based in clumped isotope thermometry of carbonate veins in peridotite. Carbonates in typical, partially serpentinized mantle peridotites in the Samail ophiolite yield crystallization temperatures between 25-50℃, using δ^{18}O exchange tem-

peratures and clumped isotope thermometry (Kelemen et al. 2011; Streit, Kelemen, and Eiler 2012).

Magnesium mobility has been documented in the mantle section of the Samail ophiolite. On average, typical partially serpentinized harzburgites might have lost up to 2% (Monnier et al. 2006) though, alternatively, in some cases Si-gain rather than Mg-loss led to increased Si/Mg ratios (Obeso and Kelemen 2018). Heavily weathered samples within 10 meters of a Cretaceous unconformity in Wadi Fins lost 30% of their initial Mg to the alteration fluid (de Obeso and Kelemen, submitted). The presence of meter-wide veins of magnesite provides more evidence of Mg-mobility (Figure 6). A significant fraction of such magnesite veins records measureable ^{14}C, corresponding to ages less than $\sim$ 50ka (Kelemen et al. 2011; Mervine et al. 2014), indicating recent mobility.

We used the results of an EQ3/6 reaction path model (Paukert et al. 2012) to estimate Mg isotope composition in the modern alteration system. This model has three stages. In the first stage, rain water in equilibrium with the atmosphere infiltrates the peridotite leading to the formation of chrysotile, calcite, hydromagnesite and magnetite. The resulting "Type I" fluid has an Mg^{2+}-HCO_3^- rich composition. In the second stage, the "Type I" fluid reacts with fresh peridotite isolated from the atmosphere to form magnesium-rich carbonates, chrysotile and brucite, plus "Type II" fluid rich in Ca^{2+}-OH^-. In the third stage (not explicitly modeled by Paukert et al. 2012) "Type II" fluids emerge on the surface and react with atmospheric CO_2 to form calcite. We used the phase proportions produced at each stage of the model to estimate Mg isotope compositions of the fluid and secondary minerals as reaction progresses. Using a model of assimilation and fractional crystallization (DePaolo 1981) we estimate isotope compositions as the fluid assimilates

mantle minerals with δ^{26}Mg=-0.25‰ and crystallizes chrysotile, hydromagnesite and calcite in the first stage, chrysotile, brucite and Mg-rich carbonates (dolomite and magnesite) in the second stage, and calcite in the third stage. We assume that the starting Mg isotope composition of water is in equilibrium with the overlying limestones with a composition similar to the global limestone average compiled by Teng (2017), yielding an initial $\delta^{26}Mg_{fluid}$ of -2.0‰. We assume that products of isochemical serpentinization do not fractionate Mg isotopes from the fluid (α=1.0000 for chrysotile and brucite) (Beinlich et al. 2014; Liu et al. 2017). Carbonates fractionate Mg isotopes in the model, we used a fractionation factor of α=0.9990 for hydromagnesite (Shirokova et al. 2013) in the first stage. For the second stage, we used a range of fractionation factors for magnesite and dolomite, as reported in Table 2.

We track the fluid isotopic composition as a function of water/rock ratio (W/R). In the open system small extents of water rock interaction (high W/R) results in an evolved fluid that goes from its initial δ^{26}Mg of -2‰ to a value of -0.25‰ (Figure 7). With the formation of hydromagnesite the fluid gets slightly enriched in heavy isotopes before reaching a steady state at δ^{26}Mg=-0.15‰ with W/R less than 100. The evolved fluid is Mg-HCO_3 rich. This evolved fluid is then used as the reactant in the closed system, that runs until pH reaches 12 (maximum pH measured in the field). We track the fluid isotopic composition as a function of water/rock ratio (W/R). This stage produces Mg- and C-depleted waters with high pH and extremely low fO_2 (Paukert et al. 2012). The reaction path is characterized by the co-precipitation of Mg-rich carbonates (magnesite and dolomite) and chrysotile at W/R between 100-100,000. While the system co-precipitates chrysotile and isotopically light carbonates, Mg isotope ratios in the fluid and serpentine become

heavier (Figure 8). Once the system becomes carbon-depleted, carbonates disappear from the precipitating mineral assemblage and the fluid/serpentine system rapidly evolves to mantle-like isotope ratios (Figure 8).

The evolution of Mg isotope ratios from the model is consistent with isotopic ratios measured in our samples and could explain the presence of isotopic heavy serpentine with pure serpentization not affecting magnesium isotope ratios as reported in previous studies (Beinlich et al. 2014; Liu et al. 2017). Co-precipitation of serpentine and magnesite/dolomite forms isotopically heavy fluid and serpentine compositions at high W/,R similar to those observed in Wadi Fins serpentine veins (δ^{26}Mg>0.5‰). Also at high W/R, precipitated carbonates are very light, similar to those in massive carbonate veins (Figure 6). As W/R decreases (and reaction progress increases) in the model, carbonates disappear from the precipitating assemblage, the fluid evolves to δ^{26}Mg=-0.25‰, and serpentine forms from fluids with this mantle-like Mg isotope ratio consistent with the values observed in partially serpentinized harzburgites and dunites. While the carbonate and serpentine samples in this study are not co-genetic, our measurements show that serpentine and carbonates occur with magnesium isotopic ratios different from those of the original protolith. Our proposed mechanism reproduces the observed data while staying consistent with previous studies that concluded that serpentinization does not fractionate Mg isotopes (Beinlich et al. 2014; Liu et al. 2017).

Massive carbonate vein samples OM07-27, OM07-39 and OM07-07 have ^{14}C ages of 40, 32 and 37ka (Kelemen et al. 2011) respectively. Similar Mg-rich carbonate veins have ^{14}C ages as low as 7ka ((Kelemen et al. 2011; Mervine et al. 2014). Thus, our modeling and observations of Mg isotope variation in the Samail ophiolite is consistent with the

inference that serpentinization occurs along with carbonation during ongoing weathering of the Samail ophiolite mantle peridotites, with timescales less than or equal to the ages of the carbonates.

In the natural system, the "Type II" hyper-alkaline Ca-rich fluid comes in contact with the atmosphere in springs, where it combines with CO_2 from air to form extensive travertine deposits (Chavagnac et al. 2013b; Clark and Fontes 1990; Kelemen and Matter 2008; Kelemen et al. 2011; Mervine et al. 2014; Neal and Stanger 1985). The Mg isotope composition of travertines measured in this study are δ^{26}Mg of -1.14‰ and -0.89‰. Our modeling shows that, at pH 12, the fluid has an isotope ratio identical to mantle values, δ^{26}Mg=-0.25‰. The $\Delta^{26}Mg_{cal-fl}$ of the travertine is lower that what expected from equilibrium fractionation with such a fluid ($\sim$3‰) (Li et al. 2012; Mavromatis et al. 2017; Wang et al. 2019). Mavromatis et al. 2013 showed that $\Delta^{26}Mg_{cal-fl}$ is dependent on the calcite growth rate, with $\Delta^{26}Mg_{cal-fl}$ decreasing with increasing growth rate. Based on this, the observed $\Delta^{26}Mg_{cal-fl}$ in Oman travertines suggests calcite growth rates of 10^{-5} mol/m^{2}s. Such rapid growth rates are consistent with non-equilibrium, high Mg contents in peridotite-hosted travertines in the Samail ophiolite and other massifs (e.g Barnes and O'Neil 1969, 1971; Chavagnac et al. 2013b; Kelemen and Matter 2008; Kelemen et al. 2011; Streit, Kelemen, and Eiler 2012). Assuming that between 1-10% of the total estimated travertine area in the Samail ophiolite ($\sim 10^7$ m^2 Kelemen and Matter 2008) is actively precipitating, this growth rate yields a total uptake of 10^3-10^4 tons atmospheric CO_2/yr, similar to previous estimates of carbon uptake to form travertine in the ophiolite (Kelemen and Matter 2008; Kelemen et al. 2011; Mervine et al. 2014). The whole carbonation-serpentinization system is shown conceptually in figure 9.

4.6 Conclusions

Dunite and harzburgites in the mantle section of the Samail ophiolite have δ^{26}Mg indistinguishable from average mantle values. Serpentinization at low W/R does not fractionate Mg isotopes, but deviations from mantle like δ^{26}Mg are observed as a result of extensive Mg leaching at higher W/R. Heavily altered peridotites recording up to 30% Mg loss and containing secondary Mg-clay minerals have the heaviest δ^{26}Mg ever reported for ultramafic rocks. We propose a mechanism in which the modern alteration system forms Mg-rich carbonates with light δ^{26}Mg at high W/R, together with heavy δ^{26}Mg fluids and serpentine, similar to those observed in serpentine veins in Wadi Fins and massive carbonate veins in Wadi Tayin. The fact that most peridotite-hosted carbonate veins have finite ^{14}C ages is consistent with other observations indicating that both serpentinization and carbonation are ongoing. The proposed mechanism can be further explored, likely with co-genetic carbonate-serpentine veins, in the newly drilled cores from the Oman Drilling Project. Travertine δ^{26}Mg is heavier than expected from equilibrium fractionation between calcite and fluid with mantle-like Mg isotope ratios, suggesting rapid, disequilibrium crystallization. We infer calcite growth rates of 10^{-5} mol/m$_2$s, leading to uptake of atmospheric CO_2 at a rate of 10^6-10^7 kg CO_2/yr to form travertine in Oman.

References

Asimow, Paul D. (1999). "A model that reconciles major- and trace-element data from abyssal peridotites." In: *Earth and Planetary Science Letters* 169.3, pp. 303–319. ISSN: 0012821X. DOI: 10.1016/S0012-821X(99)00084-9.

Baker, Michael B. and John R Beckett (1999). "The origin of abyssal peridotites: a reinterpretation of constraints based on primary bulk compositions." In: *Earth and Planetary Science Letters* 171.1, pp. 49–61. ISSN: 0012-821X. DOI: https://doi.org/10.1016/S0012-821X(99)00130-2.

Barnes, Ivan, V. C. LaMarche, and G. Himmelberg (1967). "Geochemical Evidence of Present-Day Serpentinization." In: *Science* 156.3776, pp. 830–832. ISSN: 0036-8075. DOI: 10.1126/science.156.3776.830.

Barnes, Ivan and James R. O'Neil (1969). "The Relationship between Fluids in Some Fresh Alpine-Type Ultramafics and Possible Modern Serpentinization, Western United States." In: *Geological Society of America Bulletin* 80.10, p. 1947. ISSN: 0016-7606. DOI: 10.1130/0016-7606(1969)80[1947:TRBFIS]2.0.CO;2.

Barnes, Ivan and James R. O'Neil (1971). "Calcium-magnesium carbonate solid solutions from Holocene conglomerate cements and travertines in the Coast Range of California." In: *Geochimica et Cosmochimica Acta* 35.7, pp. 699–718. ISSN: 00167037. DOI: 10.1016/0016-7037(71)90068-8.

Barnes, Ivan, James R. O'Neil, and J.J Trescases (1978). "Present day serpentinization in New Caledonia, Oman and Yugoslavia." In: *Geochimica et Cosmochimica Acta* 42.1, pp. 144–145. ISSN: 00167037. DOI: 10.1016/0016-7037(78)90225-9.

Beinlich, Andreas et al. (2014). "Inter-mineral Mg isotope fractionation during hydrothermal ultramafic rock alteration – Implications for the global Mg-cycle." In: *Earth and Planetary Science Letters* 392, pp. 166–176. ISSN: 0012821X. DOI: 10.1016/j.epsl.2014.02.028.

Braun, Michael Geoffrey (2004). "Petrologic and Microstructural Constraints on Focused Melt Transport in Dunites and Rheology of the Shallow Mantle." PhD thesis. WHOI/MIT.

Braun, Michael Geoffrey and Peter B. Kelemen (2002). "Dunite distribution in the Oman Ophiolite: Implications for melt flux through porous dunite conduits." In: *Geochemistry, Geophysics, Geosystems* 3.11, pp. 1–21. ISSN: 15252027. DOI: 10.1029/2001GC000289.

Bruni, Jessica et al. (2002). "Irreversible water–rock mass transfer accompanying the generation of the neutral, Mg–HCO3 and high-pH, Ca–OH spring waters of the Genova province, Italy." In: *Applied Geochemistry* 17.4, pp. 455–474. ISSN: 08832927. DOI: 10.1016/S0883-2927(01)00113-5.

Chavagnac, Valerie et al. (2013a). "Characterization of hyperalkaline fluids produced by low-temperature serpentinization of mantle peridotites in the Oman and Ligurian ophiolites." In: *Geochemistry, Geophysics, Geosystems* 14.7, pp. 2496–2522. ISSN: 15252027. DOI: 10.1002/ggge.20147.

Chavagnac, Valerie et al. (2013b). "Mineralogical assemblages forming at hyperalkaline warm springs hosted on ultramafic rocks: A case study of Oman and Ligurian ophi-

olites." In: *Geochemistry, Geophysics, Geosystems* 14.7, pp. 2474–2495. ISSN: 15252027. DOI: 10.1002/ggge.20146.

Clark, Ian D. and Jean-Charles Fontes (1990). "Paleoclimatic reconstruction in northern Oman based on carbonates from hyperalkaline groundwaters." In: *Quaternary Research* 33.3, pp. 320–336. ISSN: 00335894. DOI: 10.1016/0033-5894(90)90059-T.

Coleman, Robert G. and T. E. Keith (1971). "A Chemical Study of Serpentinization — Burro Moutain, California." In: *Journal of Petrology* 12.2, pp. 311–328.

Collier, Martin Lee (2012). "Spatial-Statistical Properties of Geochemical Variability as Constraints on Magma Transport and Evolution Processes at Ocean Ridges." PhD thesis. Columbia University.

DePaolo, Donald J. (1981). "Trace element and isotopic effects of combined wallrock assimilation and fractional crystallization." In: *Earth and Planetary Science Letters* 53.2, pp. 189–202. ISSN: 0012821X. DOI: 10.1016/0012-821X(81)90153-9.

Evans, Bernard W. (1977). "Metamorphism of alpine peridotite and serpentinite." In: *Annual Reviews in Earth and Planetary Sciences*, pp. 397–447. ISSN: 0084-6597. DOI: 10.1146/annurev.ea.05.050177.002145.

Evans, Bernard W. et al. (1976). "Stability of chrysotile and antigorite in the serpentinite multisystem." In: *Schweizerische mineralogische und petrographische Mitteilungen* 56, pp. 79–93.

Falk, Elisabeth S. and Peter B. Kelemen (2015). "Geochemistry and petrology of listvenite in the Samail ophiolite, Sultanate of Oman: Complete carbonation of peridotite during ophiolite emplacement." In: *Geochimica et Cosmochimica Acta* 160, pp. 70–90. ISSN: 00167037. DOI: 10.1016/j.gca.2015.03.014.

Frost, Ronald B. (1985). "On the stability of sulfides, oxides, and native metals in serpentinite." In: *Journal of Petrology* 26.June 1983, pp. 31–63. ISSN: 00223530. DOI: 10.1093/petrology/26.1.31.

Galy, Albert et al. (2001). "High-precision measurement of magnesium isotopes by multiple-collector inductively coupled plasma mass spectrometry." In: *International Journal of Mass Spectrometry* 208.1, pp. 89–98. ISSN: 13873806. DOI: 10.1016/S1387-3806(01)00380-3.

Galy, Albert et al. (2003). "Magnesium isotope heterogeneity of the isotopic standard SRM980 and new reference materials for magnesium-isotope-ratio measurements." In: *Journal of Analytical Atomic Spectrometry* 18.11, pp. 1352–1356. ISSN: 0267-9477. DOI: 10.1039/B309273A.

Gao, Caihong et al. (2018). "Theoretical calculation of equilibrium Mg isotope fractionations between minerals and aqueous solutions." In: *Chemical Geology* 488, pp. 62–75. ISSN: 0009-2541. DOI: 10.1016/J.CHEMGEO.2018.04.005.

Godard, Marguerite, David Jousselin, and Jean-Louis Bodinier (2000). "Relationships between geochemistry and structure beneath a palaeo-spreading centre: a study of the mantle section in the Oman ophiolite." In: *Earth and Planetary Science Letters* 180.1-2, pp. 133–148. ISSN: 0012821X. DOI: 10.1016/S0012-821X(00)00149-7.

Gregory, Robert T. and Hugh P. Taylor (1981). "An oxygen isotope profile in a section of Cretaceous oceanic crust, Samail Ophiolite, Oman: Evidence for δ ¹⁸ O buffering of the oceans by deep (>5 km) seawater-hydrothermal circulation at mid-ocean ridges." In: *Journal of Geophysical Research: Solid Earth* 86.B4, pp. 2737–2755. ISSN: 01480227. DOI: 10.1029/JB086iB04p02737.

Hanghøj, Karen et al. (2010). "Composition and Genesis of Depleted Mantle Peridotites from the Wadi Tayin Massif, Oman Ophiolite; Major and Trace Element Geochemistry, and Os Isotope and PGE Systematics." In: *Journal of Petrology* 51.1-2, pp. 201–227. ISSN: 0022-3530. DOI: 10.1093/petrology/egp077.

Husson, Jon M. et al. (2015). "Ca and Mg isotope constraints on the origin of Earth's deepest δ13C excursion." In: *Geochimica et Cosmochimica Acta* 160, pp. 243–266. ISSN: 00167037. DOI: 10.1016/j.gca.2015.03.012.

Kelemen, Peter B. and Jürg M. Matter (2008). "In situ carbonation of peridotite for CO2 storage." In: *Proceedings of the National Academy of Sciences* 105.45, pp. 17295–17300. ISSN: 0027-8424. DOI: 10.1073/pnas.0805794105.

Kelemen, Peter B. et al. (2011). "Rates and Mechanisms of Mineral Carbonation in Peridotite: Natural Processes and Recipes for Enhanced, in situ CO 2 Capture and Storage." In: *Annual Review of Earth and Planetary Sciences* 39.1, pp. 545–576. ISSN: 0084-6597. DOI: 10.1146/annurev-earth-092010-152509.

Li, Weiqiang et al. (2012). "Magnesium isotope fractionation during precipitation of inorganic calcite under laboratory conditions." In: *Earth and Planetary Science Letters* 333-334, pp. 304–316. ISSN: 0012-821X. DOI: 10.1016/J.EPSL.2012.04.010.

Li, Weiqiang et al. (2015). "Experimental calibration of Mg isotope fractionation between dolomite and aqueous solution and its geological implications." In: *Geochimica et Cosmochimica Acta* 157, pp. 164–181. ISSN: 00167037. DOI: 10.1016/j.gca.2015.02.024.

Liu, Ping-Ping et al. (2017). "Magnesium isotopic composition of the oceanic mantle and oceanic Mg cycling." In: *Geochimica et Cosmochimica Acta* 206, pp. 151–165. ISSN: 00167037. DOI: 10.1016/j.gca.2017.02.016.

Malvoisin, Benjamin (2015). "Mass transfer in the oceanic lithosphere: Serpentinization is not isochemical." In: *Earth and Planetary Science Letters* 430, pp. 75–85. ISSN: 0012821X. DOI: 10.1016/j.epsl.2015.07.043.

Mavromatis, Vasileios et al. (2013). "Kinetics of Mg partition and Mg stable isotope fractionation during its incorporation in calcite." In: *Geochimica et Cosmochimica Acta* 114, pp. 188–203. ISSN: 0016-7037. DOI: 10.1016/J.GCA.2013.03.024.

Mavromatis, Vasileios et al. (2017). "Impact of amorphous precursor phases on magnesium isotope signatures of Mg-calcite." In: *Earth and Planetary Science Letters* 464, pp. 227–236. ISSN: 0012-821X. DOI: 10.1016/J.EPSL.2017.01.031.

Mervine, Evelyn M. et al. (2014). "Carbonation rates of peridotite in the Samail Ophiolite, Sultanate of Oman, constrained through 14C dating and stable isotopes." In: *Geochimica et Cosmochimica Acta* 126, pp. 371–397. ISSN: 00167037. DOI: 10.1016/j.gca.2013.11.007.

Monnier, Christophe et al. (2006). "Along-ridge petrological segmentation of the mantle in the Oman ophiolite." In: *Geochemistry, Geophysics, Geosystems* 7.11, n/a–n/a. ISSN: 15252027. DOI: 10.1029/2006GC001320.

Monnin, Christophe et al. (2011). "Characterization of hyperalkaline fluids produced by serpentinization of mantle peridotites in Oman and in Liguria (Northern Italy)." In: *Mineralog. Mag* 75, p. 1490.

Nasir, Sobhi et al. (2007). "Mineralogical and geochemical characterization of listwaenite from the Semail Ophiolite, Oman." In: *Chemie der Erde - Geochemistry* 67.3, pp. 213–228. ISSN: 00092819. DOI: 10.1016/j.chemer.2005.01.003.

Neal, C. and G. Stanger (1983). "Hydrogen generation from mantle source rocks in Oman." In: *Earth and Planetary Science Letters* 66, pp. 315–320. DOI: 10.1016/0012-821X(83)90144-9.

Neal, C. and G. Stanger (1985). "Past and present serpentinization of ultramafic rocks: An example from the Semail ophiolite nappe of northern Oman." In: *The Chemistry of Weathering*. Ed. by JI Drewer. Dordrecht, Holland: D. Reidel Publishing Company, 249–275.

Noël, J. et al. (2018). "Evidence of polygenetic carbon trapping in the Oman Ophiolite: Petro-structural, geochemical, and carbon and oxygen isotope study of the Wadi Dima harzburgite-hosted carbonates (Wadi Tayin massif, Sultanate of Oman)." In: *Lithos* 323, pp. 218–237. ISSN: 0024-4937. DOI: 10.1016/J.LITHOS.2018.08.020.

Obeso, Juan Carlos de and Peter B. Kelemen (2018). "Fluid rock interactions on residual mantle peridotites overlain by shallow oceanic limestones: Insights from Wadi Fins,

Sultanate of Oman." In: *Chemical Geology*. ISSN: 0009-2541. DOI: 10.1016/J.CHEMGEO.2018.09.022.

Paukert, Amelia N. et al. (2012). "Reaction path modeling of enhanced in situ CO2 mineralization for carbon sequestration in the peridotite of the Samail Ophiolite, Sultanate of Oman." In: *Chemical Geology* 330-331, pp. 86–100. ISSN: 00092541. DOI: 10.1016/j.chemgeo.2012.08.013.

Pinilla, Carlos et al. (2015). "Equilibrium magnesium isotope fractionation between aqueous Mg2+ and carbonate minerals: Insights from path integral molecular dynamics." In: *Geochimica et Cosmochimica Acta* 163, pp. 126–139. ISSN: 00167037. DOI: 10.1016/j.gca.2015.04.008.

Ryu, Jong-Sik et al. (2016). "Experimental investigation of Mg isotope fractionation during mineral dissolution and clay formation." In: *Chemical Geology* 445, pp. 135–145. ISSN: 00092541. DOI: 10.1016/j.chemgeo.2016.02.006.

Schott, Jacques et al. (2016). "The control of carbonate mineral Mg isotope composition by aqueous speciation: Theoretical and experimental modeling." In: *Chemical Geology* 445, pp. 120–134. ISSN: 00092541. DOI: 10.1016/j.chemgeo.2016.03.011.

Shirokova, Liudmila S et al. (2013). "Using Mg Isotopes to Trace Cyanobacterially Mediated Magnesium Carbonate Precipitation in Alkaline Lakes." In: *Aquatic Geochemistry* 19.1, pp. 1–24. ISSN: 1573-1421. DOI: 10.1007/s10498-012-9174-3.

Snow, Jonathan E. and Henry J.B. Dick (1995). "Pervasive magnesium loss by marine weathering of peridotite." In: *Geochimica et Cosmochimica Acta* 59.20, pp. 4219–4235. ISSN: 00167037. DOI: 10.1016/0016-7037(95)00239-V.

Stanger, G. (1985). "Silicified serpentinite in the Semail nappe of Oman." In: *Lithos* 18, pp. 13–22. ISSN: 00244937. DOI: 10.1016/0024-4937(85)90003-9.

Streit, Elisabeth, Peter B. Kelemen, and John Eiler (2012). "Coexisting serpentine and quartz from carbonate-bearing serpentinized peridotite in the Samail Ophiolite, Oman." In: *Contributions to Mineralogy and Petrology* 164.5, pp. 821–837. ISSN: 00107999. DOI: 10.1007/s00410-012-0775-z.

Su, Ben-Xun et al. (2015). "Iron and magnesium isotope fractionation in oceanic lithosphere and sub-arc mantle: Perspectives from ophiolites."

Teng, Fang-Zhen (2017). "Magnesium Isotope Geochemistry." In: *Reviews in Mineralogy and Geochemistry* 82.1, pp. 219–287. ISSN: 1529-6466. DOI: 10.2138/rmg.2017.82.7.

Teng, Fang-Zhen et al. (2010). "Magnesium isotopic composition of the Earth and chondrites." In: *Geochimica et Cosmochimica Acta* 74.14, pp. 4150–4166. ISSN: 00167037. DOI: 10.1016/j.gca.2010.04.019.

Teng, Fang Zhen et al. (2015). "Magnesium Isotopic Compositions of International Geological Reference Materials." In: *Geostandards and Geoanalytical Research* 39.3, pp. 329–339. ISSN: 1751908X. DOI: 10.1111/j.1751-908X.2014.00326.x.

Wang, Wenzhong et al. (2019). "Equilibrium Mg isotope fractionation among aqueous Mg2+, carbonates, brucite and lizardite: Insights from first-principles molecular dynamics simulations." In: *Geochimica et Cosmochimica Acta* 250, pp. 117–129. ISSN: 0016-7037. DOI: 10.1016/J.GCA.2019.01.042.

Weyhenmeyer, Constanze E et al. (2002). "Isotope study of moisture sources , recharge areas , and groundwater flow paths within the eastern Batinah coastal plain , Sultanate of Oman." In: 38.10, pp. 1–22. DOI: 10.1029/2000WR000149.

Wimpenny, Josh et al. (2010). "The behaviour of Li and Mg isotopes during primary phase dissolution and secondary mineral formation in basalt." In: *Geochimica et Cosmochimica Acta* 74.18, pp. 5259–5279. ISSN: 00167037. DOI: 10.1016/j.gca.2010.06.028.

Wimpenny, Joshua et al. (2014). "Investigating the behaviour of Mg isotopes during the formation of clay minerals." In: *Geochimica et Cosmochimica Acta* 128, pp. 178–194. ISSN: 00167037. DOI: 10.1016/j.gca.2013.12.012.

Young, Edward D and Albert Galy (2004). "The Isotope Geochemistry and Cosmochemistry of Magnesium." In: *Reviews in Mineralogy and Geochemistry* 55.1, 197 LP –230.

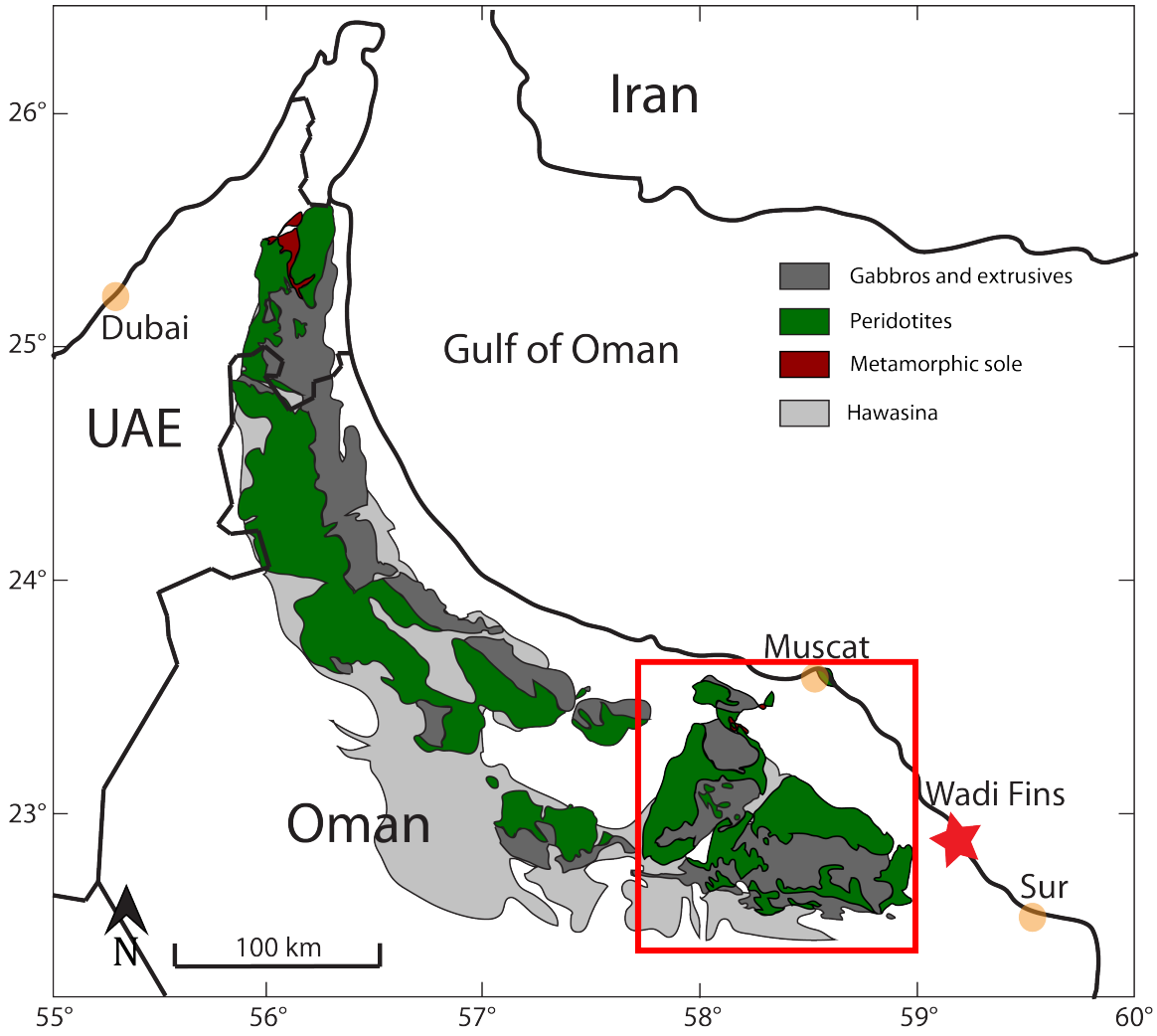

Figure 4.1: Simplified geologic map of the Samail ophiolite in Oman and the United Arab Emirates. All samples in this study come from the southern massifs (red square) and a small exposure beneath overlying Cretaceous to Eocene limestones at Wadi Fins (red star). Modified after Nicolas, Boudier, and France 2009

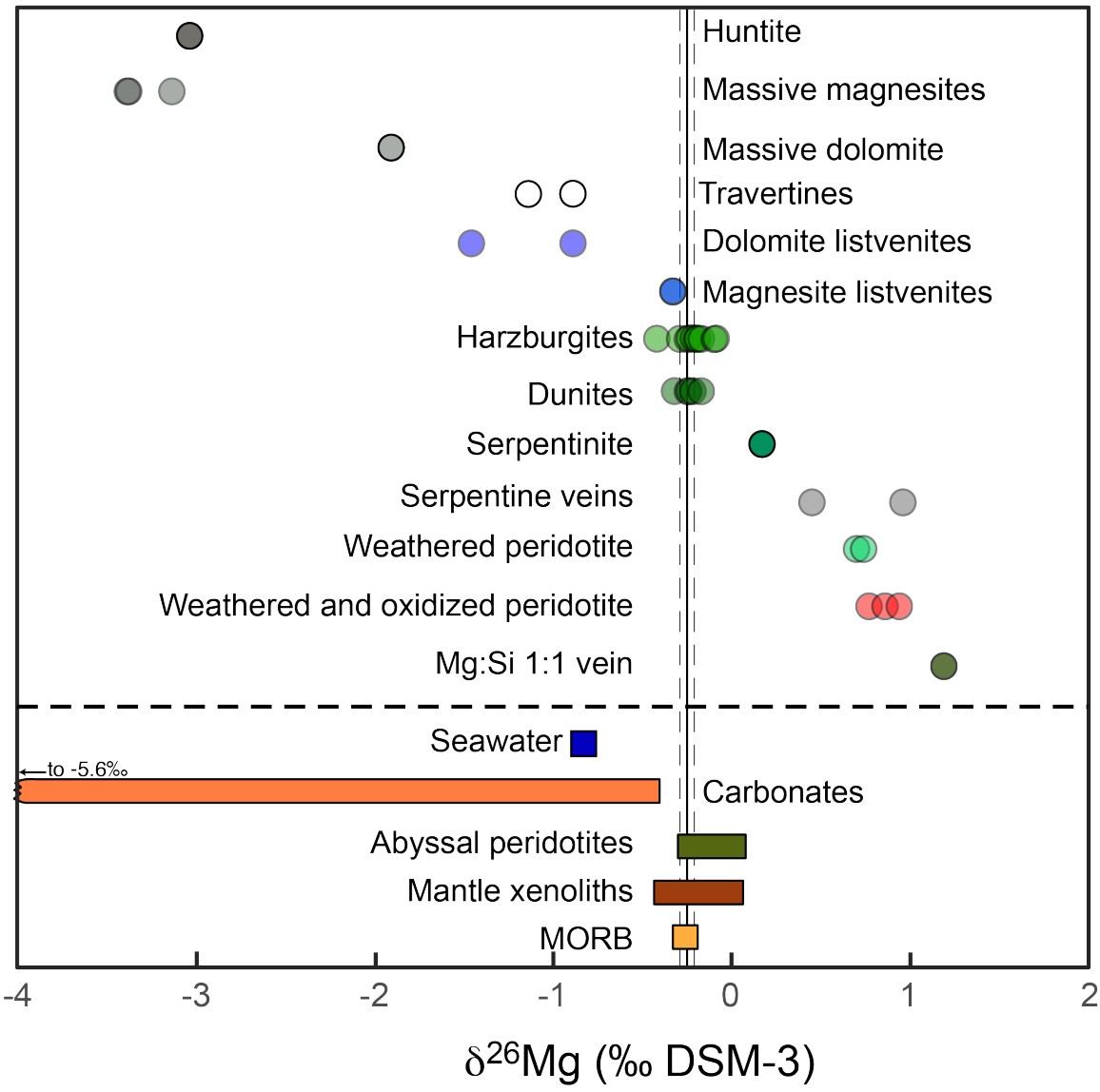

Figure 4.2: δ^{26}Mg composition for studied samples and selected terrestrial reservoirs (color squares from Teng 2017). Black solid line is mantle average and dashed black lines range of variability of mantle compositions from Teng et al. 2010 and Teng 2017

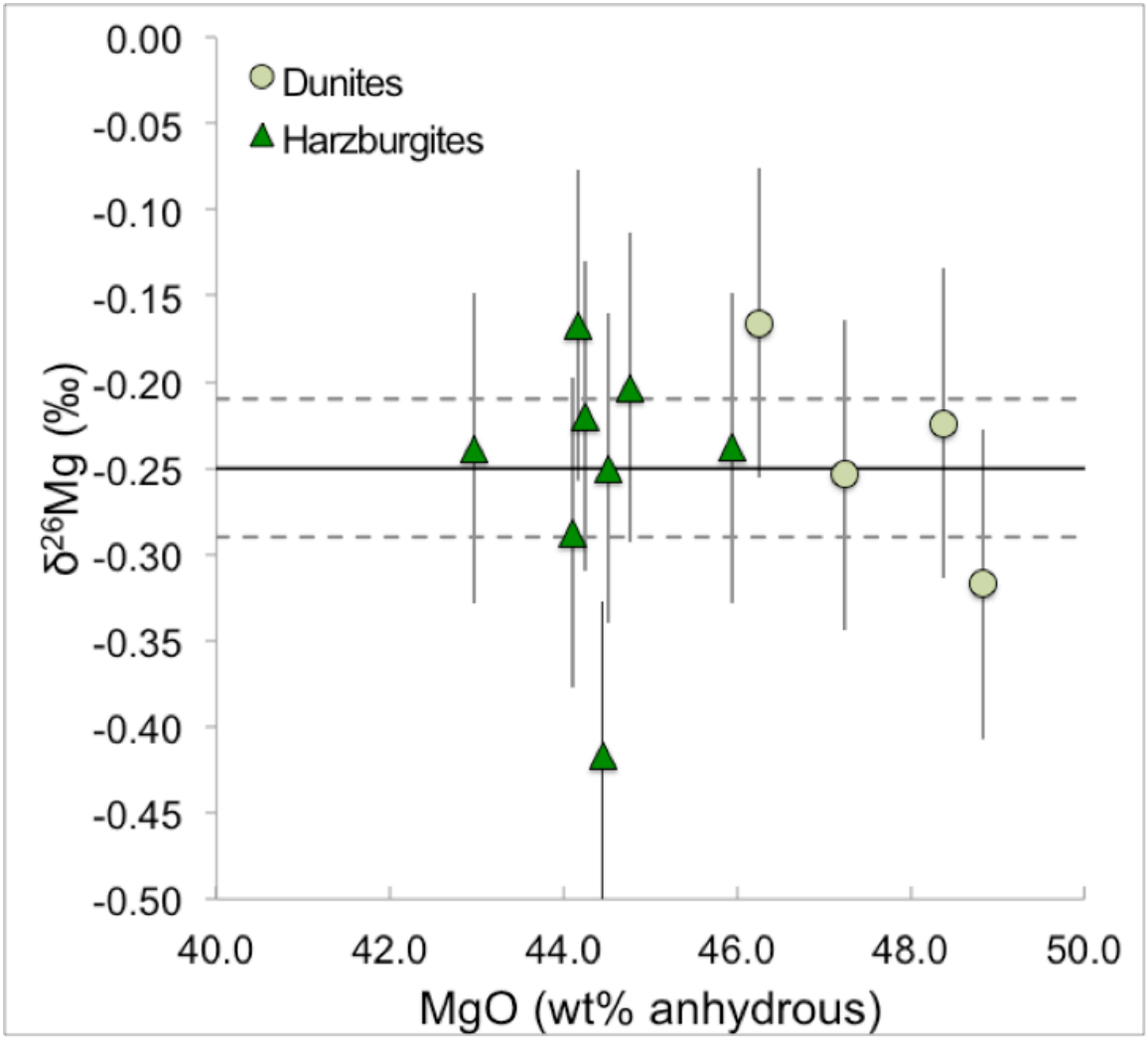

Figure 4.3: δ^{26}Mg vs. MgO (wt% anhydrous) for harzburgites and dunites. Black solid line is mantle average and dashed black lines encompass the range of variability from Teng et al. 2010 and Teng 2017

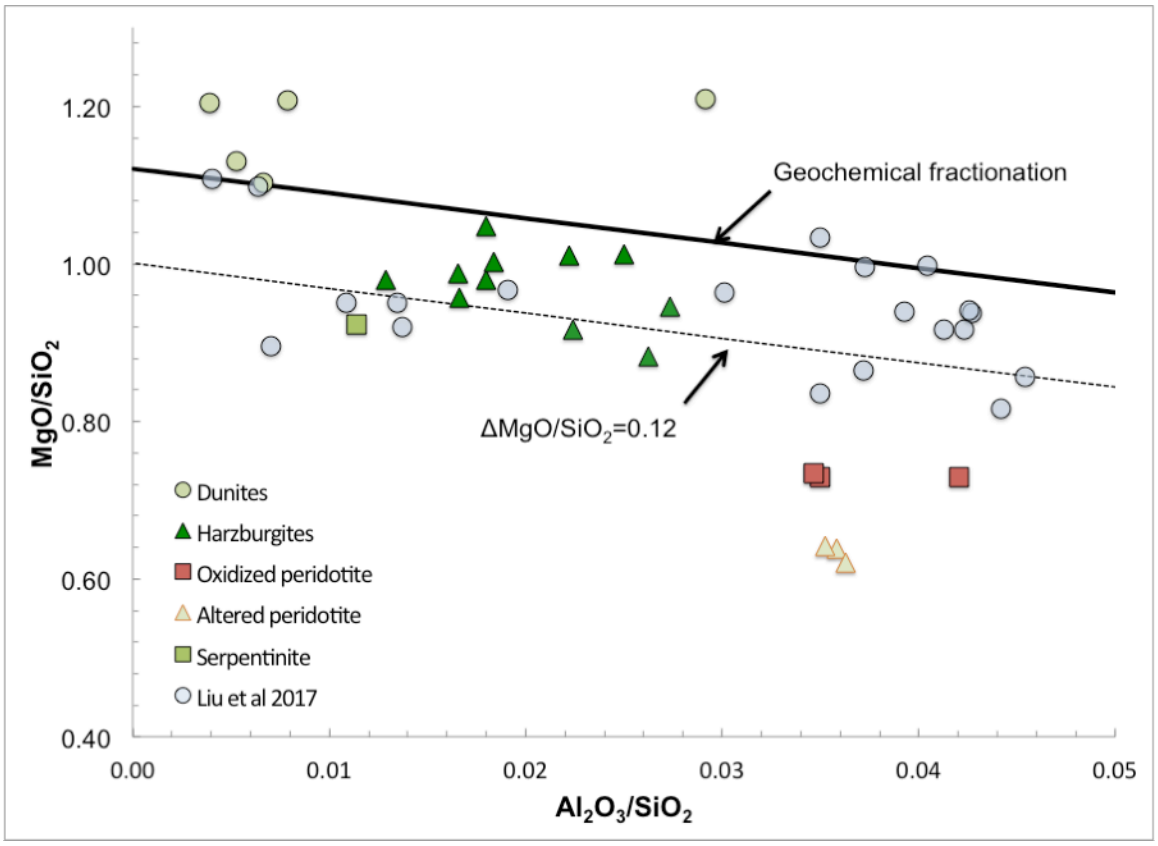

Figure 4.4: Whole rock MgO/SiO_2 vs Al_2O_3/SiO_2. Geochemical fractionation is a linear fit of theoretical and observed residues of mantle melting and melt extraction during adiabatic decompression beneath oceanic spreading ridges (Asimow 1999; Baker and Beckett 1999).

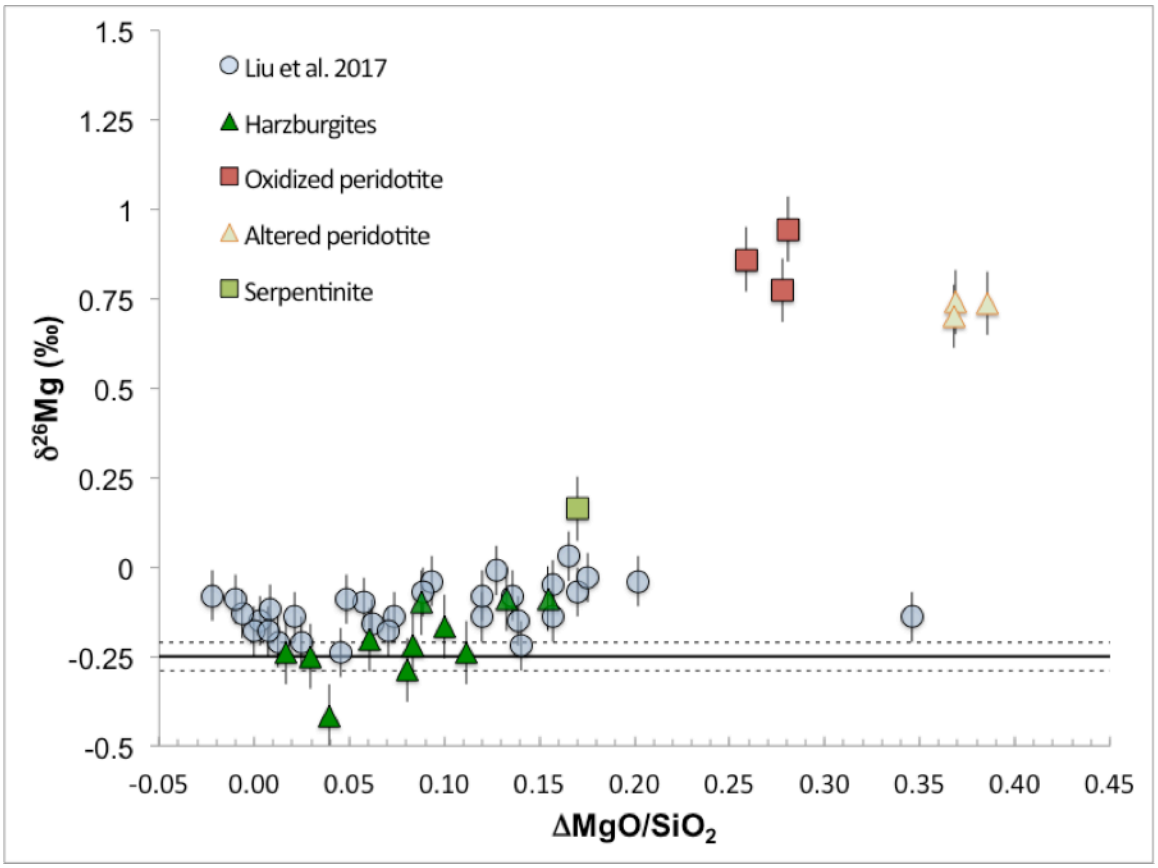

Figure 4.5: Bulk rock $\Delta(MgO/SiO_2)$ vs δ^{26}Mg for Oman samples and abyssal peridotites (Liu et al. 2017). Black solid line is mantle average and dashed black lines range of variability of mantle compositions (Teng 2017; Teng et al. 2010)

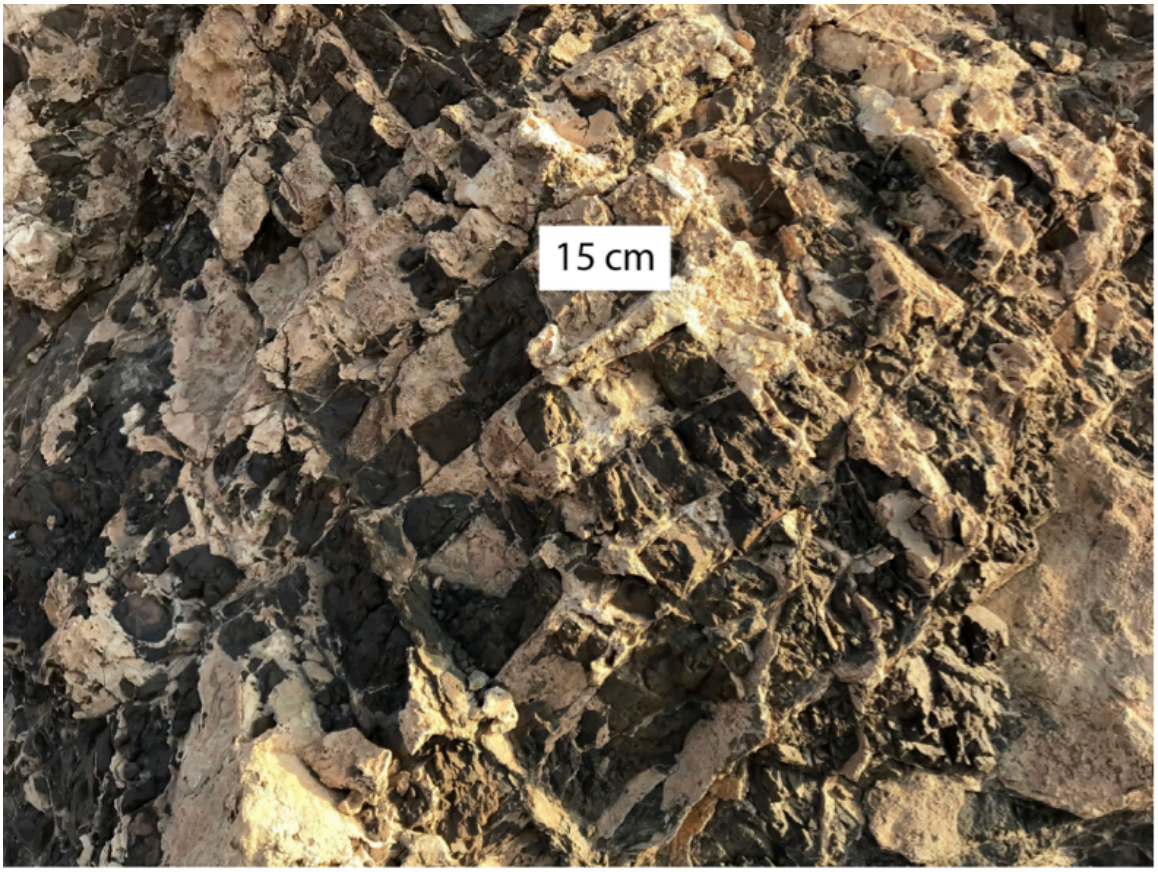

Figure 4.6: Massive magnesite veins with blocks of serpentinized harzburgite in the ophiolite (UTM 40Q E 671274 N 2536144).

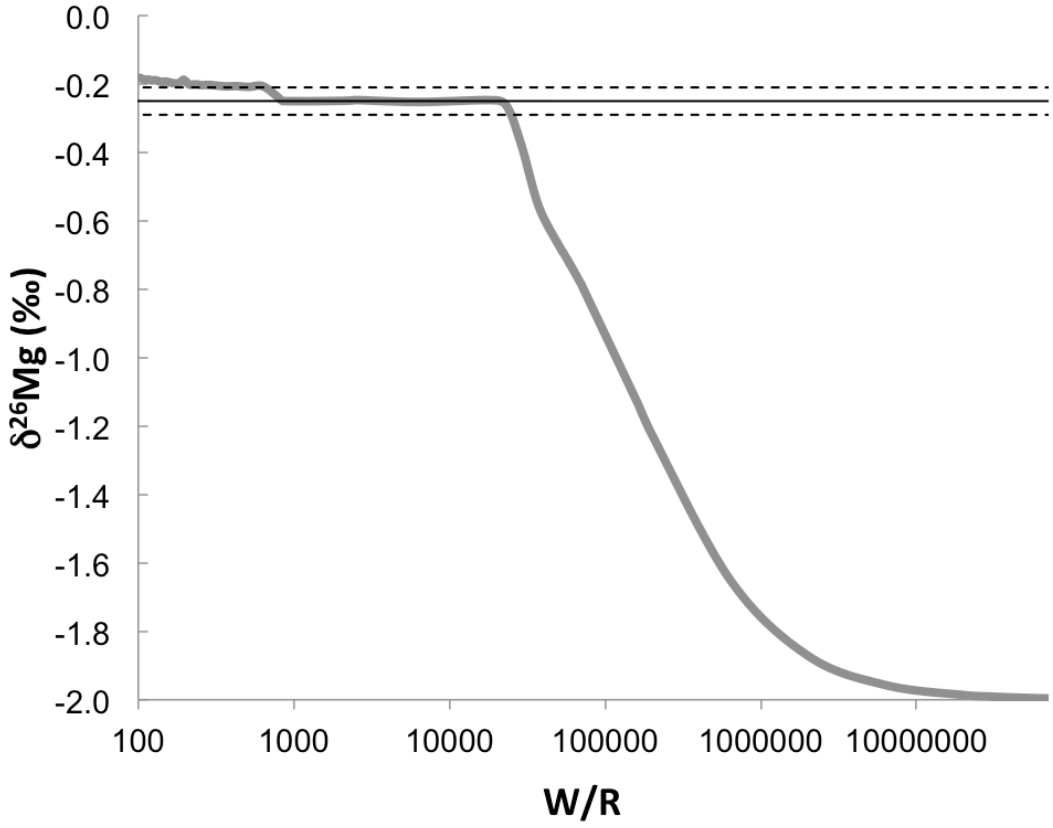

Figure 4.7: δ^{26}Mg evolution of the fluid in the open system . Black solid line is mantle average and dashed black lines range of variability of mantle compositions from Teng 2017; Teng et al. 2010.

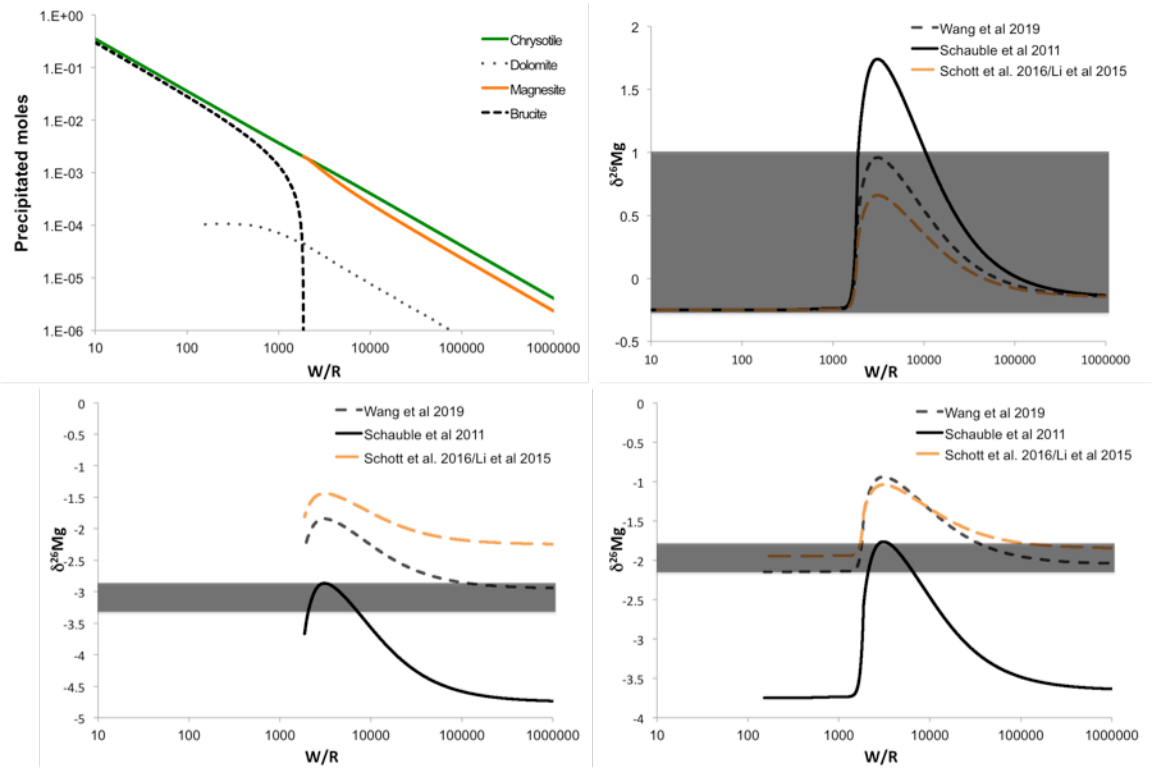

Figure 4.8: Closed system reaction path mineralogy (top left), δ^{26}Mg of fluid and serpentine (top right), magnesite (bottom left), dolomite (bottom right). Grey squares illustrate range of sample values measured for each mineral.

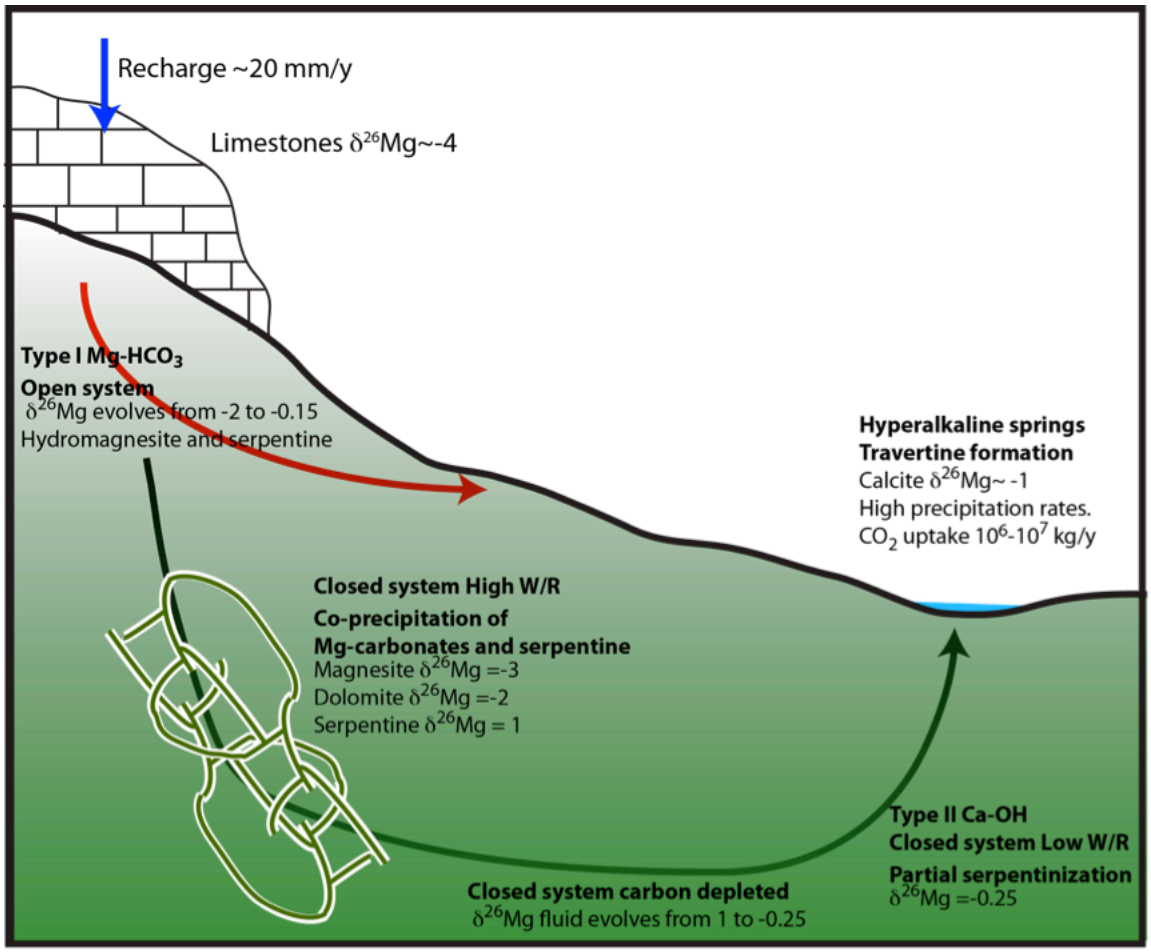

Figure 4.9: Conceptual model of Mg isotope systematics in the modern alteration system in Oman after Dewandel et al. 2005 and Neal and Stanger 1985

Table 4.1: Samples numbers, reference, lithology and Mg isotopic compositions

Sample	Reference	Lithology	δ^{26}Mg	δ^{25}Mg	2σ/2SE	n
OM94-99	Hanghøj et al 2008	Dunite	-0.22	-0.11	0.09	1
OM94-52D*	Hanghøj et al 2008	Dunite	-0.25	-0.11	0.09	1
OM94-74D	Hanghøj et al 2008	Dunite	-0.32	-0.15	0.09	1
OM94-110*	Hanghøj et al 2008	Dunite	-0.17	-0.06	0.09	1
OM94-67	Hanghøj et al 2008	Harzburgite	-0.25	-0.12	0.09	1
OM94-103	Hanghøj et al 2008	Harzburgite	-0.22	-0.11	0.09	1
OM94-61	Hanghøj et al 2008	Harzburgite	-0.24	-0.09	0.09	1
OM94-98	Hanghøj et al 2008	Harzburgite	-0.20	-0.09	0.09	1
OM94-101	Hanghøj et al 2008	Harzburgite	-0.29	-0.16	0.09	1
OM94-52H	Hanghøj et al 2008	Harzburgite	-0.42	-0.22	0.09	1
OM13-19	De Obeso and Kelemen 2018	Harzburgite	-0.17	-0.09	0.09	1
OM13-2	De Obeso and Kelemen 2018	Harzburgite	-0.24	-0.14	0.09	1
OM13-4	De Obeso and Kelemen 2018	Dunite	-0.24	-0.09	0.09	1
OM15-5-4	De Obeso & Kelemen submitted	Harzburgite	-0.10	-0.07	0.09	1
OM15-6-4	De Obeso & Kelemen submitted	Harzburgite	-0.09	-0.03	0.09	1
OM15-7-4	De Obeso & Kelemen submitted	Harzburgite	-0.09	-0.07	0.09	1
OM15-5-3	De Obeso & Kelemen submitted	Oxidized harzburgite	0.94	0.49	0.09	1
OM15-6-3	De Obeso & Kelemen submitted	Oxidized harzburgite	0.86	0.46	0.09	1
OM15-7-3	De Obeso & Kelemen submitted	Oxidized harzburgite	0.77	0.41	0.09	1
OM15-6-2	De Obeso & Kelemen submitted	Altered harzburgite	0.74	0.38	0.09	1
OM15-7-2	De Obeso & Kelemen submitted	Altered harzburgite	0.74	0.40	0.09	1
OM15-5-2	De Obeso & Kelemen submitted	Altered harzburgite	0.70	0.37	0.09	1
OM13-15A	This Study	Serpentinite	0.17	0.08	0.09	1
OM15-5-5	This Study	”Waxy” vein	1.19	0.60	0.09	1
OM13-15B	This Study	Serpentine vein	0.45	0.20	0.09	1
OM13-17A WP	This Study	Serpentine vein	0.96	0.51	0.09	1
OM09-11	Falk and Kelemen 2015	Magnesite Listvenite	-0.33	-0.18	0.09	1
OM10-26	Falk and Kelemen 2015	Magnesite Listvenite	-0.33	-0.16	0.09	1
OM10-14	Falk and Kelemen 2015	Dolomite Listvenite	-1.46	-0.78	0.09	1
OM10-15	Falk and Kelemen 2015	Dolomite Listvenite	-0.89	-0.48	0.09	1
OM07-39	Streit et al. 2012	Massive magnesite vein	-3.14	-1.64	0.09	1
OM07-27	Streit et al. 2012	Massive dolomite vein	-1.91	-1.02	0.09	1
OM17 Magnesite	This study	Massive magnesite vein	-3.38	-1.77	0.01	5
OM07-18	Kelemen et al 2011 only mineralogy	Travertine forming now	-1.14	-0.56	0.07	2
OM07-34A	Kelemen et al 2011 only mineralogy	Old travertine	-0.89	-0.44	0.05	2
OM07-07	Kelemen et al 2011 only mineralogy	Carbonate vein	-3.39	-1.75	0.09	1
BA1B 11-2 17-27 cm	This study from mineralogy	Huntite vein	-3.04	-1.57	0.09	1

2σ=long-term external reproducibility of Cambridge-1; applied to all samples that were run only once through column chemistry + Neptune (i.e. not replicated)

2SE=applied to samples that were replicated, that is, run through column chemistry + Neptune more than once

Table 4.2: Magnesium isotope fractionation factors

Reference	$\alpha_{mgs-fluid}$	$\alpha_{dol-fluid}$
Wang et al 2019	0.9972	0.9981
Schauble et al 2011	0.9954	0.9965
Schott et al. 2016^/Li et al 2015	0.9979	0.9983

^ Schott is extrapolated from batch reaction data

Appendix A: Supplementary Figures

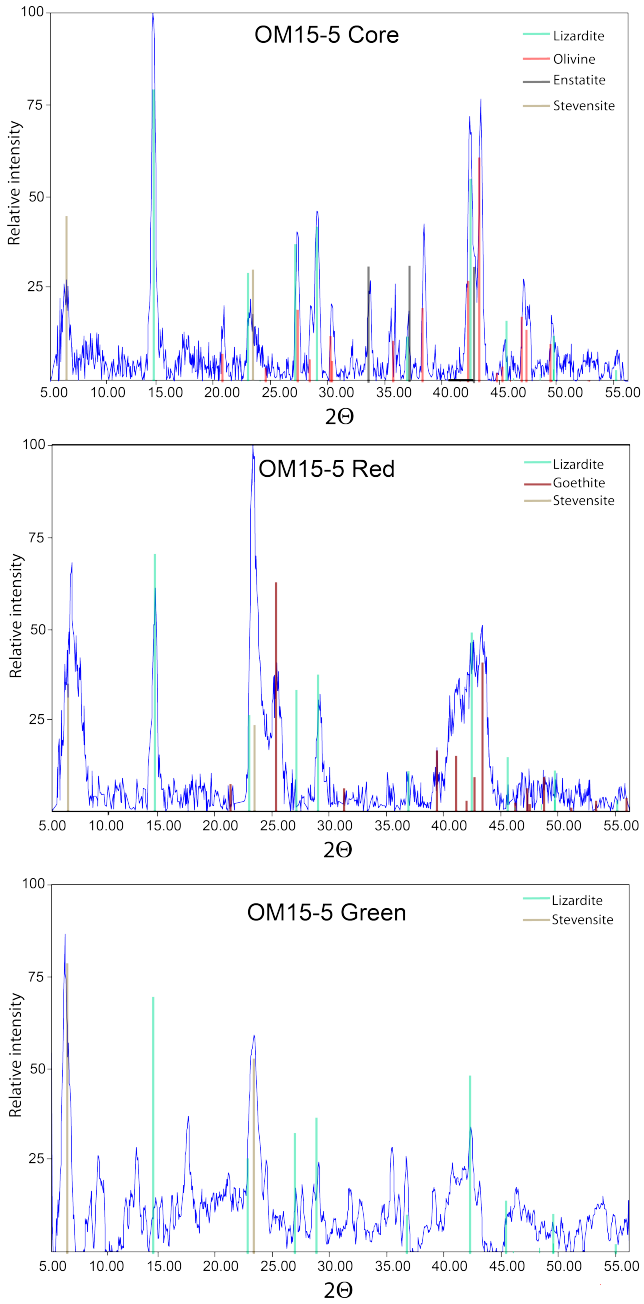

Supplementary figure 1. Representative XRD spectra of three alteration zones. Spectra were processed using Match! software. Background was removed using Match! automatic background removal tool for clarity.

Appendix B: Supplementary Tables

Supplementary Tables for Chapter 2: Fluid rock interactions on residual mantle peridotites overlain by shallow oceanic limestones: Insights from Wadi Fins, Sultanate of Oman can be downloaded here

Supplementary Tables for Chapter 3: Magnesium and iron mobility during serpentinization, oxidation and weathering of mantle peridotite at low temperatures: The case of Wadi Fins, Oman can be downloaded here

Supplementary Tables for Chapter 4: Carbon mineralization accompanying serpentinization in the Oman ophiolite: A magnesium isotope perspective can be downloaded here